PREPARATION AND CHARACTERIZATION OF ZEOLITE CONFINED COBALT(0) NANOCLUSTERS AS CATALYST FOR HYDROGEN GENERATION FROM THE HYDROLYSIS OF SODIUM BOROHYDRIDE AND AMMONIA BORANE

A THESIS SUBMITTED TO
THE GRADUATE SCHOOL OF NATURAL AND APPLIED SCIENCES
OF
MIDDLE EAST TECHNICAL UNIVERSITY

BY

MURAT RAKAP

IN PARTIAL FULFILLMENT OF THE REQUIREMENTS
FOR
THE DEGREE OF DOCTOR OF PHILOSOPHY
IN
CHEMISTRY

JULY 2011

Approval of the thesis:

PREPARATION AND CHARACTERIZATION OF ZEOLITE CONFINED COBALT(0) NANOCLUSTERS AS CATALYST FOR HYDROGEN GENERATION FROM THE HYDROLYSIS OF SODIUM BOROHYDRIDE AND AMMONIA BORANE

submitted by **MURAT RAKAP** in partial fulfillment of the requirements for the degree of **Doctor of Philosophy in Chemistry Department, Middle East Technical University** by,

Prof. Dr. Canan Özgen __________________
Dean, Graduate School of **Natural and Applied Sciences**

Prof. Dr. İlker Özkan __________________
Head of Department, **Chemistry**

Prof. Dr. Saim Özkar
Supervisor, **Chemistry Dept., METU** __________________

Examining Committee Members:

Prof. Dr. Ceyhan Kayran __________________
Chemistry Dept., METU

Prof. Dr. Saim Özkar __________________
Chemistry Dept., METU

Prof. Dr. Gülsün Gökağaç __________________
Chemistry Dept., METU

Assoc. Prof. Dr. Ayşen Yılmaz __________________
Chemistry Dept., METU

Assist. Prof. Dr. Emrah Özensoy __________________
Chemistry Dept., Bilkent University

Date: 08.07.2011

I hereby declare that all information in this document has been obtained and presented in accordance with academic rules and ethical conduct. I also declare that, as required by these rules and conduct, I have fully cited and referenced all material and results that are not original to this work.

Name, Last name: MURAT RAKAP

Signature:

ABSTRACT

PREPARATION AND CHARACTERIZATION OF ZEOLITE CONFINED COBALT(0) NANOCLUSTERS AS CATALYST FOR HYDROGEN GENERATION FROM THE HYDROLYSIS OF SODIUM BOROHYDRIDE AND AMMONIA BORANE

RAKAP, Murat
Ph.D., Department of Chemistry
Supervisor: Prof. Dr. Saim ÖZKAR

July 2011, 123 pages

Because of the growing concerns over the depletion of fossil fuel supplies, environmental pollution and global warming caused by a steep increase in carbon dioxide and other greenhouse gases in the atmosphere, much attention has been given to the development of renewable energy sources that are the only long-term solution to the energy requirements of the world’s population, on the way towards a sustainable energy future. Hydrogen has been considered as a clean and environmentally benign new energy carrier for heating, transportation, mechanical power and electricity generation. However, the lack of effective, safe, and low-cost hydrogen storage materials for mobile, portable, and stationary applications is one of the major hurdles to be overcome for the implementation of hydrogen economy. Among various solid state hydrogen storage materials, chemical hydrogen storage materials such as sodium borohydride ($NaBH_4$) and ammonia borane (H_3NBH_3) have received much attention as promising candidates for fuel cell applications under ambient conditions due to their high gravimetric and volumetric hydrogen storage capacities. Both sodium borohydride and ammonia borane generate hydrogen upon hydrolysis in the presence of suitable metal catalysts.

Transition metal nanoclusters can be used as active catalysts to catalyze the hydrolysis reactions of sodium borohydride and ammonia borane for hydrogen generation since they exhibit unique properties that differ from their bulk counterparts. Although the catalytic activity of metal nanoclusters increases with decreasing particle size, they are unstable with respect to agglomeration into the bulk metal leading to a significant decrease in activity in their catalytic applications. Therefore, the exploitation of microporous and mesoporous materials with ordered porous structures as hosts to encapsulate metal nanoclusters has attracted great interest since the pore size restriction of these host materials could limit the growth of nanoclusters leading to an increase in the percentage of the catalytically active surface atoms. In this dissertation, we report the preparation, characterization and the investigation of the catalytic activities of zeolite confined cobalt(0) nanoclusters in the hydrolysis of sodium borohydride and ammonia borane. The zeolite confined cobalt(0) nanoclusters were prepared by the reduction of cobalt(II)-exchanged zeolite-Y by sodium borohydride in aqueous solution at room temperature with no alteration in the framework lattice or loss in the crystallinity. The characterization of zeolite confined cobalt(0) nanoclusters were done by using inductively coupled plasma optical emission spectroscopy (ICP-OES), X-ray diffraction (XRD), high resolution transmission electron microscopy (HRTEM), scanning electron microscopy (SEM), energy dispersive X-ray spectroscopy (EDX), X-ray photoelectron spectroscopy (XPS), diffuse reflectance UV-visible spectroscopy (DR-UV-Vis), infrared spectroscopy (IR), Raman spectroscopy, and N_2 adsorption-desorption technique. The catalytic activity of zeolite confined cobalt(0) nanoclusters and the kinetics of hydrogen generation from the hydrolysis of sodium borohydride and ammonia borane were studied depending on catalyst concentration, substrate concentration and temperature. The rate laws and the activation parameters (Arrhenius activation energy, Ea; activation enthalpy, $\Delta H^{\#}$; and activation entropy, $\Delta S^{\#}$) for both catalytic hydrolysis reactions were calculated from the obtained kinetic data.

Keywords: Nanoclusters, Cobalt, Zeolite, Catalyst, Hydrolysis, Sodium Borohydride, Ammonia Borane.

ÖZ

ZEOLİT GÖZENEKLERİ İÇİNE HAPSEDİLMİŞ KOBALT(0) NANOKÜMELERİN HAZIRLANMASI, TANIMLANMASI VE SODYUM BORHİDRÜR İLE AMONYAK BORANIN HİDROLİZİNDEN HİDROJEN ÜRETİMİNDE KATALİZÖR OLARAK KULLANILMASI

RAKAP, Murat
Doktora, Kimya Bölümü
Tez Yöneticisi: Prof. Dr. Saim ÖZKAR

Temmuz 2011, 123 sayfa

Fosil yakıt rezervlerinin azalması, çevre kirliliği ve atmosferdeki karbon dioksit ve diğer sera gazlarındaki artışın sebep olduğu küresel ısınma konusunda giderek artan endişeler nedeniyle, sürdürülebilir bir enerji geleceği için dünya nüfusunun enerji gereksinimine uzun süreli çözüm olarak düşünülen yenilenebilir enerji kaynaklarının geliştirilmesi üzerine yapılan çalışmalar büyük önem kazanmaktadır. Bu bağlamda hidrojen ısınma, ulaşım, mekanik enerji ve elektrik üretimi için temiz ve çevresel olarak zararsız bir enerji taşıyıcı olarak düşünülmektedir. Bununla birlikte, hareketli, taşınabilir ve sabit uygulamalar için etkin, güvenilir ve düşük maliyetli hidrojen depolama malzemelerinin eksikliği hidrojen ekonomisinin hayata geçirilmes için aşılması gereken en büyük engellerden biridir. Çeşitli katı hidrojen depolama malzemeleri arasında, sodyum borhidrür ve amonyak boran gibi kimyasal hidrojen depolama malzemeleri, sahip oldukları yüksek gravimetrik ve volumetrik hidrojen depolama kapasiteleri sayesinde ılımlı koşullar altında yakıt pili uygulamaları için potansiyel adaylar olarak büyük dikkat çekmektedirler. Hem sodyum borhidrür hem de amonyak boran, uygun katalizörler eşliğinde suda hidroliz olduğunda hidrojen gazı oluşturmaktadır.

Geçiş metal nanokümeleri külçe karşıtlarından ayıran eşsiz özelliklere sahip olduklarından, hidrojen eldesi için sodyum borhidrür ve amonyak boranın hidroliz tepkimelerinde katalizör olarak kullanılabilirler. Metal nanokümelerinin katalitik etkinliği küçülen parçacık boyutuyla artış göstermesine rağmen, bu nanokümeler topaklanmaya karşı kararsız olduklarından külçe metale dönüşme eğilimindedirler ve bu durum katalitik uygulamalarda aktivitenin önemli ölçüde azalmasına neden olmaktadır. Bu yüzden, nanokümelerin hazırlanmasında zeolitler gibi düzenli gözenekli yapılara sahip malzemelerin kullanılması, gözenek boyut sınırlaması nanokümelerin büyümelerini önleyeceğinden ve dolayısıyla katalitik olarak aktif yüzey atomlarının sayısını arttıracağından büyük ilgi görmektedir. Bu tezde, zeolit gözeneklerine hapsedilmiş kobalt(0) nanokümelerinin hazırlanmasını, tanımlanmasını ve sodyum borhidrür ile amonyak boranın hidroliz tepkimelerindeki katalitik etkinliklerinin incelenmesini sunuyoruz. Zeolit gözenekleri içine hapsedilmiş kobalt(0) nanokümeleri, kobalt(II) iyonlarıyla değiştirilmiş zeolitin oda sıcaklığında sodium borhidrür ile indirgenmesi sonucu hazırlanmıştır ve bu işlemler zeolit yapısında herhangi bir değişikliğe yol açmamıştır. Bu şekilde hazırlanan metal nanokümeleri, İndüktif olarak çiftleşmiş plazma-optik emisyon spektroskopisi (ICP-OES), X- ışınları kırınımı (XRD), yüksek çözünürlüklüklü geçirgenli elektron mikroskopisi (HRTEM), taramalı elektron mikroskopisi (SEM), Enerji dağıtımı X-ışını spektroskopisi (EDX), X-ışını fotoelektron spektroskopisi (XPS), Dağınık yansıtma-UV-görünür bölge elektronik soğurma spektroskopisi (DR-UV-Vis), İnfrared spektroskopisi (IR), Raman spektroskopisi ve N_2 adsorpsiyon-desorpsiyon tekniği kullanılarak tanımlandı. Zeolit gözenekleri içine hapsedilen kobalt(0) nanokümelerinin katalitik etkinliği ile bu katalizörlerin varlığında sodium borhidrür ve amonyak boranın hidroliz tepkimelerinin kinetiği, farklı katalizör ve substrat konsantrasyonuna ve sıcaklığa bağlı olarak çalışıldı. Her iki katalitik hidroliz tepkimesine ilişkin hız kanunu ve aktivasyon parametreleri (Arrhenius aktivasyon enerjisi (Ea), aktivasyon entalpisi ($\Delta H^{\neq}$) and aktivasyon entropisi ($\Delta S^{\neq}$)), Elde edilen kinetik veriler kullanılarak hesaplandı.

Anahtar Kelimeler: Nanokümeler, Kobalt, Zeolit, Katalizör, Hidroliz, Sodyum Borhidrür, Amonyak Boran.

To my wife, Asiye, and my son, Ahmet Faruk, for being the meaning of my life

ACKNOWLEDGMENTS

I would like to express my sincerest gratitude to Prof. Dr. Saim Özkar for his precious support, guidance, patience, and encouragement throughout the course of my PhD studies and in the completion of this dissertation. I am profoundly honored to have a chance to work with him, and to be alumni of his highly loved research group.

I am grateful for the help and advice provided by my committee members, Prof. Dr. Ceyhan Kayran and Assist. Prof. Dr. Emrah Özensoy.

Appreciation is extended to all former and current members of 'Nanoclusters and Organometallic Research Group' for their good friendship, scientific collaborations, endless help and motivation.

I would like to thank The Scientific and Technological Research Council of Turkey (TÜBİTAK) for 2211-National Scholarship for PhD students and METU-DPT-OYP on the behalf of Yüzüncü Yıl University.

I would like to thank my parents, brother, and sister for countless love and support. I could not pay you for what you have done for me in every moment of my life.

Most importantly, I would like to thank my wife and best friend Asiye, who was always there for me. Her endless moral support, love, patience, dedication, and encouragement during my PhD studies were truly needed for this work to be completed.

Finally, I would like to thank my lovely son, Ahmet Faruk, for taking his time and hopefully, I will not keep him waiting in the evenings anymore.

TABLE OF CONTENTS

LIST OF FIGURES

FIGURES

LIST OF TABLES

TABLES

LIST OF ABBREVIATIONS

AB : Ammonia borane

TON : Turnover number

TOF : Turnover frequency

$Ea^{apparent}$: Apparent activation energy

k_{app} : Apparent rate constant

nm : Nanometer

FAU : Faujasite

PV : Photovoltaic

ICE : Internal combustion engine

IT : Information technology

FCV : Fuel cell vehicle

ICEV : Internal combustion engined vehicle

MTL : Mass transfer limitation

ppm : Parts per million

rpm : Revolution per minute

$\Delta H^{\#}$: Activation enthalpy

$\Delta S^{\#}$: Activation entropy

dba : Dibenzylideneacetone

CHAPTER 1

INTRODUCTION

1.1. Energy Related Global Problems and Hydrogen as an Energy Carrier

Most of the world's energy requirements for heating, transportation, mechanical power and electricity generation are currently supplied from fossil fuels like petroleum, coal or natural gas [1]. However; because of the growing concerns over the depletion of fossil fuel supplies, environmental pollution and global warming caused by a steep increase in carbon dioxide and other greenhouse gases in the atmosphere, much attention has been given to the development of renewable energy sources that are the only long-term solution to the energy requirements of the world's population, on the way towards a sustainable energy future [2]. In the past 20 years, a hydrogen economy has often proposed by the media, and also by some economists and scientists, as a means to solve the problems caused by the use of fossil fuels. At first sight, the idea sounds quite simple: (i) hydrogen is one of the most plentiful elements on Earth; (ii) some vehicle manufacturers have demonstrated that hydrogen can be used directly in an internal combustion engine, and fuel cell-powered prototype cars have also been constructed; (iii) combustion of molecular hydrogen, H_2, with oxygen produces heat, and combination of molecular hydrogen and oxygen in a fuel cell generates electricity and heat; (iv) the only byproduct is water, whereas burning of fossil fuels generates CO_2 and a variety of pollutants. Therefore, if hydrogen could promptly replace fossil fuels, both the energy and environmental problems of our planet woud have been solved [3].

Hydrogen is the most abundant element in the universe, making up 75 % of normal matter by mass, and is the third most abundant element on Earth's surface.

Due to its high reactivity, hydrogen in Nature is nearly always combined with other elements. It is present in water (H_2O) and thereby in every living organism. It is also present in hydrocarbons (e.g. methane, CH_4), in organic compounds, and in several other natural as well as artificial compounds. Hydrogen is invisible, non toxic, light, odorless, and tasteless gas. Combustion of hydrogen with pure oxygen generates only water as s byproduct. Currently, more than 95 % of hydrogen is produced from fossil fuels in a variety of processes that generate, besides hydrogen, carbon dioxide. For example, the extraction of hydrogen from steam reforming of methane takes place via C and CO as intermediate products. A very minor fraction of hydrogen is produced by electrolysis of water. Hydrogen is mainly used in the synthesis of ammonia and refining processes (Figure 1) [3a].

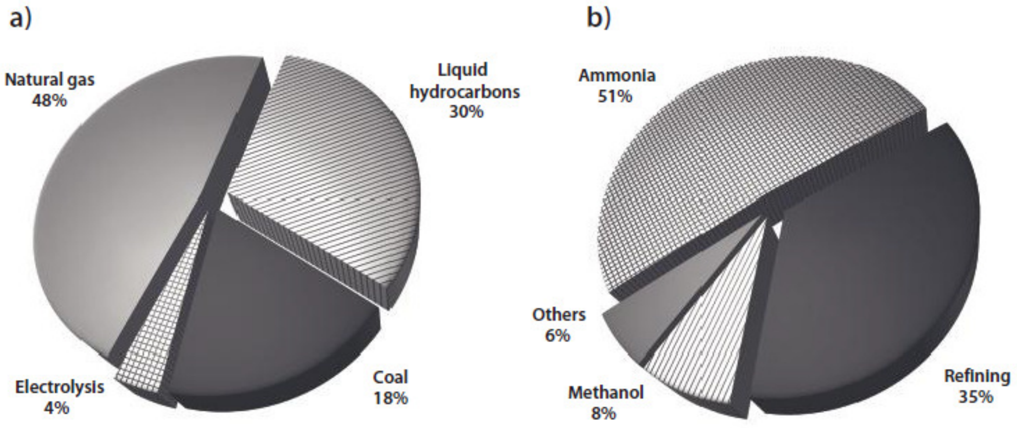

Figure 1. (a) Hydrogen production sources currently used in the world. (b) The main hydrogen-consuming sectors in the world [3a].

Unfortunately, however, there is no molecular hydrogen on Earth. Molecular hydrogen has to be produced by using energy, starting from hydrogen rich compounds. Therefore, hydrogen is rather an energy carrier, not an alternative fuel [4]. The various kinds of primary energy sources that can be used for the production of hydrogen and potential applications for this energy vector, including both renewable and nonrenewable sources are schematically summarized in Figure 2 [5]. As seen from this figure, hydrogen can be produced from primary energy sources including coal, natural gas, biomass, solar, thermal, wind, hydro, or nuclear power, and may be used to convey energy to where it may be utilized.

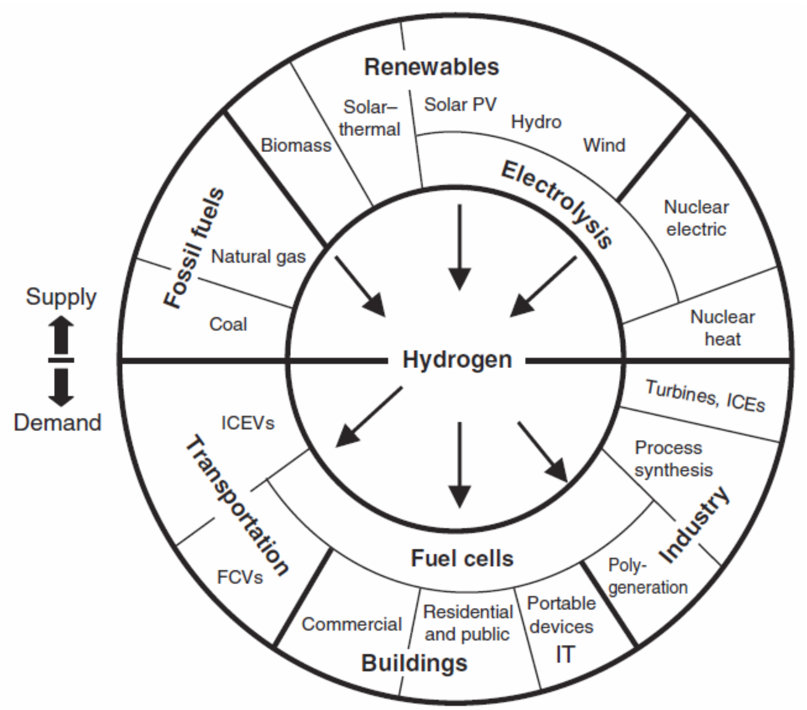

Figure 2. Hydrogen supply options and major uses [6]. PV, photovoltaic (cells); ICEs, internal combustion engines; IT, information technology; FCVs, fuel cell (electric) vehicles; ICEVs, internal-combustion-engined vehicles.

However, energy production from the renewable sources needs relatively high cost and has low efficiency and discontinuity problem. For instance, sunlight or wind energy is not continuously available. Also, the use of fossil fuels for hydrogen production causes some environmetal problems. Therefore, the storage of energy is the obvious solution to this predicament. Hydrogen, similar to electricity, is a high-quality energy carrier that can be used with a high conversion efficiency and zero or near-zero emissions of greenhouse gases and air pollutants at the point of use [7]. As an energy carrier, electricity and hydrogen are used either parallel or in place of each other (Figure 3) [3a]. It has been shown that hydrogen can be used for transportation, heating, and power generation, and therefore could replace current fuels in all their present uses [8]. However, development of improved technologies for production, storage, distribution, and consumption of hydrogen (called as hydrogen economy) is difficult since some technological challenges must be overcome. The storage of hydrogen is one of those challenges.

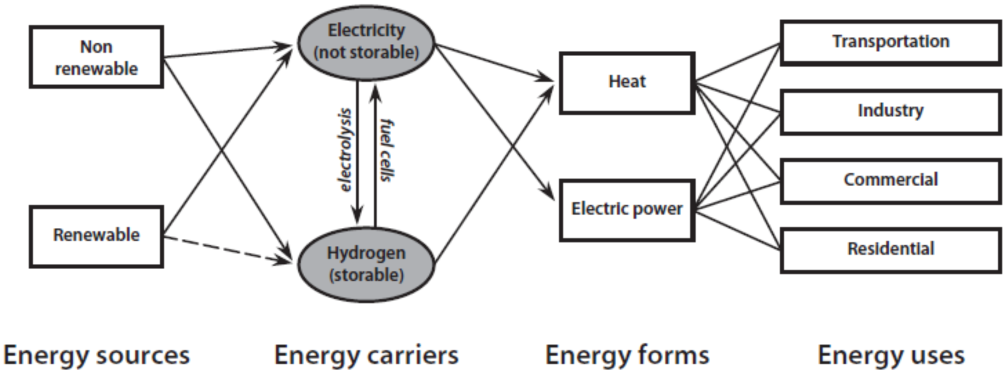

Figure 3. Hydrogen and electricity as parallel and interchangeable energy carriers [3a].

1.2. A Big Challenge in Hydrogen Economy: The Storage of Hydrogen

One of the major hurdles toward hydrogen powered society as a long-term solution for a secure energy future is the lack of effective, safe, and low-cost hydrogen-storage materials for mobile, portable, and stationary applications [1,9]. In attempt to find a convenient way to store hydrogen in vehicles, both physical storage (liquefied or compressed hydrogen) and chemical storage (absorption by metals or other materials) are being intensively investigated. In this context, various kinds of solid materials including metal/complex hydrides [10], metal nitrides and imides [11], carbon materials like carbon nanofibers and single-wall carbon nanotubes [12], TiO_2 nanotubes [13], inorganic nanostructures [14], metal-organic frameworks [15], and intermetallic hydrides [16] have been investigated for hydrogen storage to meet the 2010 targets (6 wt % and 45 g L^{-1}) and potentially meet the 2015 targets (9 wt % and 81 g L^{-1}) set by the U.S. Department of Energy (DOE) [17] since they require less space than the others. Among these solid state hydrogen storage materials, chemical hydrogen storage materials (Figure 2) have received much attention as promising candidates for fuel cell applications under ambient conditions due to their high gravimetric/volumetric hydrogen storage capacities [18].

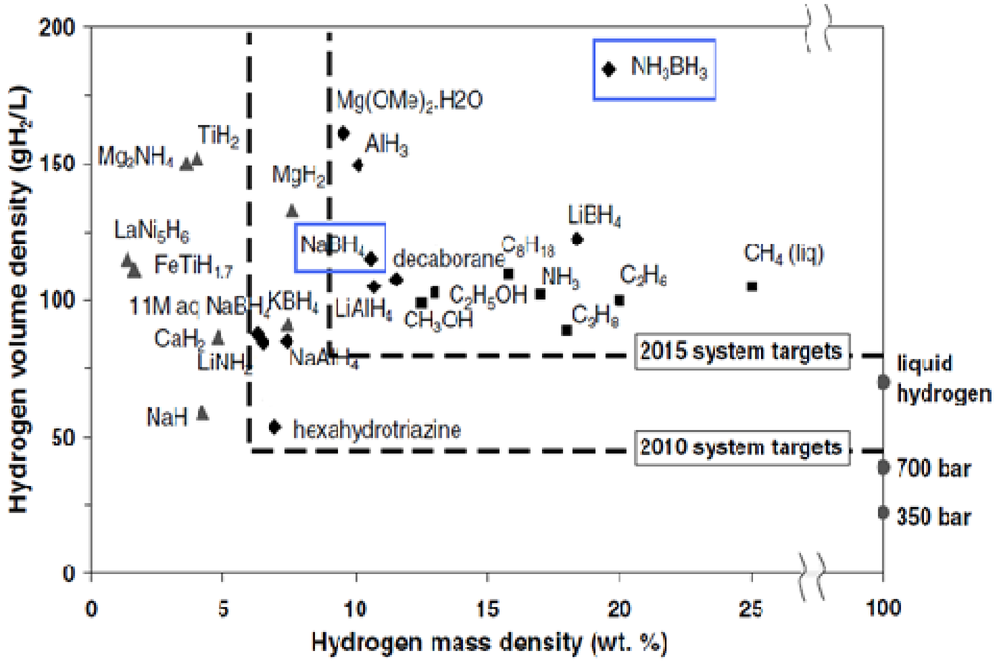

Figure 4. Plot of hydrogen weight fraction and hydrogen volume density for some representative hydrogen storage materials [19].

1.2.1. Sodium Borohydride as a Hydrogen Storage Material

Sodium borohydride ($NaBH_4$) is a well-known chemical because it is often used in organic chemistry as a reducing agent. As a hydrogen storage material, $NaBH_4$ has a 60 year-old history [20]. It was discovered in the 1940s and its as a hydrogen releasing material was remarked by the US Army and soon drew scientist's attention [21]. However, it was given up for a while from the middle of the 1960s, but since the late 1990s, it met a new interest [25a]. Hydrogen stored in $NaBH_4$ can be recovered either by thermolysis [22] or by hydrolysis [23]. Hydrogen generation from the hydrolysis of sodium borohydride, among the most promising chemical hydrides for vehicular fuel cell applications with a 10.8 wt % gravimetric hydrogen storage capacity, has been most widely investigated [24]. Although $NaBH_4$ is stable in alkaline solution, hydrogen gas is generated by following hydrolysis reaction (Eq. 1) only in the presence of a suitable catalyst, with the important advantage of producing half of the hydrogen from the water solvent [25]. By this way hydrogen gas can be safely produced for fuel cells.

$$NaBH_4(aq) + 2H_2O(l) \xrightarrow{\text{catalyst}} NaBO_2(aq) + 4H_2(g) \qquad (1)$$

The reaction can also be written as follows by considering the fact that $NaBO_2$ is always dissolved in water forming of Na^+ and $B(OH)_4^-$;

$$NaBH_4\,(aq) + 4H_2O\,(l) \xrightarrow{\text{Catalyst}} Na^+(aq) + B(OH)_4^-(aq) + 4H_2(g) \qquad (2)$$

Catalytic hydrogen generation from the hydrolysis of alkaline $NaBH_4$ solutions via Eq.1 has the following advantages [26]:

- $NaBH_4$ solutions are nonflammable and stable in air for months,
- H_2 generation only occurs in the presence of a suitable catalyst at room temperature,
- reaction products are environmentally benign,

- H_2 generation rates can be easily controlled,
- volumetric and gravimetric H_2 storage efficiencies are high,
- the reaction products can be recycled, and
- H_2 can be generated even at 0 ºC.

These properties are unique among metal hydride systems that generate H_2 by reaction with water. This hydrolysis reaction of $NaBH_4$ would occur to some extent even without a catalyst if the solution $pH < 9$. However, $NaBH_4$ solutions are typically maintained as a strongly alkaline solution by adding NaOH in order to increase shelf life of $NaBH_4$ solutions and to prevent H_2 gas from being slowly produced upon standing. Occurrence of H_2 gas generation in alkaline $NaBH_4$ solutions ($pH > 14$) only when these solutions are allowed to contact selected heterogeneous catalysts is the key feature of using this reaction to produce hydrogen. Strongly alkaline $NaBH_4$ solutions do not produce appreciable amount of H_2 without catalysts present. Since H_2 is generated only when selected catalysts contact $NaBH_4$ solution, this ensures a rapid, dependable, and controllable response to H_2 demand. Moreover, H_2 generation stops when the catalyst is separated from the alkaline $NaBH_4$ solution. No energy input is needed to generate hydrogen since the hydrolysis reaction is highly exothermic. This hydrolysis reaction of $NaBH_4$ can also be accelerated under increased temperatures [27] or by the addition of suitable metal catalysts [28] or acids [29].

Sodium metaborate ($NaBO_2$), the only byproduct of this hydrolysis reaction of alkaline $NaBH_4$, is water soluble, environmentally benign and can be utilized as a starting material in regenerating $NaBH_4$. Hydrolysis of $NaBH_4$ produces virtually no fuel cell poisons such as sulfur compounds, CO, soot, or aromatics since it is totally inorganic and does not contain sulfur. Therefore, the hydrolysis of $NaBH_4$ can be considered as safe, efficient, and easily controllable reaction than producing H_2 by other chemical methods [26]. Carrying $NaBH_4$ solutions onboard, a vehicle is far safer than carrying an equivalent amount of gasoline since aqueous $NaBH_4$ solutions cannot be easily ignited [25a].

The generated hydrogen can be directly fed to fuel cell, which is a device that produces electricity from the reaction of a reductant (fuel) with an oxidant (oxygen) in the presence of electrolyte [30]. As an example, proton exchange membrane (PEM) fuel cell device is shown in Figure 5. In PEM fuel cells [31], hydrogen entering the fuel cell is split with the help of a platinum catalyst on the anode side into electrons and protons. The protons migrate to the cathode through a polymer electrolyte membrane and the electrons are forced to travel through an external circuit generating electric power. At the cathode, protons and electrons are recombined with oxygen of the air in a platinum catalyzed process to form water as a waste product [3a].

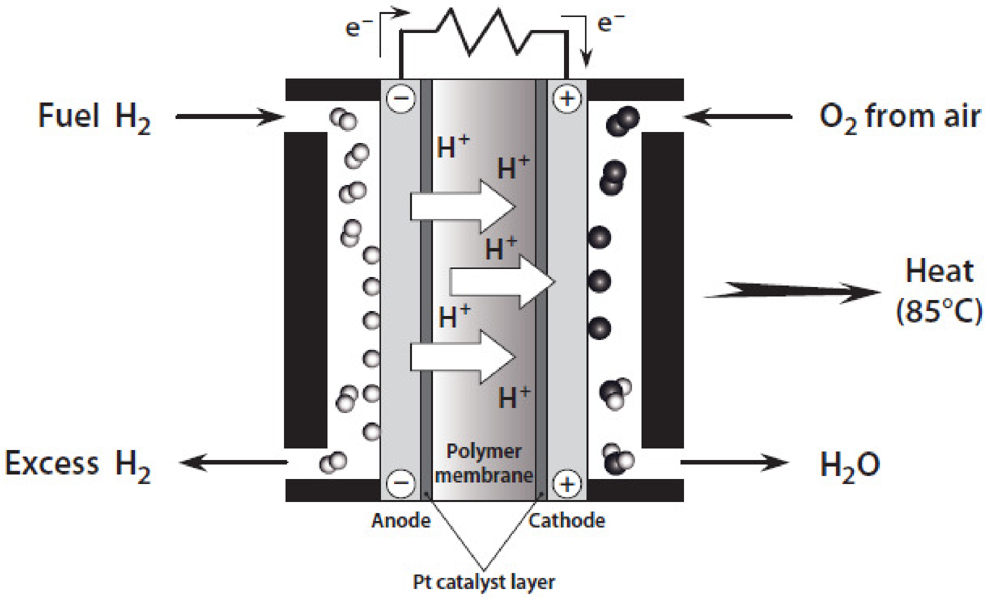

Figure 5. Proton exchange membrane (PEM) hydrogen fuel cell [3a].

1.2.2. A New Hydrogen Storage Material: Ammonia Borane

In November 2007, the US DOE published an independent report that recommended a no-go for $NaBH_4$ for on-board vehicle hydrogen storage [32]. This decision is not so surprising since the aqueous solution of $NaBH_4$ does not meet US DOE criteria in terms of storage capacity, spent fuel recycling and cost [32]. The report's conclusion is not completely negative. It consistently remarks that the improvements obtained for $NaBH_4$ can benefit ammonia borane (H_3NBH_3, AB). Actually, AB is today the most promising boron hydride for on-board hydrogen storage while $NaBH_4$ has still potential for portable applications [33].

Ammonia borane complex has attracted increasing attention as an efficient and lightweight material for hydrogen storage owing to its potential to store a significant percent of hydrogen chemically (19.6 wt % H_2) and low molecular weight (30.7 g/mol) [34]. The $H_3N\text{-}BH_3$ molecule is a typical example of an electron donor-acceptor complex. The lone pair of electrons of NH_3 interact with the empty p_z-orbital of boron in BH_3 to form a dative bond [35]. AB is a colorless and nontoxic molecular crystal at room temperature. It is water soluble and stable in air [36]. For the laboratory-scale preparation of AB, several methods including reaction of ammonium salts with lithium or sodium borohydride and direct reaction of ammonia with diborane have been developed. However, the reaction of $NaBH_4$ with ammonium formate (HCO_2NH_4) in dioxane has been found to be the most efficient way to prepare AB with high purity (> 98 %) and high yield (> 95 %) [37,84].

AB effectively releases large amounts of hydrogen either pyrolysis or hydrolysis. It has been reported that AB decomposes at around 112 °C and releases only 6.5 wt % of hydrogen. The release of more hydrogen requires higher temperatures (> 500 °C) [38]. However, formation of several volatile by-products such as borazine, cycloborazanes, polyaminoborane, and ammonia beyond 123 °C can poison the fuel cell systems [39]. Therefore, the catalytic hydrolysis of aqueous AB solution can be regarded as more practical and efficient way for the rapid release of hydrogen since the hydrolysis reaction provides 3 moles of hydrogen per mole of AB in the presence of a suitable catalyst at room temperature (Eq.3) [40].

$$H_3NBH_3(aq) + 2H_2O(l) \xrightarrow{\text{catalyst}} NH_4^+(aq) + BO_2^-(aq) + 3H_2(g) \qquad (3)$$

The reaction can also be written as follows by considering the fact that NH_4BO_2 is always dissolved in water forming NH_4^+ and $B(OH)_4^-$;

$$NH_3BH_3\,(aq) + 4H_2O\,(l) \xrightarrow{\text{Catalyst}} NH_4^+(aq) + B(OH)_4^-(aq) + 3H_2(g) \qquad (4)$$

The hydrolysis of AB has the following advantages [41,17a,42b]: (i) AB has high solubility in water (33.6 g/ 100 g water), (ii) AB is highly stable in aqueous solution with respect to the self-hydrolysis and therefore, there is no need to stabilize the solution by the addition of any base, (iii) the hydrolysis reaction occurs only in the presence of a suitable catalyst at room temperature, (iv) the hydrolysis reaction is exothermic. In order to accelerate the hydrogen release from aqueous AB solution acids [42] or metal catalyst [43] can be employed.

1.2.3. The Catalysts Tested for the Hydrolysis of Sodium Borohydride and Ammonia Borane

So far, various kinds of catalysts have been used to catalyze the hydrolysis reactions of $NaBH_4$ and H_3NBH_3. For the hydrolysis of $NaBH_4$; ruthenium [25a], $Pt/LiCoO_2$ [44], carbon supported platinum [45], $PtRu/LiCoO_2$ [46], Ru/IRA-400 [47], nickel [48], electrodeposited Co and Co-P [49], $Co/\gamma\text{-}Al_2O_3$ [50], Co-B [51], Pt/C [52], nickel-cobalt-boride [53], Co-Mn-B nanocomposite [54], cobalt-boron/nickel foam [55], $Ru/LiCoO_2$ [56], cobalt-tungsten-boron/nickel foam [57], Co/C [58], electrolessly deposited Co-P [59], $Ru/\gamma\text{-}Al_2O_3$ [60], Co-B/MWCN [61], Ru-promoted sulphated zirconia [62], Ni-Ru nanocomposite [63], fluorinated cobalt [64], PtPd-carbon nanotubes [65], aluminum chloride [66], acetic acid [67], Co-Cr-B [68], porous Fe-Co-B/Ni foam [69], Ru/Graphite [70], clay-supported Co-B [71], Co-Ni-B [72], attapulgite CoB [73], Co-Cu-B [74], Pd/C [75], Ni_xB [76], Co-powder [77], Ru/IR-120 [78], BMR07 (Ni based) [79], Ru/C [80], Ru-Pd-Pt [81], mono- and di-carboxylic acids [82], and $(Ni_{3.6}Co_{0.7}Mn_{0.4}Al_{0.3})_{1.15}$ hydride electrodes [83] have been tested as catalysts.

For the hydrolysis of H_3NBH_3; $RuCl_3$, $PdCl_2$, and $CoCl_2$ [84], non noble metals supported on γ-Al_2O_3, carbon, and SiO_2 [85], solid acid catalysts [42b], K_2PtCl_6 [86], $Ni_{1-x}Pt_x$ hollow spheres [87], Ru/C [88], colloidal Rh(0), Ir(0), and Co(0) catalysts [89], Cu@Cu_2O core shell catalysts [90], hollow Ni-SiO_2 nanosphere [91], Pt- and Ni-based alloys [92], Fe(0) [93], magnetically recyclable Fe-Ni alloy [94], cobalt(0) [95], water/air-stable Ni [96], Pt_xNi_{1-x} nanoparticles [97], palladium(0) [98], cobalt-molybdenum-boron/nickel foam [99], hollow Co-B nanospindles [100], nanoparticle-assembled Co-B thin film [101], bimetallic Au-Ni nanoparticles embedded in SiO_2 nanospheres [102], Cu/Co_3O_4 [103], electroless Co-Ni-P/Pd-TiO_2 [104], Pd-PVB-TiO_2 [105], and Co-SiO_2 nanosphere [106] have been tested as catalysts.

As the catalytic activity in the heterogeneous catalysis is directly related to the particle size and dispersion degree of the catalyst, the use of small size and highly dispersed particles can make the catalysts contact with the reactant sufficiently, increase the reaction rate and decrease the amount of the catalyst used [107]. Thus, the use of metal nanoclusters with controllable sizes and large surface areas provides a potential route to the preparation of highly active catalysts. For this purpose, some metal(0) nanoclusters including acetate-stabilized ruthenium(0) nanoclusters [108], hydrogenphosphate- or polymer-stabilized nickel(0) [109], ruthenium(0) and palladium(0) [110] nanoclusters have been recently prepared and tested as a catalyst in the hydrolysis of both $NaBH_4$ and H_3NBH_3 by our group.

The aim of this study is to develop efficient, reusable, and economical metal catalysts to further improve the kinetic and thermodynamic properties of the hydrolysis reactions of sodium borohydride ($NaBH_4$) and ammonia borane (H_3NBH_3) under moderate conditions.

CHAPTER 2

TRANSITION METAL NANOCLUSTERS

2.1. General Introduction and Key Definitions

Transition metal nanoclusters can be defined as metal particles with a diameter in the 1-10 nm range [111]. They have received great attention in recent years due to their unique properties, that result from the fact that their properties lie somewhere between those of bulk and single-particle species [112]. Transition metal nanoclusters are smaller in size, isolable and redissolvable (bottleable), soluble in organic solvents, compositionally well-defined, and reproducible [113]. They also offer the possibility of controlling both the nanocluster size and the surface ligands in a quantitative and modifiable way. They have found many applications in such diverse fields of science as homogeneous and heterogeneous catalysts [114], fuel cell catalysts [30], electronics [115], optics [116], magnetism [117], material sciences [118], and even in biological and medical sciences [119].

Since a large percentage of a nanocluster's metal atoms lie on the surface, and that surface atoms do not necessarily order themselves in the same way that those in the bulk do, metal nanoclusters have unique chemical and physical properties [112a]. Moreover, the electrons in a nanocluster are confined to spaces that can be as small as a few atom-widths across, giving rise to quantum size effects [120]. The electronic situation in bulk metals is characterized by the existence of energy bands. They result from the combination of an infinite number of energetically very similar orbitals. The valence band contains the relevant valence electrons, in case of transition metals these are usually s- and d- electrons. The conduction band of metals overlaps to some extent with the valence band and so becomes partially occupied with electrons. These electrons are finally responsible for the electric conductivity of metals. In contrast to the electrons in a filled band, those in the conduction band are fully mobile and make conductivity possible. In semiconductors, valence and conduction bands are separated by a material-specific energy gap, which is too large in insulators to be surmounted under reasonable conditions. If a metal particle is continuously reduced in size, the overlap of valence band and conduction band is some when disappearing, resulting in a situation to be compared with that in a semiconductor. Further reduction will end up in a situation where the bands turn into more or less discrete energy levels. At this step, the bulk properties of the particles disappear to be substituted to that of a 'quantum dot', following quantum mechanical rules. Finally, the development ends up in the formation of a typical molecular situation (Figure 6) [121].

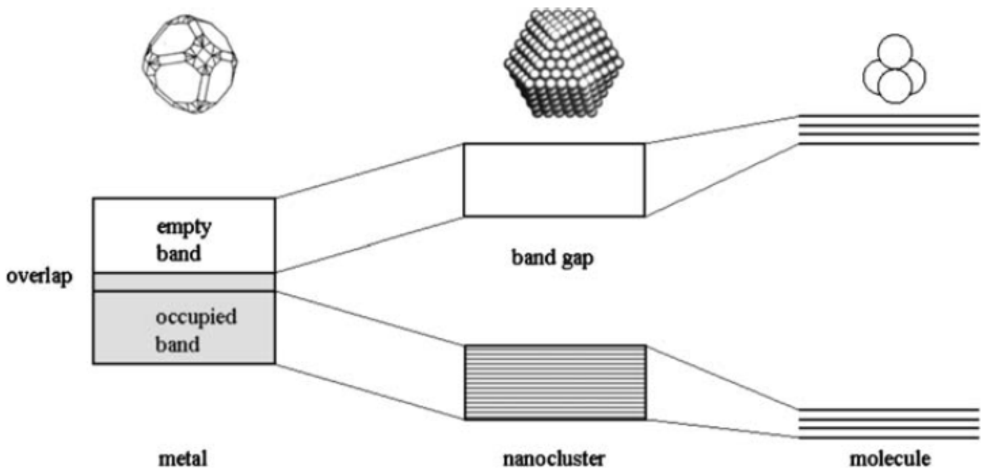

Figure 6. Formation of discrete electronic energy levels on the way from bulk to molecule [120,121].

2.2. Preparation of Transition Metal Nanoclusters

There are two general approaches for the production of metal nanoclusters, namely the top-down (physical method) and the bottom-up (chemical method) approaches. The top-down approach relies on breaking down of the bulk material into nanosized material with subsequent stabilization by appropriate stabilizers [122], while the bottom-up approach works on the principle of building nanoclusters by generating individual atoms that group to form a stable nucleus that are then stabilized. For this reason, it is very difficult to obtain monodispersed particles by the top-down approach, whereas this is the hallmark of the bottom-up approach [123].

The bottom-up methods of wet chemical nanocluster preparation rely basically on the following methods:

- chemical reduction of metal salts [124] including electrochemical pathways
- thermolysis [125], including photolytic [126], radiolytic [127], and sonochemical [128] pathways
- controlled decomposition of pre-formed metastable organometallics.

The chemical reduction of transition metal salts in the presence of stabilizing agents to generate zerovalent metal nanoclusters in aqueous or organic media was first published in 1857 by Faraday on the preparation of gold nanoparticles [129]. This method is the most widely used one to prepare the metal nanoclusters and includes the reduction of positively charged metal atoms to nanosized metal particles as simple ions or as metal complex centers in solution [130]. The current general understanding is that metals salts are reduced to give zerovalent metal atoms in the embryonic stage of nucleation, which can collide in solution with other metal ions, metal atoms, or clusters, to form an irreversible seed of metal nucleus. The size of the resulting metal colloid is determined by the relative rates of nucleation and particle growth (Figure 7) [123].

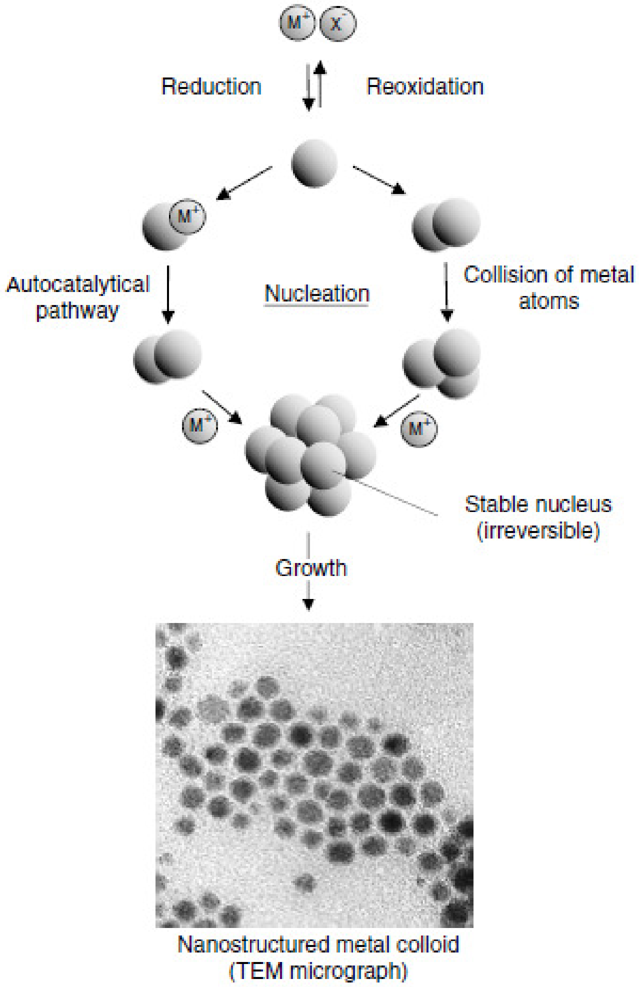

Figure 7. Formation of nanostructured metal colloids via the salt reduction method [123].

Many organometallic compounds are thermally decomposed to respective zerovalent element under mild conditions. Some Pd and Pt organosols were obtained with broad size distribution by the thermolysis of precursors such as palladium acetate, palladium acetylacetonate, or platinum halides in the presence of high boiling point-solvents without using stabilizing agents [131]. Photochemical synthesis of metal nanoclusters can be accomplished either by the reduction of transition metal salt by radiolytically produced reducing agents or degradation of an organometallic complex by radiolysis [132]. Additionally, some zerovalent organometallic complexes can be converted into colloidal suspension of metals by reduction or ligand displacement. For example, $Pt(dba)_2$ and $Pd(dba)_2$ were reduced to nanoparticle organosols with carbon monoxide in the presence of cellulose acetate or cellulose nitrate in THF [133].

2.3. Stabilization of Transition Metal Nanoclusters

Since the surface areas of metal nanoclusters are enormous relative to their masses, they have an excess surface free energy comparable to the lattice energy, making them only kinetically stable and thermodynamically unstable against agglomeration to the bulk. Protective agents are therefore essential in order to be able to outweigh the attractive van der Waals forces by the repulsive electrostatic and steric forces between adsorbed ions and associated counterions. To achieve sufficient interparticle separation, it can be helpful to use sterically demanding substituents. In addition, the solubility of the metal in organic or aqueous phases can be tailored by introducing and varying lipo- and hydrophilic end groups [121].

Based on the type of protecting shell, the mode of stabilization can be classified as follows:

- electrostatic [134]
- steric (using polymers) [135]
- ligand (P, N, S donor) [136]
- electrosteric [137]
- solvent (such as THF [138] and propylene carbonate [139])

Electrostatic stabilization results from the electrical double layer formed by the anions and cations interacting with the metallic particle surface. This results in coulombic repulsion between particles. If the electric potential associated with the double layer is sufficiently high, electrostatic repulsion will prevent the particles from agglomeration. The level of stabilization can be influenced by altering the total charge on the metal cluster surface. The polarity of the solvent affects the degree of particle dispersion [121].

Steric stabilization is brought about by large organic molecules such as poly(N-vinyl-2-pyrrolidone) (PVP) that are firmly adsorbed on the surface of the metal nanoclusters [140]. Polymeric stabilizers establish many weak bonds with the nanoclusters' surface rather than forming less strong bonds at specific sites of the nanoclusters [121].

Electrosteric (electrostatic as well as steric) stabilization has proved to be a very reliable means of preventing particle agglomeration. The key feature is to adsorb bulky molecules such as polymers or surfactants at the surface of the particles. These sterically demanding surface-active protecting shields coordinate strongly to the metal nanoclusters' surface and at the same time are very well solvated in the respective medium (organic phase or water). This is the main advantage of using tetra(octyl)ammonium halides as the protective agent. The halide anions of N-(octyl)$_4$X have been shown to bind to the metal surface through the negatively charged chloride while the long alkyl chains shield the metallic core like an umbrella (Figure 8) [121].

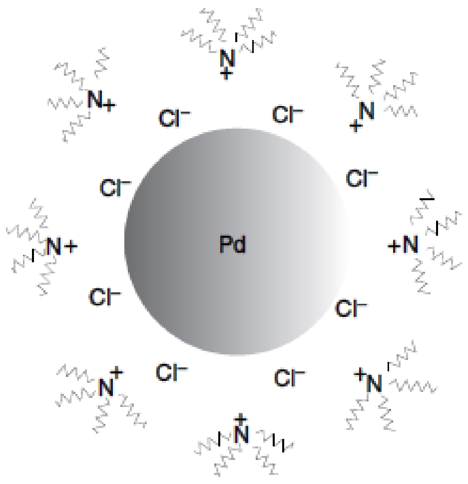

Figure 8. Electrosteric stabilization of a Pd nanoparticle by the tetra(octyl)ammonium halide stabilizer [121].

2.4. Transition Metal Nanoclusters and Catalysis

2.4.1. General Principles in Catalysis

A catalyst is defined as a substance that increases the reaction rate, without being consumed in the process. The phenomenon occurring when a catalyst acts in called catalysis. Since the catalyst is not consumed by significant amounts in the process, each catalyst molecule can participate in many consecutive cycles, so we need only a small amount of catalyst relative to substrate. There are many different types of catalysts ranging from proton, through Lewis acids, organometallic complexes, organic and inorganic polymers, all the way to enzymes. However, the catalysis can be divided into three categories as homogeneous catalysis, heterogeneous catalysis, and biocatalysis to simplify things [141].

Catalysts can be classified as homogeneous or heterogeneous depending upon the existence of catalyst in the same phase as the substrate or not. In homogeneous catalysis, the catalyst is in the same phase as the reactants and products. In the classic case, the reactant molecules and the catalyst are reacted in a solvent. The transesterification of fatty acid triglycerides with methanol is catalyzed by hydroxide ions can be given as an example. Many transition metal atoms that are stabilized by ligands can be considered as homogeneous catalysts. The ligands are generally organic molecules that attach to the metal atoms. The properties of the catalysts can be varied by changing the ligands. Heterogeneous catalysis includes all the cases where the catalyst and the substrate are in different phases. In this case, the reactant molecules diffuse to the catalyst surface and adsorb onto it via chemical bond formation. The products desorb from the surface and diffuse away after reaction. The surface area of the catalyst is very crucial for solid heterogeneous catalysts since it determines the availability of catalytically active sites [141]. Due to their easy separation from reaction products, reusability, stability, low-cost, and low-toxicity [142], the majority of industrial processes involve heterogeneous catalysts [143]. Biocatalysis is a quite special case, somewhere between homogeneous and heterogeneous catalysis. In most cases, the biocatalyst is an enzyme - a complex protein that catalyzes the reactions in living cells [144]. An enzyme typically completes 1000 catalytic cycles in one second. Therefore, it is very fast and efficient compared to conventional homogeneous and heterogeneous catalysts.

Catalysts increase the reaction rate by providing an alternative mechanism that involves a different transition state with a lower activation energy. They increase the frequency of collisions between reactants and alter the orientation of reactants so that more collisions are effective. A larger proportion of the collisions now have enough energy to overcome the activation energy for the reaction and the rate of reaction increases. As a result, the activation energy for a catalyzed reaction is smaller than for the same uncatalyzed reaction (Figure 9). Therefore, reactions blocked or slowed by a kinetic barrier can be enabled by catalysts. Since the catalytic reaction has many steps due to the many ways to product side and thus there are many rate constants (k_{app}) that are affected by temperature, this type of activation energy is called as apparent activation energy ($Ea^{apparent}$). The $Ea^{apparent}$ is the combination of these rate constants. Since the catalysts have the same effect on the forward and back reactions, they do not change the extent of a reaction, and thus equilibrium.

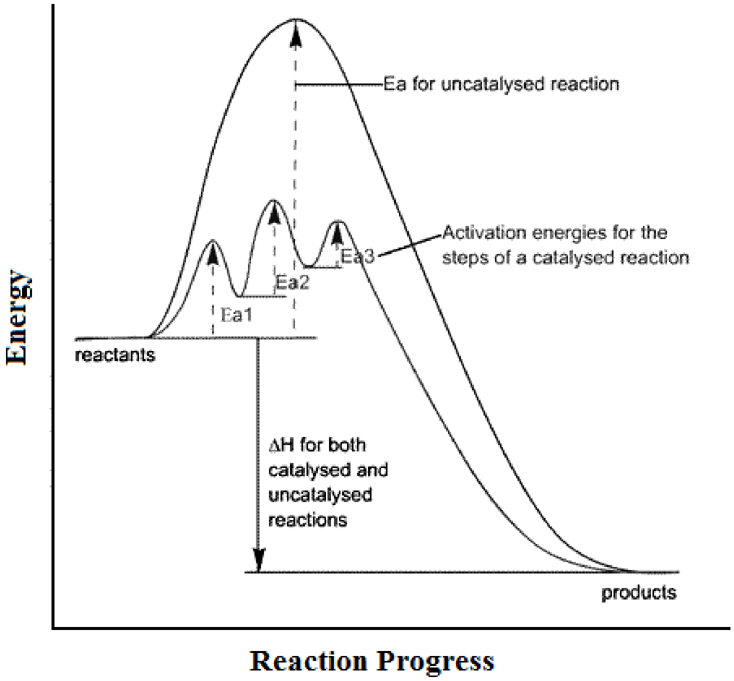

Figure 9. Potential energy diagram for an exothermic reaction under both catalyzed and uncatalyzed conditions [145].

2.4.2. Key Definitions in Catalysis

The catalyst turnover number (TON) and the turnover frequency (TOF) are two important quantities used to compare the catalyst efficiency. Their definitions vary slightly among the three catalysis fields. As a general definition, total turnover number indicates the number of total catalytic cycles before deactivation of the active catalyst in a given process and is equal to the number of moles of product per mole of catalyst. Turnover frequency is defined as the catalytic turnover number per time (number of moles of product per mole of catalyst per unit time). Selectivity is another important parameter that shoul be taken into account to evaluate the performance of any catalyst. It can be defined as acceleration of one of the competing reactions and/or selection of one reagent out of a complex mixture. A selective catalyst provides a high proportion of the desired product with minimum amount of the side products [141].

2.4.3. Transition Metal Nanoclusters as Catalysts

As pointed out earlier, there is a considerable change in the intrinsic properties of materials by going from macroscale to nanoscale. The increasing catalytic activity of the heterogeneous catalysts with the reduction of particle size is one of the most important example of these changes since the catalytic activity of heterogeneous catalysts is directly related to the their surface areas [146]. Particularly, metal nanoclusters show unusual surface morphologies and possess more reactive surfaces. Therefore, they have been involved in different applications in catalysis due to their large surface areas. Having many atoms lie on the surface provides a good ‘atom economy’ in surface-gas, surface-liquid, and surface-solid reactions [123].

Klabunde and co-workers (Figure 10) have determined the percentage of surface atoms on spherical iron(0) nanoclusters depending on their size. The number of the surface atoms increases with the decreasing particle size of the particles. It makes the metal nanoclusters more active catalysts compared to their bulk counterparts since the surface atoms are the active centers in catalytic processes.

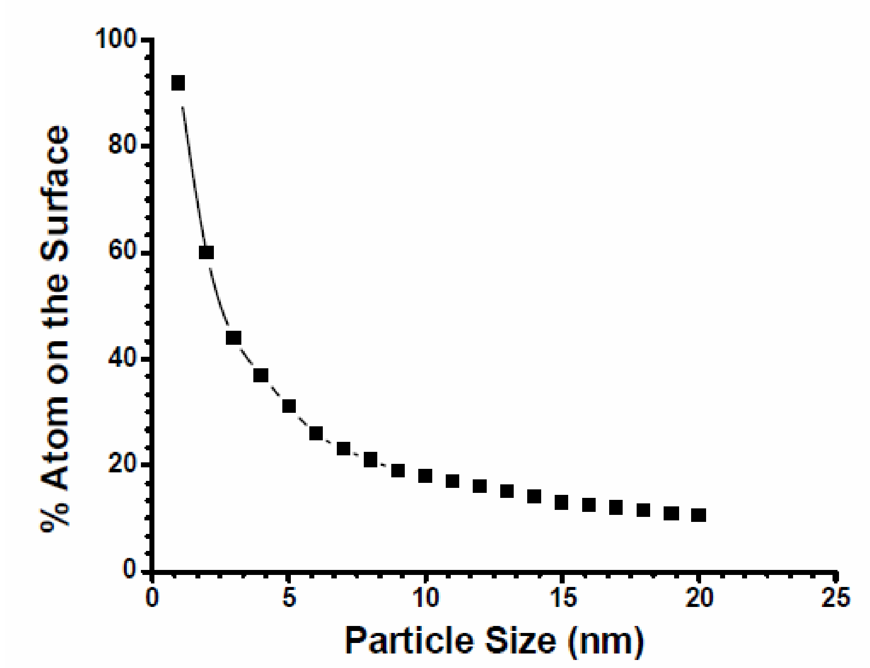

Figure 10. The change in percentage of surface iron atoms depending on the size of iron(0) nanoclusters [147].

Transition metal nanoclusters have been found to be more active catalysts than their bulk counterparts in various reactions like spanning hydrogenations [148], enantioselective hydrogenations [149], hydropyrolysis and hydrogenolysis [150], hydrosilylations [151], oxidative acetoxylation [152], oxidation of CO and CO/H_2 [153], [3+2] cycloaddition reactions [154], and couplings like McMurry [155], Suzuki [156], and Heck [157], as reported in the literature.

2.5. The Motivation of the Dissertation

The preparation of transition metal nanoclusters with controllable sizes and size distributions is of scientific importance due to their various applications in different fields including catalysis [158]. However, the agglomeration of metal nanoclusters to the bulk material despite of using the best stabilizing agents [159] is one of the most important problems that should be overcome because their agglomeration into the bulk material leads to a significant loss in activity and catalyst lifetime in their catalytic applications. Therefore, the exploitation of microporous and mesoporous materials with ordered porous structures as the hosts to encapsulate metal nanoclusters, and thus to prevent aggregation, has attracted great interest in catalysis because the pore size limitation of these host materials could hinder the growth of guest metal nanoclusters, and therefore, leads to an enhancement in the proportion of the catalytically active surface atoms. Additionally, metal nanoclusters encapsulated in the cavities of zeolite [160] could provide kinetic control for the catalytic processes.

In this context, zeolite-Y (from FAU framework) can be regarded as the suitable host material for the preparation of metal nanoclusters among the huge number of microporous and mesoporous materials. The FAU structure consists of sodalite cages (α-cage) and hexagonal prisms, connected in such a way that they create an open three dimensional pore system with large supercages (β-cage) (Figure 11) [161]. So far, the preparation of nanoparticles or clusters of noble metals such as Pd, Pt, and Rh within faujasite zeolites have been intensively studied [162]. The most convenient procedure to synthesize the metal nanoclusters encapsulated in the zeolite is to introduce metal cations into the zeolite by the ion-exchange followed by the reduction of the ion-exchanged zeolite with gaseous H_2 or CO [163]. When this procedure is applied to the synthesis of nonnoble transition metals such as Fe and Co, the reduction of metal cationic precursors inside the cages or pores of zeolite becomes difficult at moderate temperatures of less than 500 ºC [164]. However, higher reduction temperatures may be destructive to the zeolite framework or may lead to the migration of a large part of metals out of the zeolite cavities [165]. This difficulty in the reduction of the nonnoble metal cations can be explained by the strong interaction between the cationic precursor and the anionic zeolite framework. Therefore, the present method to generate the zeolite confined metal nanoclusters in such a way that hinders the sintering of nanoclusters and migration of them out of zeolite structure should be improved as the most important and challenging issue in this research area. The use of other reductants, like sodium borohydride, stronger than H_2, to reduce the nonnoble metal ions exchanged in the faujasite zeolite can be considered as an alternative to the existing method since the borohydride reduction of some nonnoble metals in solution is well studied [166].

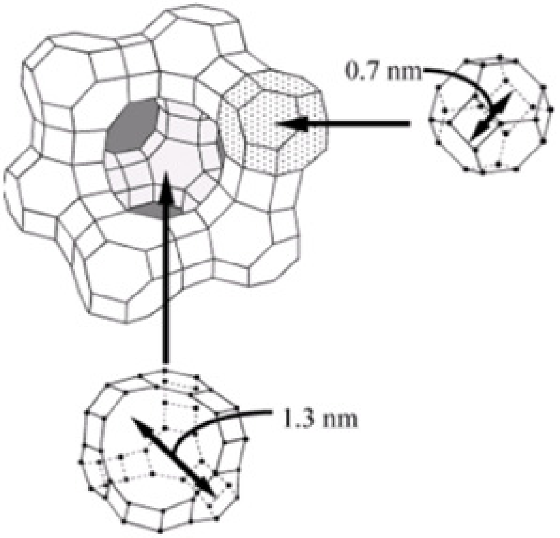

Figure 11. The framework structure and the cavities of zeolite-Y.

The development of efficient, economical, stable, long-lived, and reusable metal catalysts to futher improve the kinetic and thermodynamic properties of the hydrolysis reactions given in Eq. (1) and (3) under moderate conditions is very important for the practical applications [167]. Therefore, in the scope of this dissertation, we present our detailed study on the preparation and characterization of zeolite confined cobalt(0) nanoclusters and their use as catalyst for hydrogen generation from the hydrolysis of $NaBH_4$ and H_3NBH_3.

2.6. The Composition and the Structure of Zeolites

Zeolites are naturally occurring minerals found in volcanic rocks where they have been formed by hydrothermal processes. The term ‘zeolite’ introduced in 1756 by the Swedish mineralogist Cronstedt who gave the name according to the observation of the large amount of water they release upon heating. ‘Zeolite’ is indeed derived from the Greek words ‘zein’ (to boil) and ‘lithos’ (stone) [168].

Zeolites are microporous crystalline aluminosilicates, composed of TO_4 tetrahedra (T = Si, Al) with oxygen atoms connecting neighboring tetrahedra. For a completely siliceous structure, combination of TO_4 (T = Si) units in this fashion leads to silica (SiO_2), which is an uncharged solid. Upon incorporation of Al into the silica framework, the +3 charge on the Al makes the framework negatively charged, and requires the presence of extraframework cations (inorganic and organic cations can satisfy this requirement) within the structure to keep the overall framework neutral (Figure 12). The zeolite composition can be best described as having three components [169]:

$$\underset{\text{extraframework cations}}{M^{m+}_{n/m}} \quad \bullet \quad \underset{\text{framework}}{[Si_{1-n}Al_nO_2]} \quad \bullet \quad \underset{\text{sorbed phase}}{nH_2O}$$

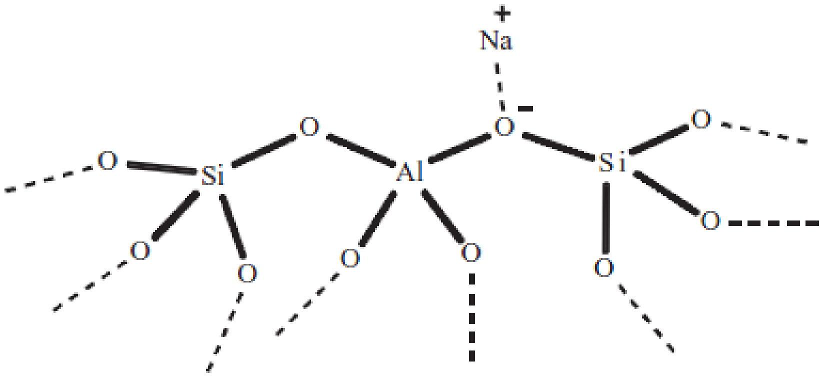

Figure 12. Compensation of a negative framework charge by a Na^+ cation [168].

The extraframework cations are ion exchangeable and give rise to the rich ion exchange chemistry of these materials. The novelty of zeolites stems from their microporosity and is a result of the topology of the framework. The amount of Al within the framework can vary over a wide range, with Si/Al = 1 to infinite, the completely siliceous form being polymorphs of SiO_2. Lowenstein proposed that the lower limit of Si/Al = 1 of a zeolite framework arises because placement of adjacent AlO_4^- tetrahedra is not favored because of electrostatic repulsions between the negative charges. The framework composition depends on the synthesis conditions. Postsynthesis modifications that insert Si or Al into the framework have also been developed. As the Si/Al ratio of the framework increases, the hydrothermal stability as well as the hydrophobicity increases [169].

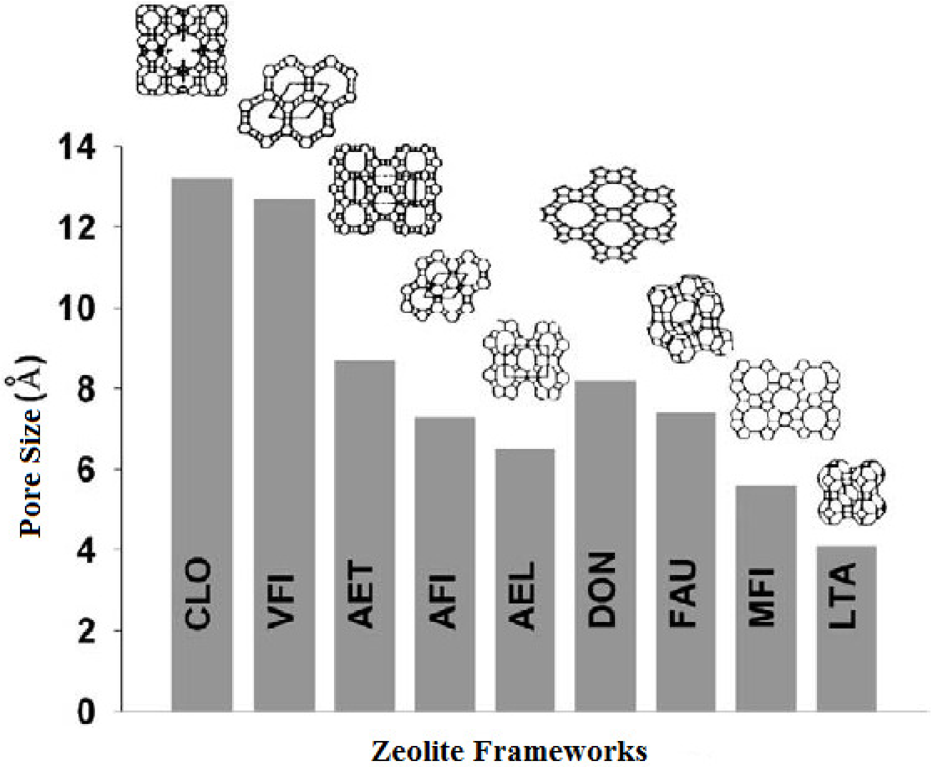

Figure 13. Comparison of pore sizes of different framework structures [169].

Typically, in as-synthesized zeolites, water present during synthesis occupies the internal voids of the zeolite. The sorbed phase and organic non-framework cations can be removed by thermal treatment/oxidation, making the intracrystalline space available. The framework projections and the ring sizes for commonly studied frameworks are shown in Figure 13.

Their unique properties (microporosity, high surface area, acid-base character, shape) have made zeolites a material of choice in a great number of applications. Zeolites are intensively used in gas separation due to their ability to adsorb selectively a large variety of molecules and are also known as molecular sieves. Furthermore, these materials are also used as ion exchangers (water softeners) and catalysts in petrochemistry (Figure 14).

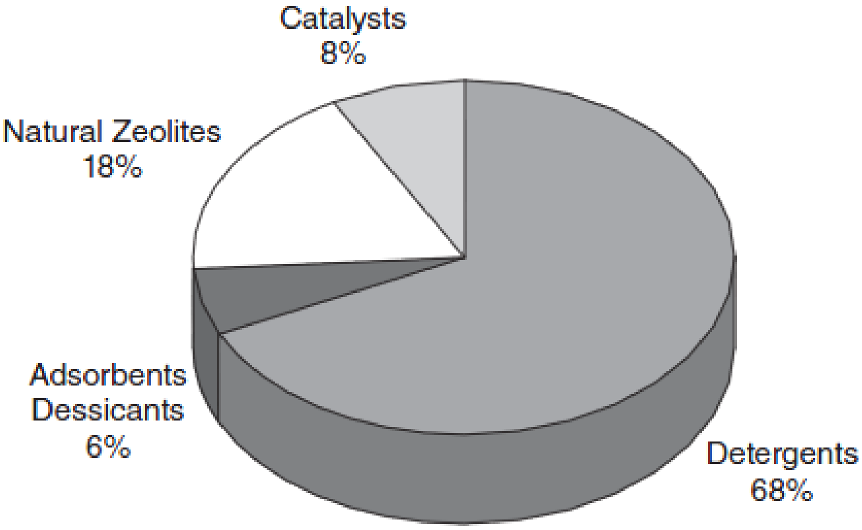

Figure 14. Main uses of zeolites [168].

Zeolite structure types are commonly described in terms of identifiable structural units that are often referred to as secondary building units (SBUs) within the frameworks. It is helpful to describe the SBUs and frameworks in terms of rings made up of alternating tetrahedral cations and oxygens. These are named in terms of the number of cations in the ring, so for instance, a six-membered ring (6MR) contains six cations and six oxygens, a twelve-membered ring (12MR) contains twelve cations and so on. Other SBUs are most easily described as being built up of two rings linked together as a prism, so two four-membered rings linked together in this way are known as double four-membered ring, D4R, two 6MRs as a D6R, etc. (Figure 15) [170].

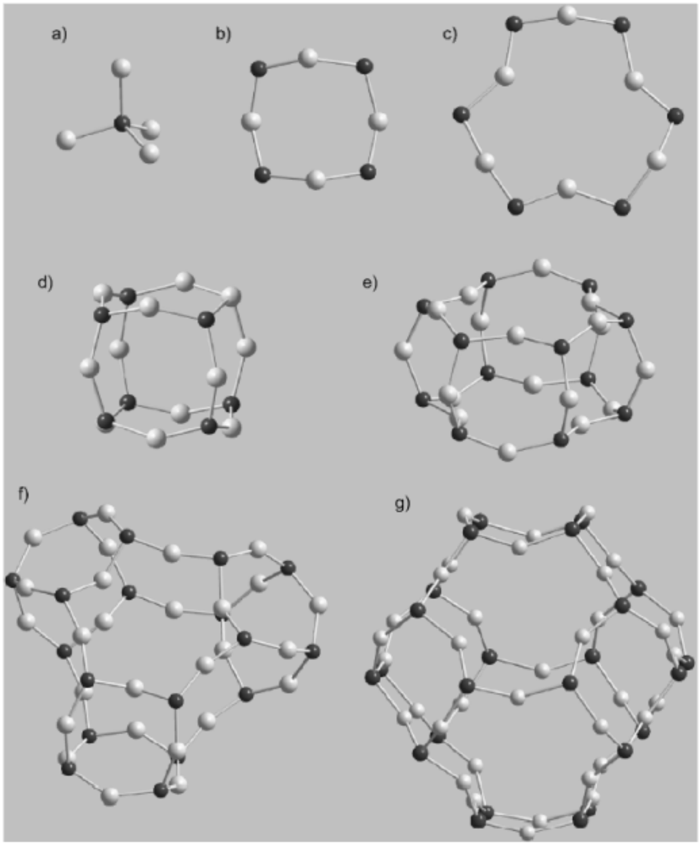

Figure 15. Building units commonly found in zeolite frameworks. a) tetrahedral primary building unit, b) 4-membered ring (4MR), c) 6-membered ring (6MR), d) double 4-membred ring (D4R), e) double 6-membered ring (D6R), f) cancrinite cage, g) sodalite cage (β-cage) [170].

Another convenient shorthand way to describe cages in the framework structure is to write them in terms of the rings that make up the faces of the cage. For example, a D6R is described [$4^6 6^2$] and a sodalite cage [$4^6 6^8$] (Figure 16).

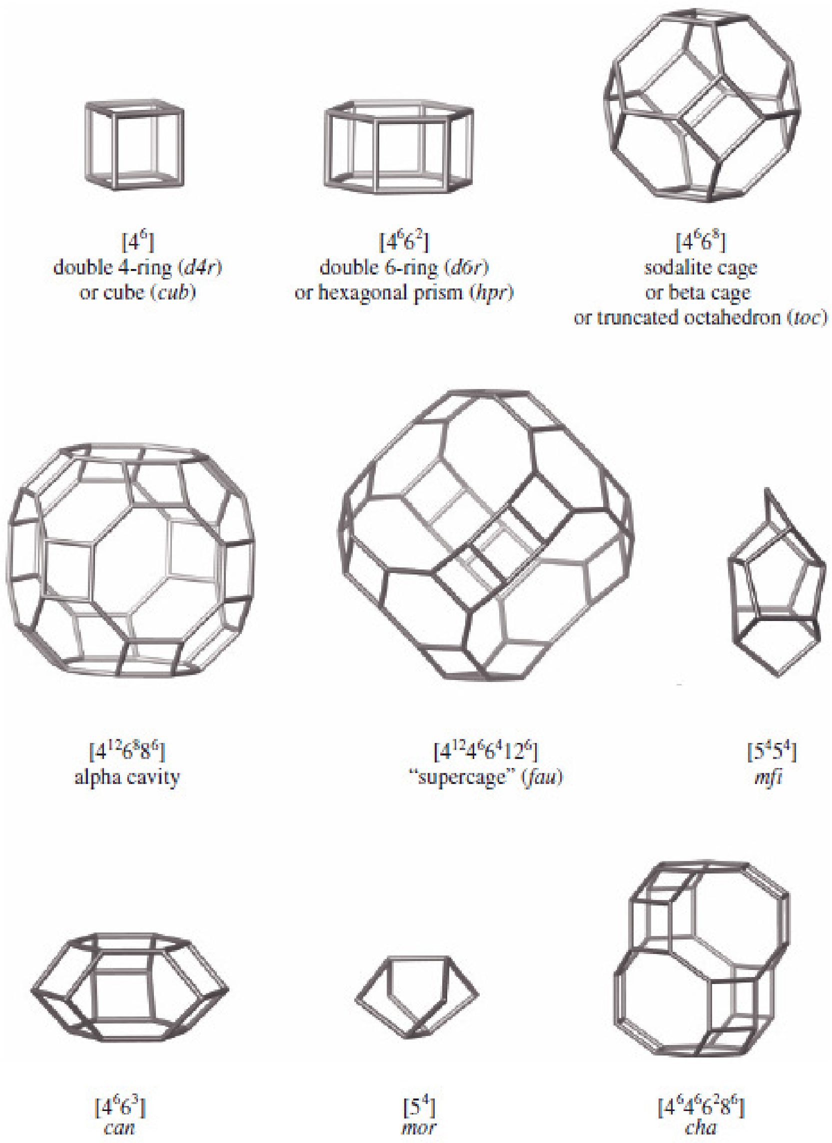

Figure 16. Some examples of polyhedral building units with their corresponding pore symbols and common names. The nodes are tetrahedrally coordinated atoms such as Si or Al. Bridging oxygen atoms have been left out for clarity [171].

CHAPTER 3

EXPERIMENTAL

3.1. Materials

Cobalt (II) nitrate hexahydrate ($Co(NO_3)_2.6H_2O$, 98+ %), sodium borohydride ($NaBH_4$, 99 %), sodium Zeolite-Y (Si/Al=2.5), borane-ammonia complex (H_3NBH_3, AB, > 97 %), and sodium hydroxide were purchased from Sigma-Aldrich. All chemicals were used as received. Deionized water was distilled by water purification system (Milli-Q system). All glassware and Teflon coated magnetic stir bars were cleaned with acetone, followed by copious rinsing with distilled water before drying in an oven at 150 ^{0}C.

3.2. Characterization

The cobalt content of the samples was determined by ICP-OES (inductively coupled plasma optical emission spectroscopy) using Leeman, Direct Reading Echelle after each sample was completely dissolved in a mixture of HNO_3/HCl (1/3 ratio). Powder X-ray diffraction (XRD) patterns of the samples were recorded with a Rigaku X-ray diffractometer using Cu Kα radiation (wavelength 1.5406 Å, 30 kV, 15 mA). Scanning electron microscope (SEM) images were measured using a JEOL JSM-5310LV at 15 kV and 33 Pa in a low-vacuum mode without metal coating by sticking the powder samples on SEM sample holder. High resolution transmission electron microscopy (HRTEM) analysis was performed on a JEM-2010F microscope

(JEOL) operating at 200 kV. A small amount of powder sample was placed on the copper grid of the transmission electron microscope. Samples were examined at magnification between 100 and 400K. The elemental analyses of the powder samples were recorded during the SEM analyses with an energy dispersive X-ray (EDX) analyzer (KEVEX Delta series) mounted on the Hitachi S-800 modulated to JEM-2010F microscope. The XPS analyses of the samples were performed on a Physical Electronics 5800 spectrometer equipped with a hemispherical analyzer and using monochromatic Al Kα radiation (1486.6 eV, the X-ray tube working at 15 kV, 350 W and pass energy of 23.5 keV). Diffuse reflectance UV-Vis spectra of the samples were recorded on a Cary 5000 (Varian) UV-Vis spectrophotometer, in the analyses of the all samples the background correction was done by using $BaSO_4$ as a reference sample with zero reflectance. The Raman spectra of the powder samples were recorded on Bruker RFS-100/S series Raman spectrometer equipped with Nd-YAG laser at 1064 nm using the FT-Raman technique. The nitrogen adsorption-desorption experiments were carried out at 77 K using a NOVA 3000 series instrument (Quantachrome Instruments). The powder samples were outgassed under vacuum at 573 K for 3 h before the adsorption of nitrogen. ^{11}B-NMR spectra were recorded on a Bruker Avance DPX 400 MHz spectrometer with an operating frequency of 128.15 MHz for ^{11}B.

3.3. The Preparation and the Catalytic Activity of Zeolite Confined Cobalt(0) Nanoclusters in the Hydrolysis of Sodium Borohydride in Aqueous Medium

3.3.1. Preparation of the Cobalt(II)-Exchanged Zeolite-Y (Co^{2+}-Y)

The sodium form of Zeolite-Y (1.0 g) was added to a solution of $Co(NO_3)_2 \cdot 6H_2O$ in 100 mL H_2O in a 250 mL round bottom flask. The concentration of the aqueous solution was adjusted to control the cobalt content in the sample. This mixture was stirred for three days at room temperature until the supernatant solution became colorless indicating the completion of ion-exchange. The sample was then filtered, washed thoroughly with deionized water (3x20 mL), and dried in oven at 80 ^{0}C for 6 h.

3.3.2. In Situ Preparation of Zeolite Confined Cobalt(0) Nanoclusters and Their Catalytic Activities in the Hydrolysis of Sodium Borohydride

The zeolite confined cobalt(0) nanoclusters were generated in situ from the reduction of the Co^{2+}-exchanged Zeolite-Y with sodium borohydride and their catalytic activity was determined by measuring hydrogen generation in the hydrolysis of sodium borohydride in aqueous medium. Before starting the formation of cobalt(0) nanoclusters and their catalytic activity test, a jacketed reaction flask (75 mL) containing a Teflon-coated stir bar was placed on a magnetic stirrer (Heidolph MR-301) and thermostated to 25.0 ± 0.1 ^{0}C by circulating water through its jacket from a constant temperature bath. Then, a graduated glass tube filled with water was connected to the reaction flask to measure the volume of the hydrogen gas to be evolved from the reaction (Figure 17). Next, 284 mg (7.47 mmol) $NaBH_4$ was dissolved in 50 mL water. The solution was transferred with a 50 mL glass-pipette into the reaction flask thermostated at 25.0 ± 0.1 °C. Then, cobalt-exchanged Zeolite-Y (Co^{2+}-Y) sample was added into the reaction flask. Cobalt(II) ions were reduced and the cobalt(0) nanoclusters were formed within the supercages of Zeolite-Y initiating the hydrolysis reaction of sodium borohydride. The volume of hydrogen gas evolved was measured by recording the displacement of water level at certain time intervals.

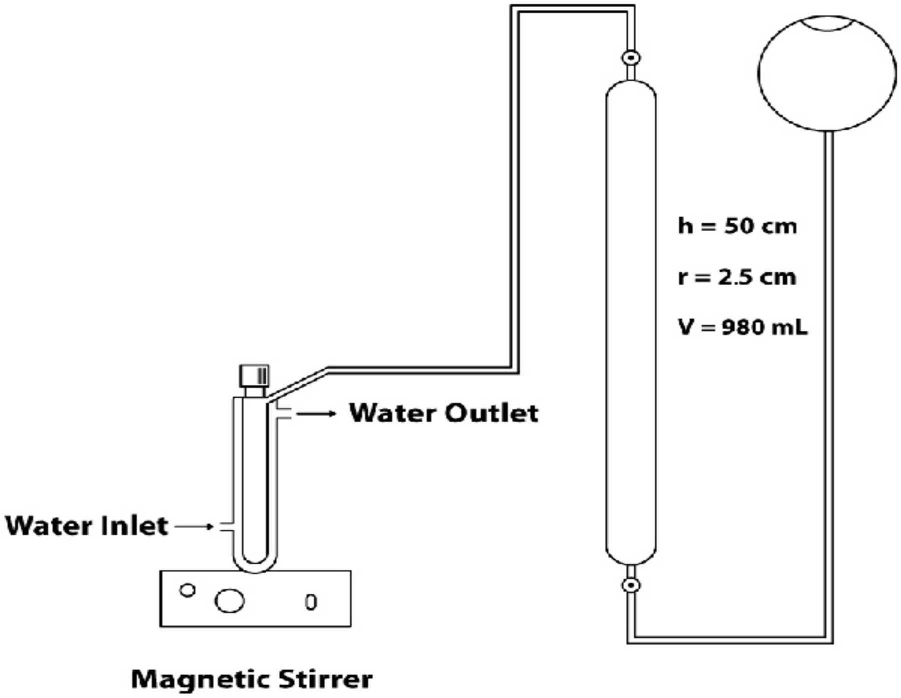

Figure 17. The experimental setup used in the measurement of the volume of hydrogen generated from the hydrolysis of sodium borohydride.

3.3.3. Control Experiment: Testing the Catalytic Activity of Cobalt-Free Zeolite-Y in the Hydrolysis of Sodium Borohydride

To determine whether host material Zeolite-Y has effect of on the catalytic activity of the zeolite confined cobalt(0) nanoclusters, the hydrolysis of sodium borohydride was carried out in the presence of Zeolite-Y. For this purpose, 284 mg of sodium borohydride (150 mM) was dissolved in 50 mL deionized water and the solution was transferred into the reaction flask thermostated at 25.0 ± 0.1 °C. Then 1041 mg Zeolite-Y (which is the highest amount of zeolite-Y that used for all reactions reported here) was added into the solution. The reaction flask was closed and the reaction was started. The same experiment was repeated at various temperatures (25, 30, 35, 40, and 45 °C) to determine the effect of temperature on the Zeolite-Y catalyzed hydrolysis of sodium borohydride.

3.3.4. Effect of Cobalt Loading on the Catalytic Activity of Zeolite Confined Cobalt(0) Nanoclusters in the Hydrolysis of Sodium Borohydride

In a series of experiments, the catalytic activities of zeolite confined cobalt(0) nanoclusters ([Co]=2 mM) with 0.20, 0.40, 0.85, 1.68, 2.52, 3.18, 4.14 wt % cobalt loading were tested in the hydrolysis of 50 mL of 150 mM (284 mg) aqueous sodium borohydride solution in order to determine the effect of cobalt loading on the hydrogen generation rate. All the experiments were carried out in the same way as described in the section of (**3.3.2.**). In case of zeolite confined cobalt(0) nanoclusters with 0.85 wt % cobalt, the highest catalytic activity was obtained. Thus, zeolite confined cobalt(0) nanoclusters with 0.85 wt % cobalt loading were used as catalyst for further kinetic experiments.

3.3.5. Kinetic Studies and the Determination of Activation Parameters for the Hydrolysis of Sodium Borohydride Catalyzed by In-Situ Formed Zeolite Confined Cobalt(0) Nanoclusters in Aqueous Medium

In order to establish the rate law for catalytic hydrolysis of $NaBH_4$ using zeolite confined cobalt(0) nanoclusters (with 0.85 wt % cobalt loading) as catalyst, two different sets of experiments were carried out in the same way described in the section of (**3.3.2.**). In the first set, $NaBH_4$ concentration was kept constant at 150 mM (284 mg $NaBH_4$, 50 mL) and the cobalt catalyst concentration was changed in the range of 1.0, 1.5, 2.0, 2.5 and 3.0 mM (347, 521, 694, 868, 1041 mg of zeolite confined cobalt(0) nanoclusters, respectively) at 25.0 ± 0.1 °C. In the second set, the cobalt catalyst concentration was kept constant at 2.0 mM Co (694 mg of zeolite confined cobalt(0) nanoclusters in 50 mL), while changing the $NaBH_4$ concentration in the range of 150, 300, 450, 600 and 750 mM (284, 568, 852, 1136, 1420 mg of $NaBH_4$, respectively) at 25 ± 0.1 °C. Finally, the catalytic hydrolysis of sodium borohydride was carried out in the presence of zeolite confined cobalt(0) nanoclusters at constant $NaBH_4$ (284 mg in 50 mL, $[NaBH_4]$ = 150 mM) and catalyst (2.0 mM Co, 694 mg zeolite confined cobalt(0) nanoclusters) concentrations at various temperatures (25, 30, 35, 40, and 45 °C) in order to determine the activation energy (Ea), enthalpy ($\Delta H^{\#}$), and entropy ($\Delta S^{\#}$), respectively.

3.3.6. Determination of the Catalytic Lifetime of Zeolite Confined Cobalt(0) Nanoclusters in the Hydrolysis of Sodium Borohydride in Aqueous Medium

The catalytic lifetime of zeolite confined cobalt(0) nanoclusters in the hydrolysis of $NaBH_4$ was calculated by measuring the total turnover number (TTO). Such a lifetime experiment was initiated with a 50 mL solution containing zeolite confined coablt(0) nanoclusters (694 mg, [Co] = 2.0 mM) and $NaBH_4$ (2.27 g, $[NaBH_4]$ = 1.2 M) at 25.0 ± 0.1 °C. After the complete conversion of $NaBH_4$, more substrate was added into the reaction medium and the reaction was lasted by this way until the evolution of hydrogen gas was slowed down to the level of the cobalt-free zeolite-Y catalyzed hydrolysis of sodium borohydride at 25 ± 0.1 °C.

3.4. The Effect of Sodium Hydroxide Concentration on the Catalytic Activity of Zeolite Confined Cobalt(0) Nanoclusters in the Hydrolysis of Sodium Borohydride

In order to study the effect of NaOH concentration on the catalytic activity of zeolite confined cobalt(0) nanoclusters in the hydrolysis of sodium borohydride (150 mM), catalytic activity tests were carried out at 25.0 ± 0.1 °C by changing the concentration of NaOH (5, 10, 15, and 20 wt %). In all the experiments, the total volume of solution was kept constant at 50 mL. All the experiments were performed in the same way as described in section of (**3.3.2.**).

3.5. The Catalytic Activity of In-Situ Formed Zeolite Confined Cobalt(0) Nanoclusters in the Hydrolysis of Sodium Borohydride in Basic Medium

3.5.1. Kinetic Studies and the Determination of Activation Parameters for the Hydrolysis of Sodium Borohydride in Basic Medium Catalyzed by Zeolite Confined Cobalt(0) Nanoclusters

To obtain the rate law for the zeolite confined cobalt(0) nanoclusters catalyzed hydrolysis of $NaBH_4$ in basic medium (in 10 wt % NaOH solution), two different sets of experiments were carried out in the same way as described in the section of (**3.3.2.**). Firstly, $NaBH_4$ concentration was kept constant at 150 mM (284 mg $NaBH_4$, 50 mL) and the cobalt catalyst concentration was changed in the range of 1.0, 1.5, 2.0, 2.5 and 3.0 mM (347, 521, 694, 868, 1041 mg of zeolite confined cobalt(0) nanoclusters, respectively) at 25.0 ± 0.1 °C. Secondly, the cobalt concentration was kept constant at 2.0 mM Co (694 mg of zeolite confined cobalt(0) nanoclusters in 50 mL), while changing the sodium borohydride concentration was in the range of 150, 300, 450, 600 and 750 mM (284, 568, 852, 1136, 1420 mg of $NaBH_4$, respectively) at 25 ± 0.1 °C. Finally, the same experiment starting with zeolite confined cobalt(0) nanoclusters (694 mg, [Co] = 2.0 mM), $NaBH_4$ (150 mM) in 50 mL of 10 wt % NaOH solution was conducted at different temperatures (25, 30, 35, 40, and 45 °C) in order to obtain the activation energy (Ea), enthalpy ($\Delta H^{\#}$), and entropy ($\Delta S^{\#}$), respectively.

3.5.2. Isolability and Reusability of Zeolite Confined Cobalt(0) Nanoclusters in the Hydrolysis of Sodium Borohydride in Basic Medium

When the first run of the hydrolysis of $NaBH_4$ (284 mg, 50 mL, 150 mM) catalyzed by zeolite confined cobalt(0) nanoclusters (694 mg, [Co] = 2.0 mM), in 10 wt % NaOH solution at 25 ± 0.1 °C is completed, the cobalt catalyst was filtered, washed three times with 20 mL of deionized water, dried under N_2 gas purging at room temperature. Then, the dried samples of zeolite confined cobalt(0) nanoclusters were used again in the hydrolysis of 150 mM basic $NaBH_4$ solution containing 10 wt % NaOH, the same procedure was repeated five times, and the results were expressed in terms of retained percent initial catalytic activity of zeolite confined cobalt(0) nanoclusters and the conversion of sodium borohydride in the hydrolysis of $NaBH_4$ in basic medium.

3.5.3. Determination of the Catalytic Lifetime of Zeolite Confined Cobalt(0) Nanoclusters in the Hydrolysis of Sodium Borohydride in Basic Medium

The catalytic lifetime of zeolite confined cobalt(0) nanoclusters in the hydrolysis of $NaBH_4$ in basic medium (in 10 wt % NaOH solution) was calculated by measuring the total turnover number (TTO). Such a lifetime experiment was initiated with a 50 mL of 10 wt % NaOH solution containing zeolite confined cobalt(0) nanoclusters (694 mg, [Co] = 2.0 mM) and $NaBH_4$ (568 mg, 300 mM) at 25.0 ± 0.1 °C. When the complete conversion is obtained, more substrate was added into the reaction medium and the reaction was lasted by this way until no hydrogen gas evolution was observed.

3.6. Zeolite Confined Cobalt(0) Nanoclusters Catalyzed Hydrolysis of Ammonia Borane

3.6.1. Control Experiments

3.6.1.1. Testing the Catalytic Activity of Cobalt-Free Zeolite-Y in the Hydrolysis of Ammonia-Borane

In order to determine the catalytic activity of zeolite-Y in the hydrolysis of ammonia-borane in the absence of catalyst, 2.0 mmol (63.6 mg) of ammonia borane was dissolved in 20 mL water and the solution was transferred into the reaction flask thermostated at 25.0 ±0.1 °C. Then weighed amount of host material (zeolite-Y) was added, the reaction flask was closed and the reaction was started. The volume of hydrogen gas evolved was measured by recording the displacement of water level at certain time intervals. It was found that in the zeolite-Y catalyzed hydrolysis of ammonia borane after one day, there is no hydrogen gas generation and additionally ^{11}B NMR spectrum of the resulting solution showed only a signal at $\delta = - 23.9$ ppm due to the unreacted AB [43].

3.6.1.2. Testing Whether the System is Under Mass Transfer Limitation

For kinetic studies in heterogeneous catalysis, it is vital to ensure that the reaction is not under mass transfer limitation [172]. For this purpose, the effect of stirring speed on the hydrogen generation rate from the hydrolysis of ammonia borane was investigated by performing the catalytic reaction at various stirring speeds (0, 200, 400, 600, 800, 1000, and 1200 rpm) at 25 ± 0.1 °C to check whether the hydrogen generation rate from the hydrolysis of ammonia-borane system is under mass transfer limitation (MTL). It was found that the hydrogen generation rate is independent of the stirring speed when it is higher than 600 rpm. This indicates that the system is in a non-mass transfer limitation regime since the present kinetic study was performed at the stirring speed of 900 rpm.

3.6.2. Effect of Cobalt Loading on Hydrogen Generation Rate

In order to determine the effect of cobalt loading on the hydrogen generation rate, the catalytic activities of zeolite confined cobalt(0) nanoclusters ([Co] = 2.0 mM) with 0.20, 0.40, 0.85, 1.68, 2.52, 3.18, and 4.14 wt % cobalt loading were tested in the hydrolysis of 20.0 mL of 100 mM aqueous ammonia-borane solution. All the experiments were performed in the same way as described in the section of (**3.6.1.1.**) to determine the catalyst with the best catalytic activity.

3.6.3. Method to Test the Catalytic Activity of Zeolite Confined Cobalt(0) Nanoclusters in the Hydrolysis of Ammonia Borane

The catalytic activity of zeolite confined cobalt(0) nanoclusters in the hydrolysis of ammonia-borane was determined by measuring the rate of hydrogen generation. In all the experiments, a jacketed reaction flask (75 mL) containing a Teflon-coated stir bar was placed on a magnetic stirrer (Heidolph MR-301) and thermostated to 25.0 ± 0.1 °C by circulating water through its jacket from a constant temperature bath. Then, a graduated glass tube filled with water was connected to the reaction flask to measure the volume of the hydrogen gas to be evolved from the reaction. Next, 63.6 mg (2.0 mmol) ammonia-borane was dissolved in 20 mL water, (corresponding to 6 mmol H_2 at 25.0 ±0.1 °C). This solution was transferred with a 50 mL glass-pipette into the reaction flask thermostated at 25.0 ±0.1 °C. Then, a certain amount of freshly prepared and dried zeolite confined cobalt(0) nanoclusters powder was added into the reaction flask. The reaction was started by closing the flask and the volume of hydrogen gas evolved was measured by recording the displacement of water level at certain time intervals. The reaction was stopped when no more hydrogen evolution was observed. The control tests using acid/base indicator showed that there was no detectable amount of ammonia evolution in our experiments due to the short reaction times and mild reaction conditions. In addition to the volumetric measurement of the hydrogen evolution, in each experiment the conversion of ammonia-borane to ammonium metaborate was also checked by comparing the intensities of signals of ammonia-borane and metaborate anion at δ = -23.9 and 9 ppm, respectively, in the ^{11}B NMR spectra of the solution [43].

3.6.4. Kinetic Study of the Hydrolysis of Ammonia Borane Catalyzed by Zeolite Confined Cobalt(0) Nanoclusters

In order to establish the rate law for catalytic hydrolysis of ammonia borane using zeolite confined cobalt(0) nanoclusters (with 0.85 wt % cobalt loading) as catalyst, two different sets of experiments were performed in the same way described in the section of (**3.6.3.**). In the first set of experiments, the hydrolysis reaction was carried out starting with different initial concentration of zeolite confined cobalt(0) nanoclusters (1.0, 1.5, 2.0, 2.5 and 3.0 mM) and keeping the initial ammonia-borane concentration constant at 100 mM. The second set of experiments were carried out by keeping the initial concentration of zeolite confined cobalt(0) nanoclusters constant at 2.0 mM and varying the ammonia-borane concentration of 100, 150, 200, 250 and 300 mM. Finally, the catalytic hydrolysis of ammonia borane was carried out in the presence of zeolite confined cobalt(0) nanoclusters at constant ammonia borane (100 mM) and catalyst (2.0 mM Co) concentrations at various temperatures in the range 25-45 °C in order to obtain the activation energy (E_a), enthalpy ($\Delta H^{\#}$) and entropy ($\Delta S^{\#}$), respectively.

3.6.5. Isolability and Reusability of Zeolite Confined Cobalt(0) Nanoclusters in the Hydrolysis of Ammonia Borane

After the first run of hydrolysis of 100 mM ammonia borane (63.6 mg in 20 mL), catalyzed by zeolite confined cobalt(0) nanoclusters (278 mg Co(0)-Y with a cobalt content of 0.85 wt %, [Co] = 2.0 mM) at 25.0 ± 0.1 °C, the catalyst was isolated by filtration, and dried under nitrogen gas purging at room temperature. The dried samples of zeolite confined cobalt(0) nanoclusters were used again in the hydrolysis of 100 mM ammonia borane and the same procedure was repeated five times and the results were expressed in terms of remaining percent activity of zeolite confined cobalt(0) nanoclusters and conversion of ammonia borane in the hydrolysis of ammonia borane solution.

3.6.6. Catalytic Lifetime of Zeolite Confined Cobalt(0) Nanoclusters in the Hydrolysis of Ammonia Borane

The catalytic lifetime of zeolite confined cobalt(0) nanoclusters in the hydrolysis of ammonia borane was determined by measuring the total turnover number (TTON). Such a lifetime experiment was started with a 20 mL solution containing 2.0 mM zeolite confined cobalt(0) nanoclusters and 500 mM ammonia borane at 25.0 ± 0.1 °C. When the complete conversion of added ammonia borane was achieved by checking the stoichiometric H_2 gas evolution (3.0 mol H_2 / mol H_3NBH_3), a new batch of ammonia borane (309 mg) was added and the reaction was continued in this way until no hydrogen gas evolution was observed.

CHAPTER 4

RESULTS AND DISCUSSION

4.1. Characterization of Zeolite Confined Cobalt(0) Nanoclusters

XRD patterns of the cobalt(II)-exchanged zeolite-Y and zeolite confined cobalt(0) nanoclusters with a 0.85 wt % cobalt content are shown in Figure 18, along with the host material, zeolite-Y. All these patterns show only the characteristic peaks of FAU structure characterized by intense reflections at 2θ equal to 7.46, 15.76, 23.71, 32.05, and 37.90° [173]. As can be seen from this figure, there is no noticeable change in both the intensities and the positions of the Bragg peaks going from host material to the zeolite confined cobalt(0) nanoclusters. When these patterns are compared, it was clearly seen that cobalt(II) ions were successfully incorporated into zeolite-Y and then zeolite confined cobalt(0) nanoclusters were formed by the reduction of these cobalt(II) ions without causing forming alteration in the framework lattice and loss in the crystallinity of zeolite-Y. Additionally, there is no peak attributable to the inclusion of cobalt into the zeolite material in XRD patterns because of relatively low cobalt content in the sample [165].

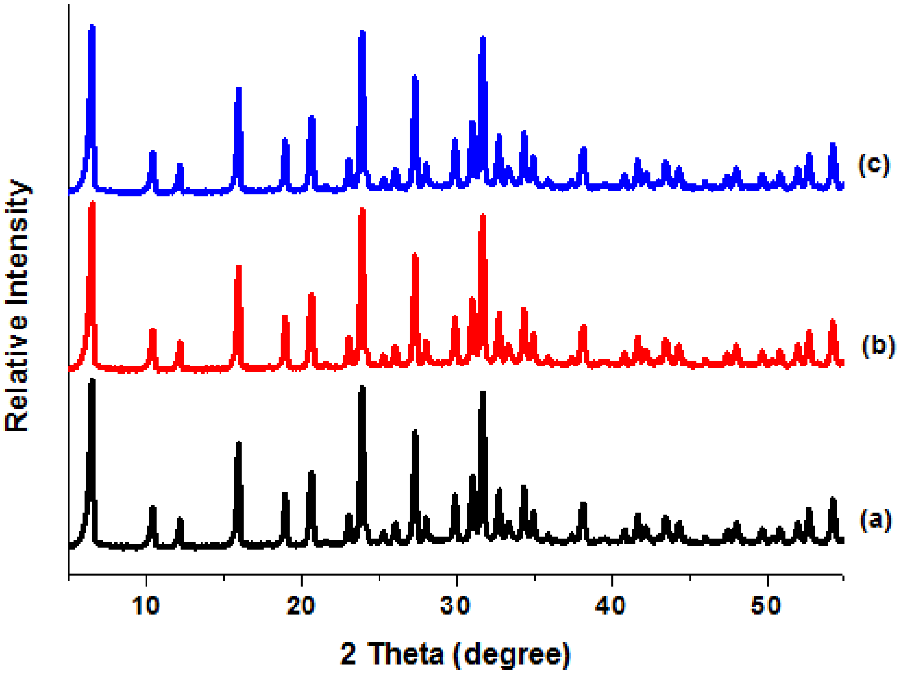

Figure 18. The powder XRD patterns of (a) zeolite-Y, (b) cobalt(II)-exchanged zeolite-Y, and (c) zeolite confined cobalt(0) nanoclusters prepared by the reduction of cobalt(II)-exchanged zeolite-Y sample with a cobalt content of 0.85 wt % by sodium borohydride.

The crystal morphology and composition of zeolite confined cobalt(0) nanoclusters were investigated by SEM, EDX, and HRTEM analyses. Figure 19 shows the SEM images taken at different magnifications for the zeolite confined cobalt(0) nanoclusters with a cobalt loading of 0.85 wt %. These SEM images show the hexagonal structure of zeolite-Y crystals, in agreement with the fact that the ion-exchange and reduction procedures for the preparation of zeolite confined cobalt(0) nanoclusters did not cause any changes in the structure of zeolite-Y, a fact that is also supported by XRD results.

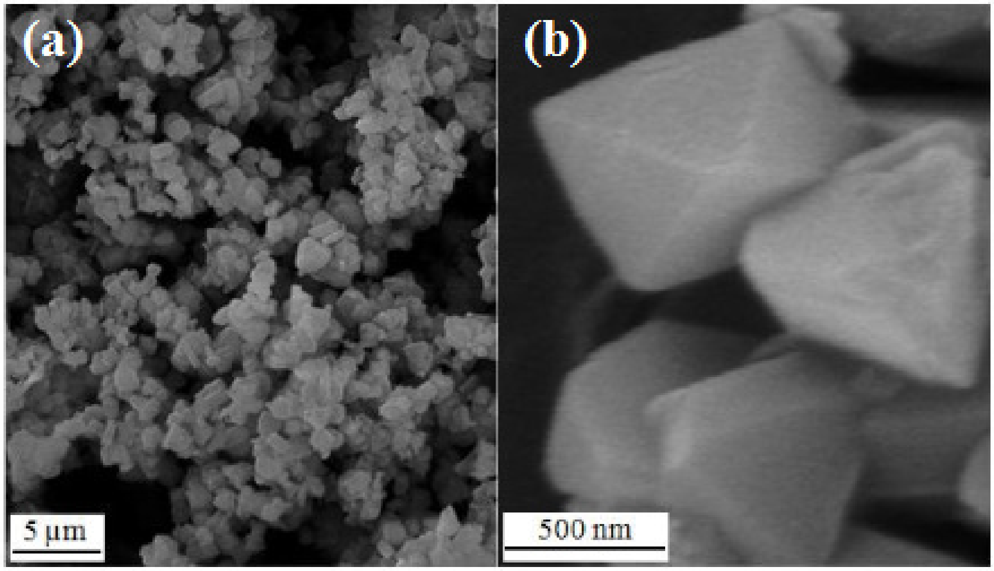

Figure 19. Scanning Electron Microscopy (SEM) images of zeolite confined cobalt(0) nanoclusters taken in different magnification scales, (a) 5.0 µm and (b) 500 nm.

SEM/EDX spectrum (Figure 20) of the zeolite confined cobalt(0) nanoclusters with 0.85 wt % cobalt content shows the existence of cobalt is the only detected element apart from the zeolite framework elements (Si, Al, O, Na) and C from the film.

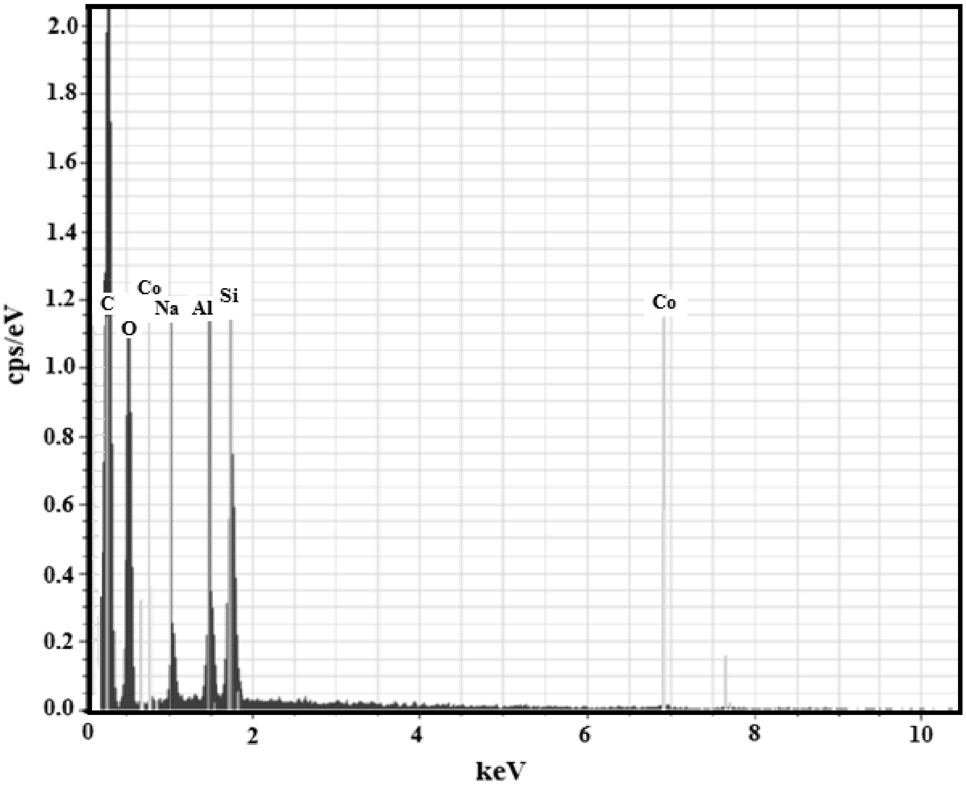

Figure 20. SEM/EDX spectrum of zeolite confined cobalt(0) nanoclusters with a cobalt content of 0.85 wt %.

Since the ICP analysis indicates the presence of cobalt metal in the catalyst sample, it can be concluded that the cobalt metal is within the cages of zeolite-Y. Indeed, the high resolution TEM image of the catalyst with 0.85 wt % cobalt content given in Figure 21 shows the distribution of cobalt within the cavities of zeolite-Y.

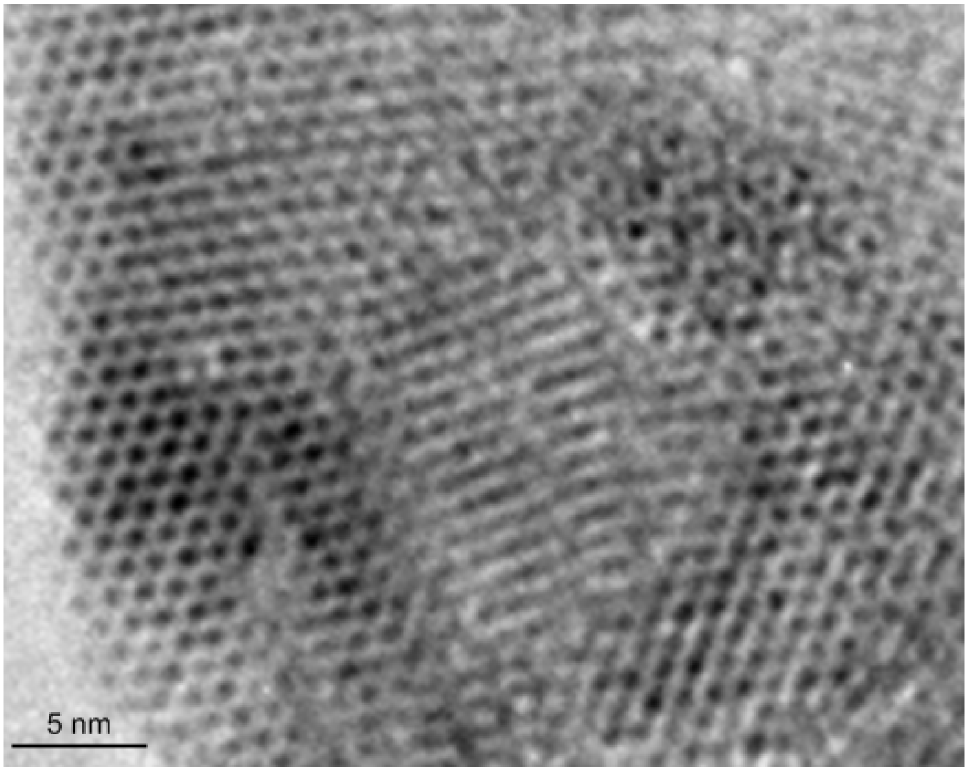

Figure 21. High resolution transmission electron microscope (HRTEM) image of zeolite confined cobalt(0) nanoclusters with a cobalt content of 0.85 wt %.

The oxidation state of cobalt and the surface composition of the zeolite confined cobalt(0) nanoclusters were investigated by X-ray photoelectron spectroscopy. The XPS survey spectrum of the catalyst prepared by the reduction of cobalt(II)-exchanged zeolite-Y sample with cobalt content of 0.85 wt % by sodium borohydride is given in Figure 22 and it confirms the existence of cobalt apart from the zeolite framework elements (O, Si, Al, Na,C) as observed by EDX analysis.

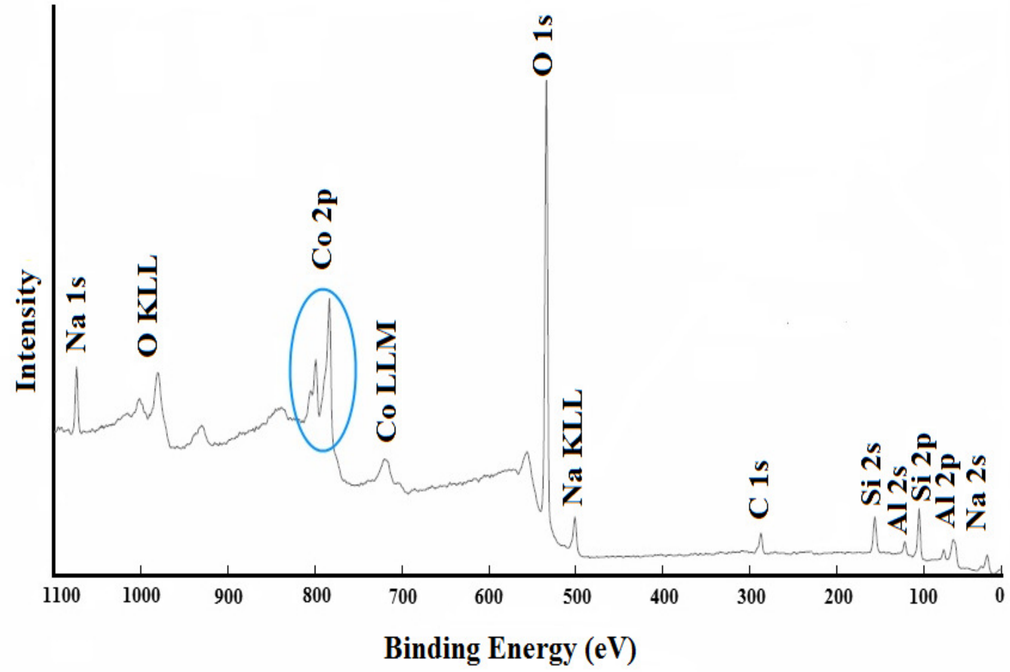

Figure 22. X-ray photoelectron survey spectrum of the zeolite confined cobalt(0) nanoclusters with a cobalt content of 0.85 wt %.

The high resolution XPS spectrum of the zeolite confined cobalt(0) nanoclusters is given in Figure 23. It shows two prominent absorption bands at 780.0 and 796.3 eV which can be readily assigned to Co(0) $2p_{3/2}$ and Co(0) $2p_{1/2}$, respectively. The binding energies of zeolite confined cobalt(0) nanoclusters are shifted by 1.5 and 1.6 eV, respectively, to the higher values compared to the values of bulk cobalt [174]. This shift might be attributed to both quantum size effect [175] and peculiar electronic properties of the zeolite matrix [176]. The interaction of cobalt(0) nanoclusters with the framework oxygen of the zeolite cages is expected to induce a positive charge on the surface metal, which would increase the binding energies of cobalt(0) nanoclusters. In addition to the matrix effect, the high energy shift in the cobalt binding energy might be due to the fact that electrons in the core level are strongly restricted by the atomic nucleus, as observed in the case of palladium(0) nanoclusters in zeolite-Y [177].

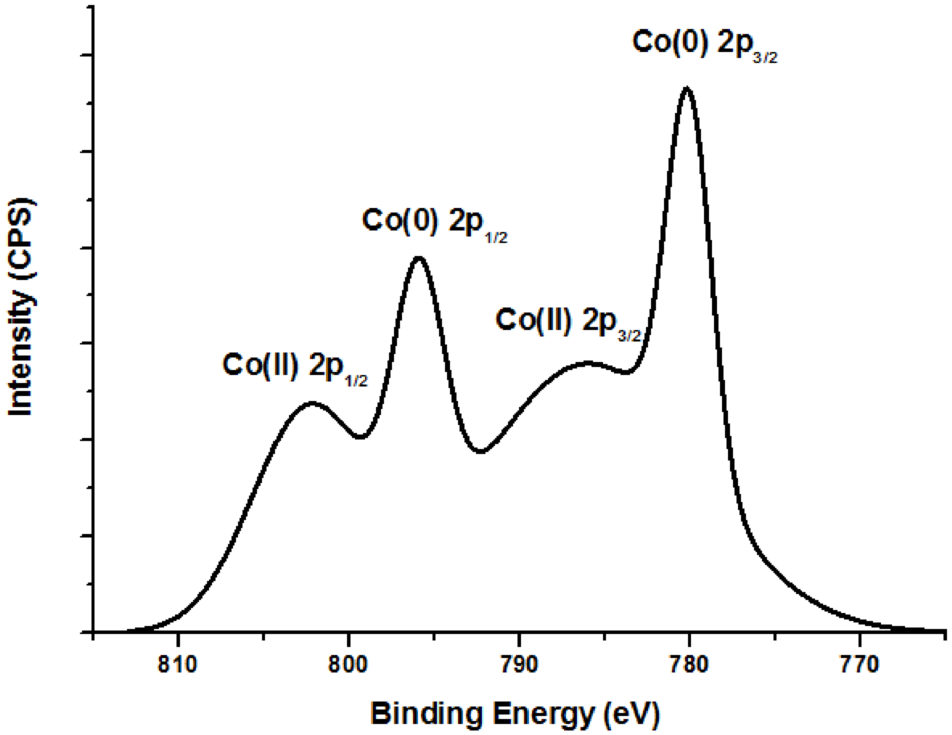

Figure 23. The high resolution Co 2p X-ray photoelectron spectrum of the zeolite confined cobalt(0) nanoclusters with a cobalt content of 0.85 wt %.

The XPS spectrum also exhibits two additional slightly higher energy features which can be attributed to a higher oxidation state of cobalt (like cobalt oxides), presumably formed by air oxidation of the sample, since the cobalt(0) nanoclusters are sensitive to aerobic atmosphere. Although the oxidation of metal nanoclusters by air oxidation is a known phenomenon [178], the existence of cobalt oxide species obtained from XPS analysis needs to be tested by using another spectroscopic technique to check whether cobalt oxide is really formed by air oxidation of the sample or in the preparation of zeolite confined cobalt(0) nanoclusters. Therefore, zeolite confined cobalt(0) nanoclusters were analyzed by Raman spectroscopy, that is a strong tool to test the presence of cobalt oxide species. The Raman spectra of zeolite-Y and zeolite confined cobalt(0) nanoclusters, taken under inert atmosphere as solid materials, shown in Figure 24 do not differ from each other significantly. They show the bands that are assigned to δ (T-O-T) bending modes at 97, 290, 375, and 504 cm^{-1}. The most prominent band of the spectrum located at 504 cm^{-1} can be associated with the four-membered rings (4MRs) in the structure since the FAU framework is composed of rings of 4 and 6 (Al,Si)O_4 tetrahedra [179]. Moreover, the characteristic Raman peaks of cobalt oxide species [180] at 480 and 690 cm^{-1} are missing in the Raman spectrum of the zeolite confined cobalt(0) nanoclusters, confirming that the formation of cobalt oxide observed in the XPS analysis is due to the surface oxidation of cobalt(0) nanoclusters by air oxidation, and therefore the cobalt particles are in zero oxidation state in the reaction medium.

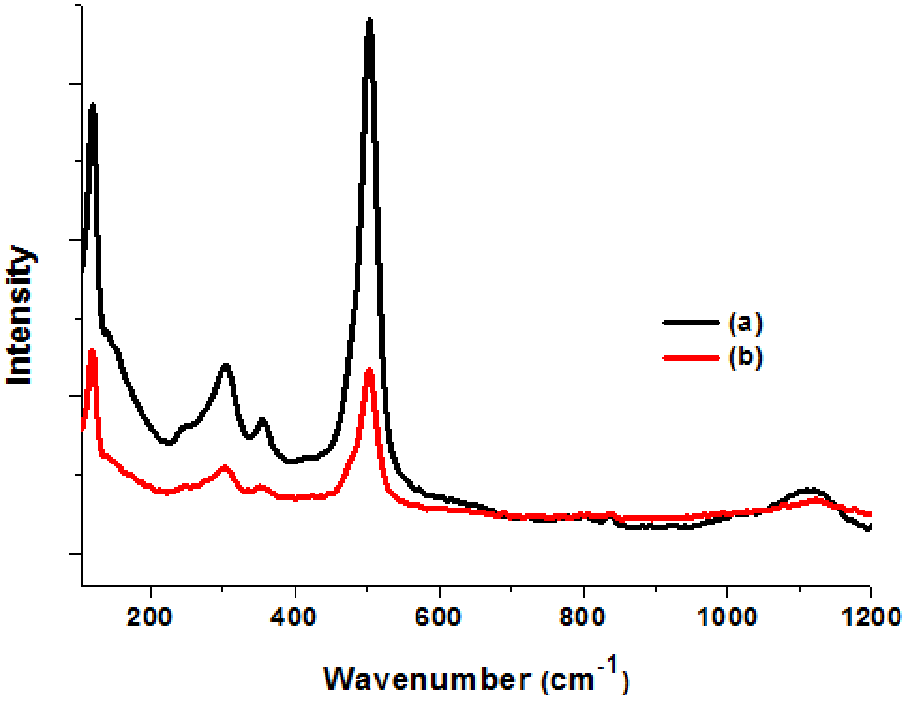

Figure 24. Raman spectrum of (a) zeolite-Y and (b) zeolite confined cobalt(0) nanoclusters with a cobalt content of 0.85 wt %.

Diffuse reflectance UV-vis spectroscopy was used to monitor the reduction of cobalt(II)-exchanged zeolite-Y to zeolite confined cobalt(0) nanoclusters (Figure 25). The only peak, located around 510 nm, observed in the DR-UV spectrum of the cobalt(II)-exchanged zeolite-Y sample can be identified as Co^{2+} ions coordinated with an octahedral configuration located in the supercages of the zeolite [181]. It is an another indication of cobalt species being located in the supercages and that peak completely disappears when the sample is reduced by sodium borohydride to form zeolite confined cobalt(0) nanoclusters. The Kubelka-Munk function of the obtained diffuse reflectance data is shown as inset in Figure 24.

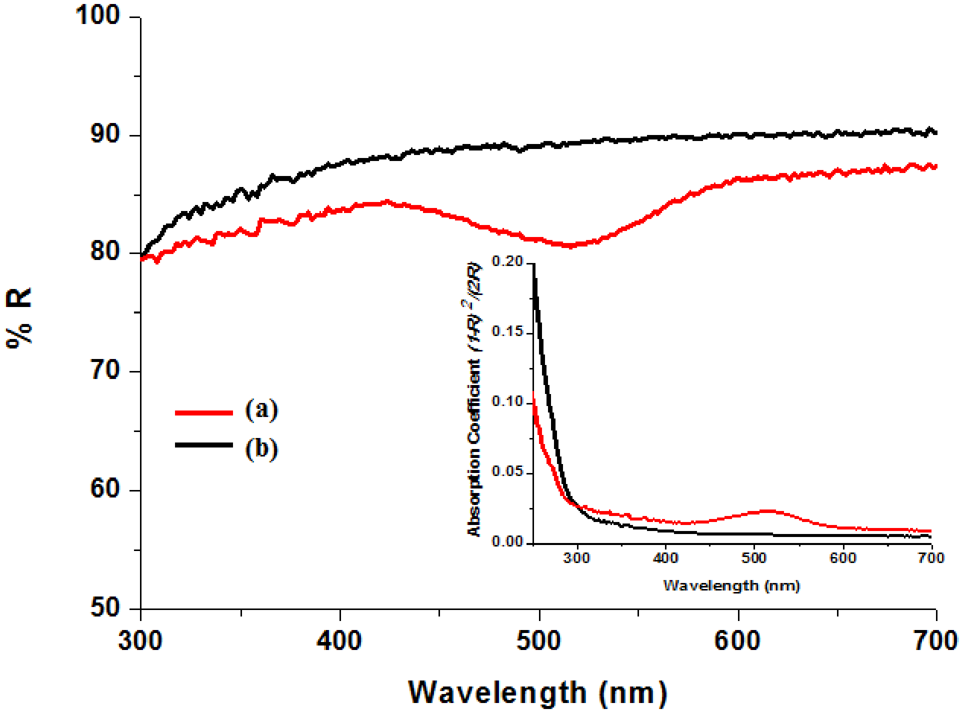

Figure 25. Diffuse reflectance UV-vis spectrum of (a) cobalt(II)-exchanged zeolite-Y and (b) zeolite confined cobalt(0) nanoclusters with a cobalt content of 0.85 wt %. Inset shows the Kubelka-Munk function of the obtained diffuse reflectance data.

Nitrogen adsorption-desorption isotherms of zeolite-Y and the zeolite confined cobalt(0) nanoclusters are shown in Figure 26 and both of them showed type I isotherm, which is typical for microporous materials [182]. The parameters of the porous structures were calculated from the nitrogen adsorption-desorption isotherms. On passing from zeolite-Y to zeolite confined cobalt(0) nanoclusters, both the micropore volume (from 0.332 to 0.254 cm^3/g) and the micropore area (from 823 to 652 m^2/g) are noticeably reduced. These remarkable decreases in both the micropore volume and micropore area are due to the encapsulation of cobalt particles in the cavities of zeolite-Y and also provide additional evidence for the presence of cobalt(0) nanoclusters within the cages.

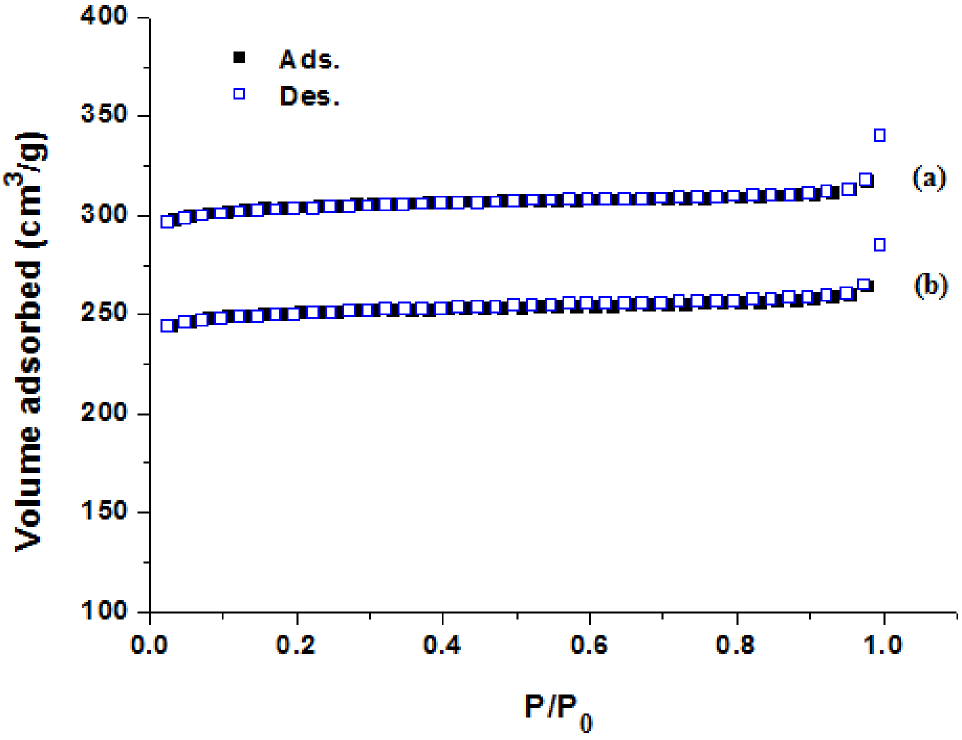

Figure 26. Nitrogen adsorption-desorption isotherms of (a) zeolite-Y and (b) zeolite confined cobalt(0) nanoclusters with a cobalt content of 0.85 wt %.

4.2. The Catalytic Activity of In-Situ Formed Zeolite Confined Cobalt(0) Nanoclusters in the Hydrolysis of Sodium Borohydride in the Aqueous Medium

4.2.1. The Catalytic Activity of Cobalt-Free Zeolite-Y in the Hydrolysis of Sodium Borohydride

To determine the catalytic activity of zeolite confined cobalt(0) nanoclusters more precisely, the effect of zeolite-Y catalyzes on the hydrolysis of $NaBH_4$ has to be checked. The hydrolysis of $NaBH_4$ in the presence of zeolite-Y was carried out at different temperatures in the range (25, 30, 35, 40, and 45 °C). It was found that the hydrogen generation from the hydrolysis of sodium borohydride in the presence of zeolite-Y increases with the increasing temperature from 1.1 to 4.2 mL H_2 min^{-1} for 25 and 45 °C, respectively. Although the hydrolysis of sodium borohydride in the presence of zeolite-Y is slow, all of the catalytic activity results of zeolite confined cobalt(0) nanoclusters in the hydrolysis of sodium borohydride given here were corrected by subtracting the amount of hydrogen gas obtained due to the hydrolysis of sodium borohydride in the presence of zeolite-Y from the values of hydrogen gas obtained from the zeolite confined cobalt(0) nanoclusters catalyzed hydrolysis of sodium borohydride.

4.2.2. The Effect of Cobalt Loading on the Catalytic Activity of Zeolite Confined Cobalt(0) Nanoclusters in the Hydrolysis of Sodium Borohydride

Zeolite confined cobalt(0) nanoclusters samples with various cobalt loading were prepared by changing the concentration of cobalt(II) nitrate solution in ion-exchange and tested to determine the effect of cobalt loading on the catalytic activity of zeolite confined cobalt(0) nanoclusters (in all [Co] = 2.0 mM) in the hydrolysis of $NaBH_4$. Figure 27 shows the change in the catalytic activity of zeolite confined cobalt(0) nanoclusters with cobalt content of the zeolite-Y.

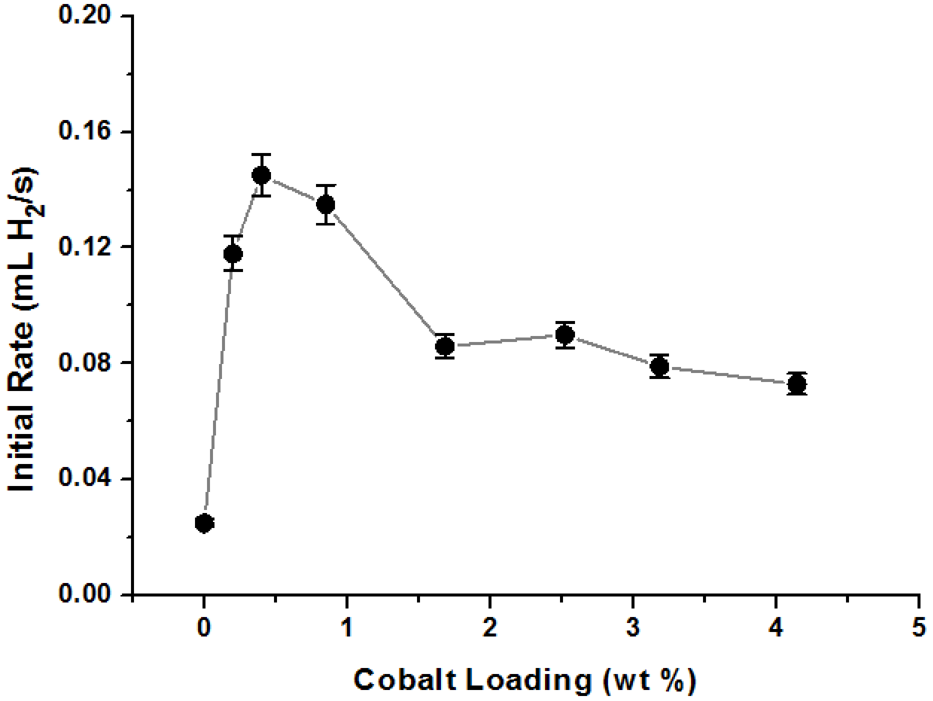

Figure 27. The initial rate of hydrogen generation (mL of H_2/s) versus cobalt loadings (in wt % Co) for the zeolite confined cobalt(0) nanoclusters (in all [Co] = 2.0 mM) catalyzed hydrolysis of $NaBH_4$ (150 mM, 50 mL) at 25 ± 0.1 °C.

The variation in catalytic activity shows the accessibility of cobalt(0) nanoclusters by the substrate molecules in the zeolite cages. The highest catalytic activity was obtained by using the zeolite confined cobalt(0) nanoclusters that have 0.40 wt % Co loading. In this loading amount, the majority of zeolite confined cobalt(0) nanoclusters should be present in the supercage (α-cage), in which the substrate molecules can easily penetrate compared to the β-cage (Figure 11). With the increasing amount of cobalt, the the formed nanoclusters might go to the less accessible sodalite cages as well, or nanoclusters in the supercages block the entrance to the supercages becoming larger. In order to keep the cobalt concentration at a certain level in the catalytic reaction using the total amount of catalyst as small as possible, the zeolite confined cobalt(0) nanoclusters catalyst with 0.85 wt % cobalt loading was selected for the further experiments.

4.2.3. Kinetic Studies and the Determination of Activation Parameters for the Hydrolysis of Sodium Borohydride Catalyzed by Zeolite Confined Cobalt(0) Nanoclusters

The zeolite confined cobalt(0) nanoclusters (with 0.85 wt % cobalt loading) were found to be highly active catalyst in the hydrolysis of $NaBH_4$ releasing hydrogen gas. Figure 28 shows the plots of the volume of hydrogen gas generated versus time during the catalytic hydrolysis of $NaBH_4$ solution in the presence of zeolite confined cobalt(0) nanoclusters in different cobalt catalyst concentrations at 25.0 ± 0.1 °C. The evolution of hydrogen gas starts without an induction period, indicating the rapid nanocluster catalyst formation.

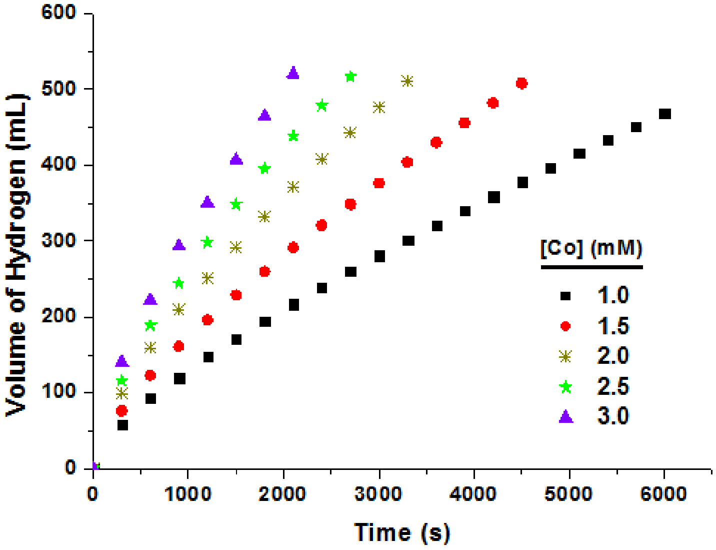

Figure 28. Plot of the volume of hydrogen (mL) versus time (s) for the hydrolysis of $NaBH_4$ (150 mM, 50 mL) catalyzed by zeolite confined cobalt(0) nanoclusters (with a cobalt content of 0.85 wt %) at different cobalt concentrations ([Co] = 1.0, 1.5, 2.0, 2. 5, and 3.0 mM) at 25.0 ± 0.1 °C.

Hydrogen generation rates calculated from the slope of the linear portion of the plots are increases with the increasing catalyst concentration, as expected. Figure 29 shows the plot of rate of hydrogen generation versus cobalt catalyst concentrations, both in logarithmic scale. A straight line with a slope of almost 1 obtained from Figure 29 indicates that hydrolysis reaction of $NaBH_4$ proceeds via first order with respect to cobalt catalyst concentration.

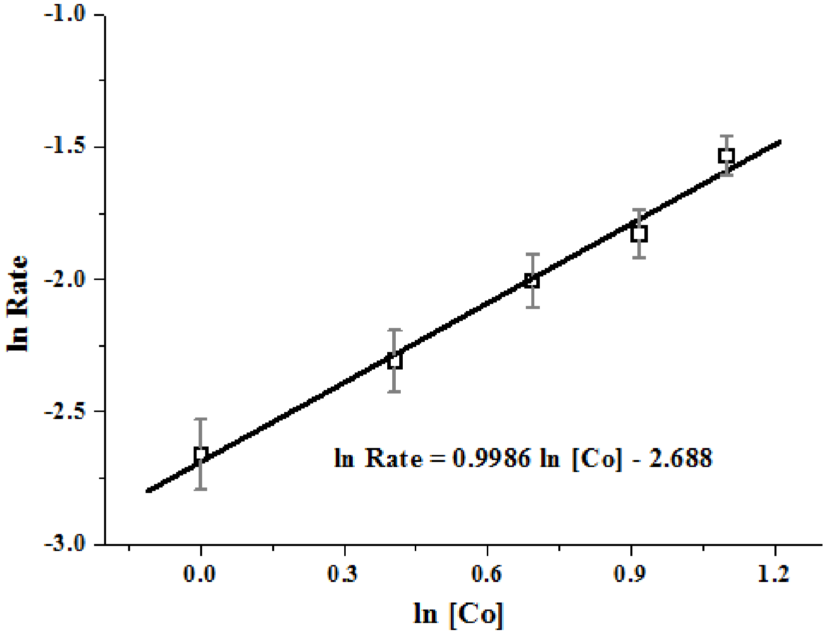

Figure 29. Plot of the rate of hydrogen generation versus the cobalt catalyst concentration (both in logarithmic scale) in the hydrolysis of $NaBH_4$ catalyzed by zeolite confined cobalt(0) nanoclusters at 25.0 ± 0.1 °C.

The effect of $NaBH_4$ concentration on the rate of hydrogen generation was also investigated by carrying out a series of experiments starting with different initial concentration of $NaBH_4$ while keeping the cobalt catalyst concentration constant at

2.0 mM. Figure 30 shows the plot of volume of hydrogen gas generated versus time for different initial concentrations of $NaBH_4$ (150, 300, 450, 600, and 750 mM).

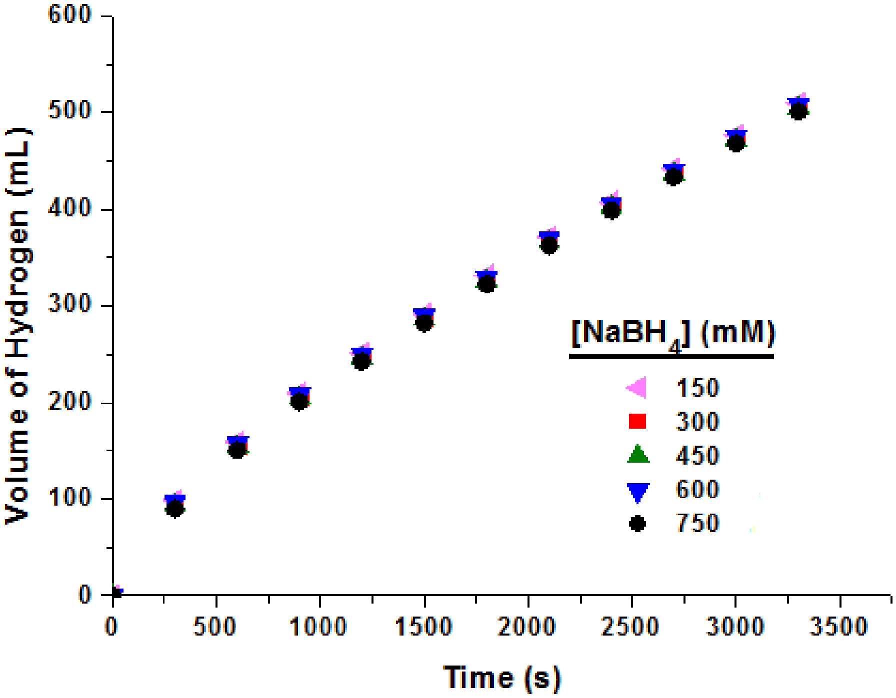

Figure 30. Plot of the volume of hydrogen gas generated (mL) versus time (s) for the zeolite confined cobalt(0) nanoclusters (with 0.85 wt % cobalt loading, [Co] = 2.0 mM) catalyzed hydrolysis of $NaBH_4$ solution (50 mL) at various concentrations ($[NaBH_4]$ = 150, 300, 450, 600, and 750 mM) at 25.0 ± 0.1 °C.

Plotting the rate of hydrogen generation, determined from the linear portion of the plots in Figure 30, versus $NaBH_4$ concentration, both in logarithmic scales (Figure 31), indicates that the catalytic hydrolysis of $NaBH_4$ is zero-order with respect to $NaBH_4$ concentration, and thus practically independent of the $NaBH_4$ concentration or in other words the rate of hydrogen generation shows no dependency on the concentration of $NaBH_4$, at least in the studied range ($[NaBH_4]$ = 150-750 mM).

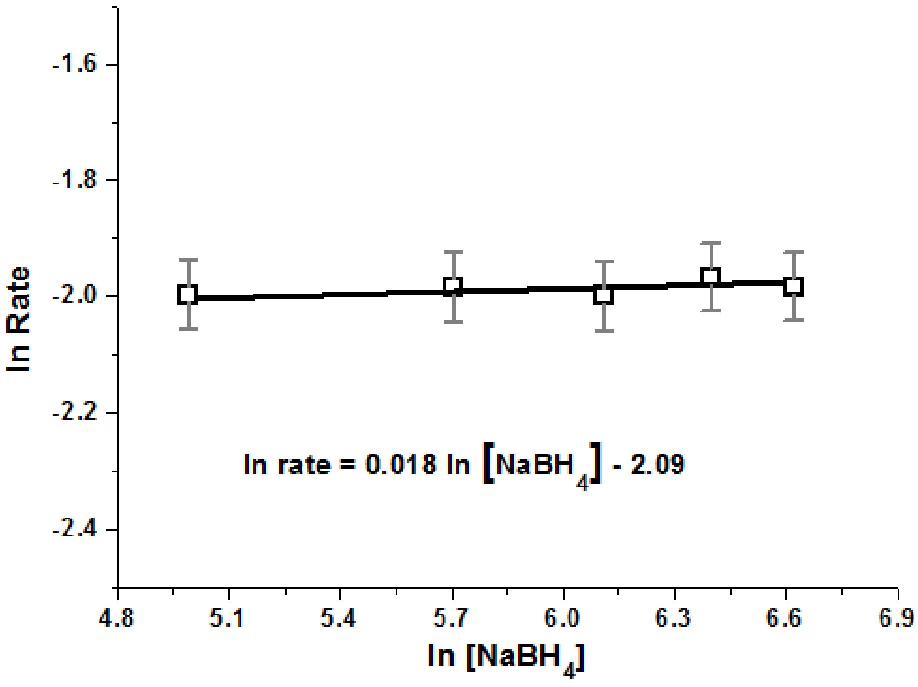

Figure 31. Plot of the hydrogen generation rate versus the substrate concentration (both in logarithmic scale) in the hydrolysis of $NaBH_4$ catalyzed by zeolite confined cobalt(0) nanoclusters at 25.0 ± 0.1 °C.

Consequently, the rate law for the catalytic hydrolysis of sodium borohydride in aqueous solution can be given as in Eq. 5,

$$\frac{-4d[NaBH_4]}{dt} = \frac{d[H_2]}{dt} = k[Co] \tag{5}$$

The hydrolysis of sodium borohydride catalyzed by zeolite confined cobalt(0) nanoclusters was performed at various temperatures (25, 30, 35, 40, and 45 °C) starting with the initial substrate concentration of 150 mM $NaBH_4$ and an initial catalyst concentration of 2.0 mM Co. Figure 32 shows the plot of hydrogen volume generated versus time at various temperatures for the hydrolysis of sodium borohydride in the presence of zeolite confined cobalt(0) nanoclusters.

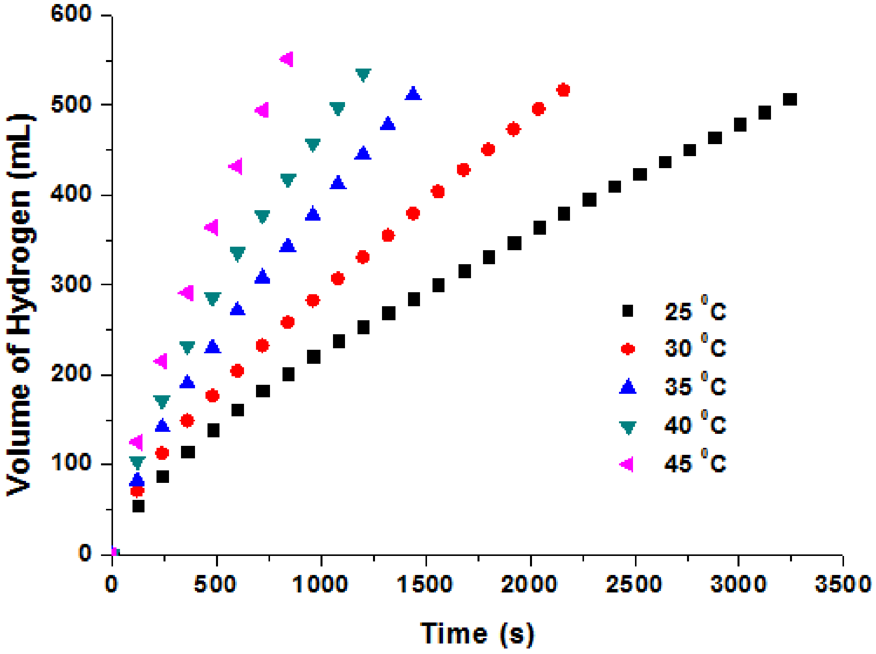

Figure 32. Plot of the volume of hydrogen (mL) versus time (s) for the hydrolysis of $NaBH_4$ (150 mM, 50 mL) catalyzed by zeolite confined cobalt(0) nanoclusters (with a cobalt content of 0.85 wt %, [Co] = 2.0 mM) at different temperatures (25, 30, 35, 40, and 45 °C).

The values of rate constant k_{app} (Table A1 in the Appendix A) determined from the linear portions of the hydrogen volume versus time plots at five different temperatures (Figure 32) are used to calculate the activation parameters, namely; activation energy, activation enthalpy, and activation entropy from the Arrhenius (Eq. 6) and Eyring (Eq. 8) plots as shown in Figue 33 and Figure 34, respectively, for the catalytic hydrolysis of sodium borohydride.

$$\mathbf{k = A.e^{-Ea/RT}} \tag{6}$$

Where Ea is the Arrhenius energy of activation, A is the preexponential factor as a characteristic contant and R is the gas constant. The Equation 6 is changed to Equation 7 by taking natural logarithm of both sides:

$$\mathbf{lnk = lnA - [Ea/RT]} \tag{7}$$

According to Figure 33, a straight line with a slope of [-Ea/R] is obtained by the plot of ln k versus 1/T.

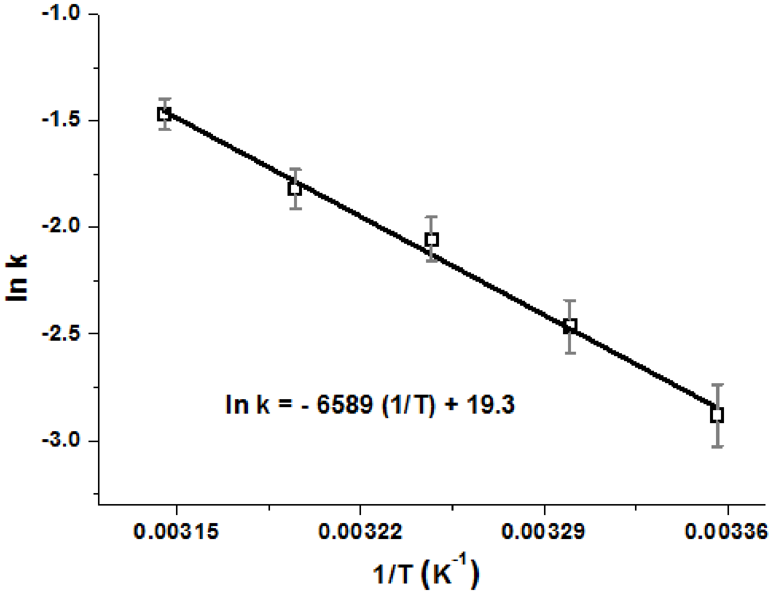

Figure 33. The Arrhenius plot for the zeolite confined cobalt(0) nanoclusters catalyzed hydrolysis of sodium borohydride.

The Arrhenius activation energy, Ea, for the hydrolysis of sodium borohydride catalyzed by zeolite confined cobalt(0) nanoclusters was calculated as E_a^{app} = 55 ± 2 kJ/mol by using the slope of Arrhenius plot. This type of activation energy should be called as E_a^{app} since it is formed by the combination of the rate constants (k_{app}) of many reaction steps for the catalytic hydrolysis of sodium borohydride. This activation energy is lower than the value found for the same hydrolysis reaction catalyzed by bulk cobalt (75 kJ/mol) and other bulk metal catalysts: 71 kJ/mol for nickel, and 63 kJ/mol for Raney nickel [28b].

The enthalpy of activation, $\Delta H^{\#}$ and the enthropy of activation, $\Delta S^{\#}$ were calculated by using of Eyring Equation:

$$\mathbf{\ln k/T = 1/T\,[-\Delta H^{\#}/R] + \ln k_b/h + \Delta S^{\#}/R} \qquad (8)$$

A straight line with a slope of $[-\Delta H^{\#}/R]$ and an intercept of $[\ln k_b/h + \Delta S^{\#}/R]$ are obtained by the plot of ln k/T versus 1/T from Figure 34.

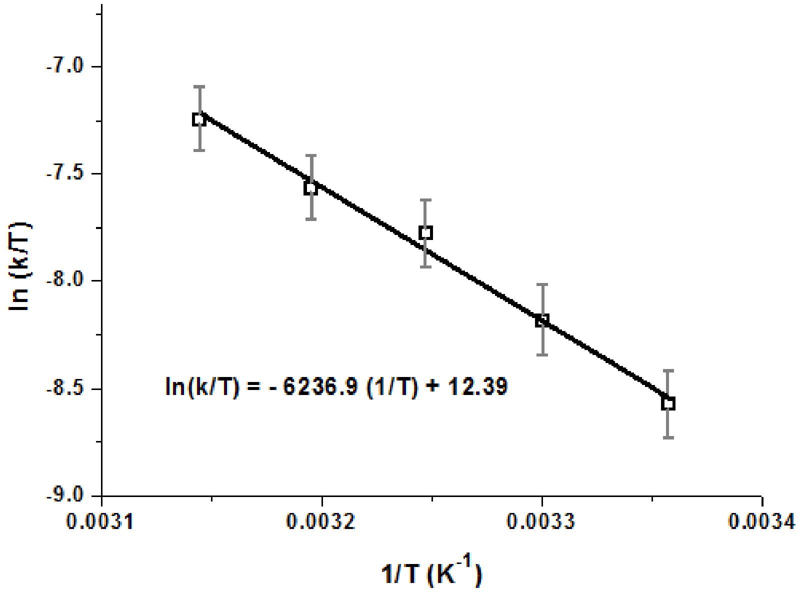

Figure 34. The Eyring plot for the zeolite confined cobalt(0) nanoclusters catalyzed hydrolysis of sodium borohydride.

The enthalpy of activation, $\Delta H^{\#}$, for the hydrolysis of sodium borohydride catalyzed by zeolite confined cobalt(0) nanoclusters is 52 ± 2 kJ/mol which was calculated by using the slope of Eyring plot while the enthropy of activation, $\Delta S^{\#}$, obtained by using the intercept of Eyring plot was calculated as - 94 ± 4 J/mol.K. The small value of activation enthalpy and the large negative value of the entropy of activation indicate an associative mechanism for the cobalt(0) nanocluster catalyzed hydrolysis of $NaBH_4$ [183]. A plausible mechanism for the metal-catalyzed hydrolysis of $NaBH_4$ including overall reaction may be as follows (Figure 35);

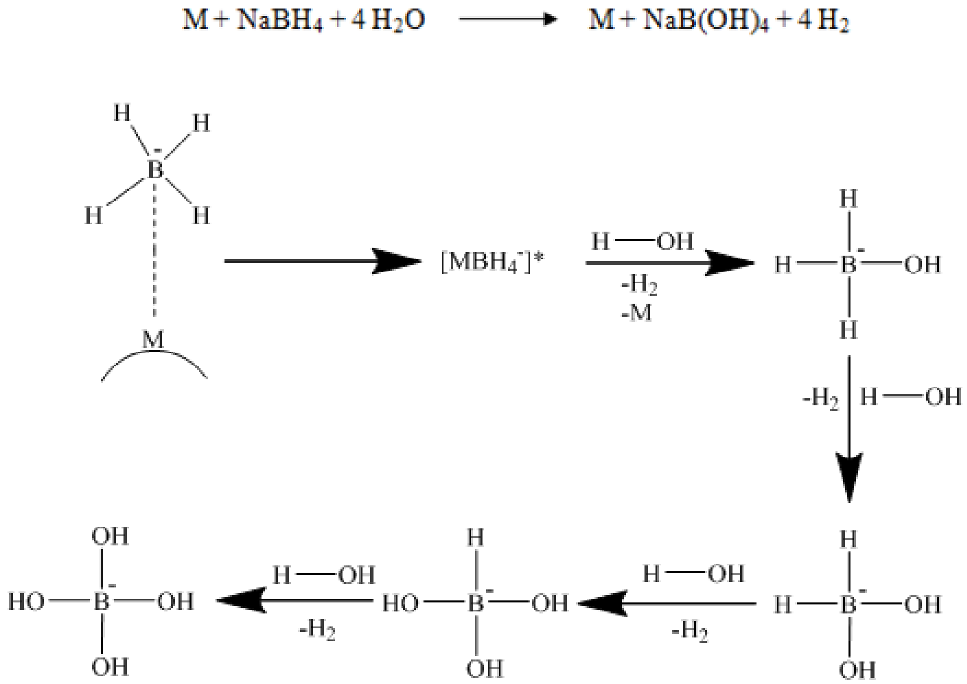

Figure 35. The overall reaction and the plausible mechanism for the metal-catalyzed hydrolysis of sodium borohydride in aqueous solution.

4.2.4. Catalytic Lifetime of Zeolite Confined Cobalt(0) Nanoclusters in the Hydrolysis of Sodium Borohydride

A lifetime experiment for the zeolite confined cobalt(0) nanoclusters catalyst in the hydrolysis of sodium borohydride was started with 2.0 mM zeolite confined cobalt(0) nanoclusters in 50 mL aqueous solution of sodium borohydride at 25.0 ± 0.1 ºC. They provide 12000 total turnovers over 75 h (Figure 36) and maximum TOF value of 250 mol H_2 (mol Co)$^{-1}$ h^{-1}. However, the rate of hydrogen generation slowed down as the reaction proceeded, may be because of increasing viscosity of the solution since the continuously added sodium borohydride was converted into the sodium metaborate. As a result, this increasing viscosity of the solution made it to be hardly stirred. Therefore, this TTO value should be considered as a lower limit and a much higher value might be obtained when the increase in viscosity is avoided.

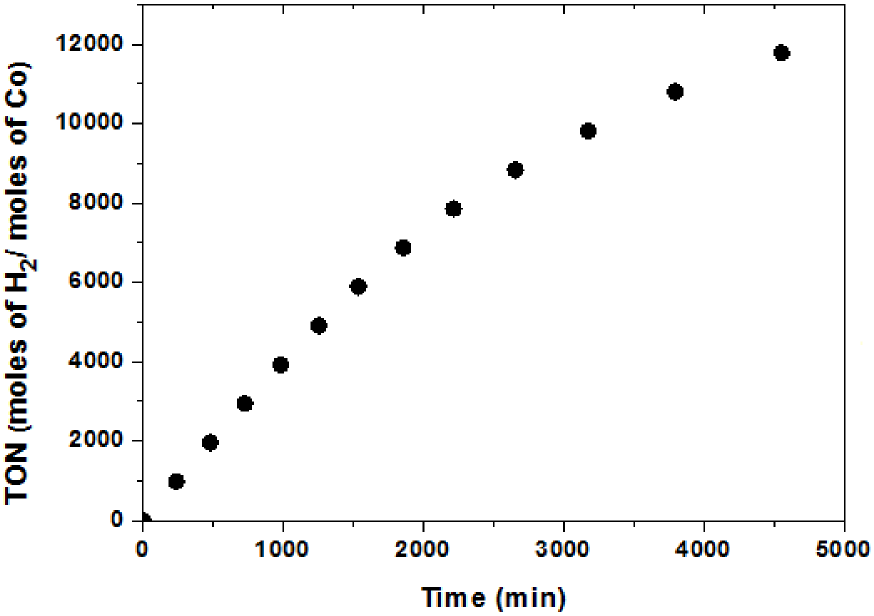

Figure 36. Graph for the variation in TON (turnover number) with time (min) for the zeolite confined cobalt(0) nanoclusters catalyzed hydrolysis of sodium borohydride at 25 ± 0.1 ºC.

4.3. The Effect of Sodium Hydroxide Concentration on the Catalytic Activity of Zeolite Confined Cobalt(0) Nanoclusters in the Hydrolysis of Sodium Borohydride

Figure 37 shows the plot of hydrogen generation rate versus concentration of NaOH in wt % for the hydrolysis of sodium borohydride catalyzed by zeolite confined cobalt(0) nanoclusters. The rate of hydrogen generation first increases with the increasing sodium hydroxide concentration, demonstrating an enhancement of reaction by NaOH. It reaches a maximum value at the concentration of 10 wt % NaOH and subsequently decreases with the further increase in sodium hydroxide concentration. This observation dictates the use of 10 wt % NaOH for the kinetic studies of the catalytic hydrolysis of $NaBH_4$ using zeolite confined cobalt(0) nanoclusters as catalyst.

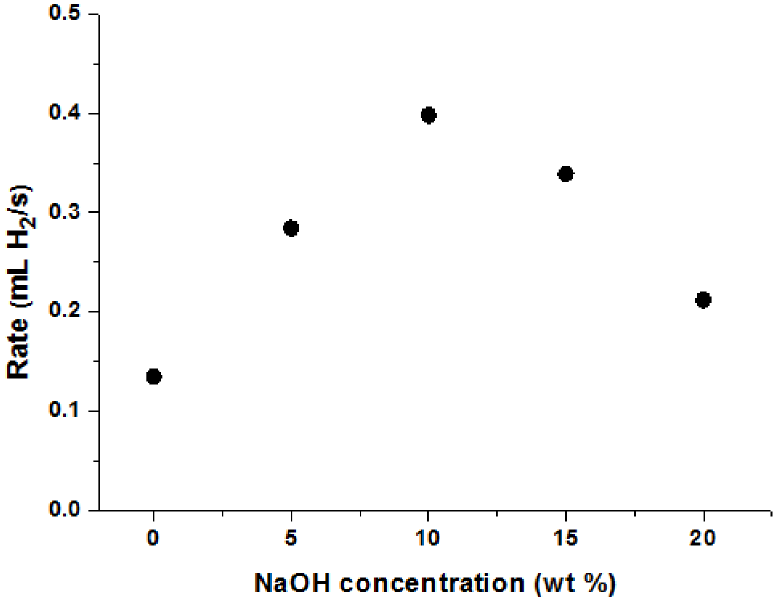

Figure 37. Plot of hydrogen generation rate (mL H_2/s) versus NaOH concentration (5.0, 10.0, 15.0, and 20.0 wt %) for the hydrolysis of $NaBH_4$ (150 mM, 50 mL) catalyzed by zeolite confined cobalt(0) nanoclusters ([Co] = 2.0 mM, with a cobalt content of 0.85 wt %) at 25 ± 0.1 °C.

Other catalysts for $NaBH_4$ hydrolysis reaction either increase or decrease the hydrogen generation rate with the increasing NaOH concentration [25a,76,184]. It was reported that some Ni- and Co-based alloy catalysts [50,76,184] exhibit faster hydrogen generation rate in basic $NaBH_4$ solution at higher NaOH concentrations, and the reverse is the case for Ru-based [25a,56] catalysts. Those results demonstrate that the effect of NaOH concentration on the $NaBH_4$ hydrolysis is greatly dependent on the nature of catalyst.

Although the accelerating effect of NaOH concentration on the hydrogen generation rate from the hydrolysis of $NaBH_4$ in the presence of metal catalysts is still not well-established, there is a plausible mechanism proposed by Holbrook and Twist [185]. According to this mechanism, metal (M)-catalyzed hydrolysis of $NaBH_4$ begins with the attachment of the borohydride ion to a catalytic site, forming two metal complexes ($M\text{-}BH_3^-$ and M-H). The $M\text{-}BH_3^-$ complex is then in equilibrium with BH_3, and this step is called as anodic step. BH_3 reacts with the OH- ion to generate $BH_3(OH)^-$ ion. The rate of reaction is determined by the cathodic step, where an electron is combined with a water molecule and an available site to form the M-H complex and OH^- ion. It is under the assumption that the reactivity of the $BH_3(OH)^-$ ion is similar to that of BH_4^-, establishing an equilibrium condition to form $MBH_2(OH)^-$ and M-H complexes. An increase in $[OH^-]$ drives the reaction (eq. 11) forward, and thus increases [M-H] through repeating reaction where $BH_3(OH)^-$-$BH_2(OH)_2^-$-$BH(OH)_3^-$-$B(OH)_4^-$ via the same mechanism. Finally, the $B(OH)_4^-$ reacts with Na^+ to produce $NaBO_2$. In cases, where the catalyst does not strongly bind the hydrogen (nonnoble metals scuh as Co or Ni), the [M-H] complex formed during the repeated reaction is rapidly converted to the overall reaction product, H_2, with the increasing reaction rates. The reverse is the case for the noble metal catalysts such as ruthenium or platinum [186].

$$2\,M + BH_4^- \longleftrightarrow MBH_3^- + M\text{-}H \tag{9}$$

$$MBH_3^- \longleftrightarrow BH_3 + M + e^- \tag{10}$$

$$BH_3 + OH^- \longrightarrow BH_3(OH)^- \tag{11}$$

$$M + e^- + H_2O \longrightarrow M\text{-}H + OH^- \tag{12}$$

$$M\text{-}H + M\text{-}H \longrightarrow 2\,M + H_2 \tag{13}$$

The decreasing trend in the hydrogen generation rate with the increasing NaOH concentration after 10 wt % is most probably due to the decreasing solubility of reaction byproduct, $NaBO_2$, and thus precipitating from the solution after exceeding the solubility limit. The precipitated $NaBO_2$ blocks the active site on the catalyst surface, hindering the contact of BH_4^- ion and the subsequent hydrolysis rate [74]. The accelerating effect of NaOH ensures a good efficiency for hydrogen generation during the hydrolysis reaction, compensating for a possible negative effect caused by reduced activity of water and a lower solubility of the reaction product at higher hydroxide concentrations [53]. It is noteworthy that a control test was performed to check whether the use of sodium hydroxide causes to leaching of cobalt from the catalyst. ICP analysis performed after the hydrolysis reaction in the presence of 10 wt % NaOH showed that the cobalt content in the catalyst is the same as before the reaction.

4.4. The Catalytic Activity of In-Situ Formed Zeolite Confined Cobalt(0) Nanoclusters in the Hydrolysis of Sodium Borohydride in Basic Medium

4.4.1. Kinetic Studies and the Determination of Activation Parameters for the Hydrolysis of Sodium Borohydride Catalyzed by Zeolite Confined Cobalt(0) Nanoclusters in Basic Medium

The zeolite confined cobalt(0) nanoclusters (with a cobalt content of 0.85 wt %) were also found to be highly active catalyst in the hydrolysis of sodium borohydride in basic medium liberating hydrogen gas. It should be noted that there is no self-hydrolysis or zeolite-Y catalyzed hydrolysis of $NaBH_4$ in basic solution. Figure 38 shows the plots of volume of generated hydrogen gas versus time during the catalytic hydrolysis of $NaBH_4$ solution in the presence of zeolite confined cobalt(0) nanoclusters with different concentrations in 10 wt % NaOH solution at 25.0 ± 0.1 °C. The hydrogen evolution starts without an induction period, indicating a rapid formation of the catalyst.

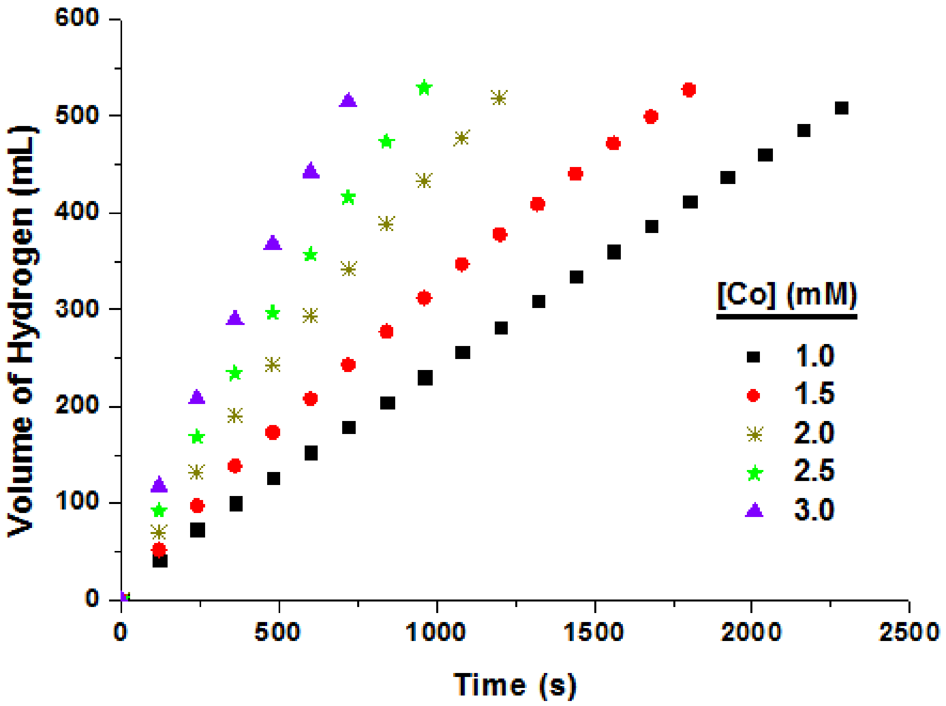

Figure 38. Plot of the volume of hydrogen (mL) versus time (s) for the hydrolysis of sodium borohydride ([$NaBH_4$] = 150 mM) in 10 wt % NaOH solution catalyzed by zeolite confined cobalt(0) nanoclusters (with a cobalt content of 0.85 wt %) at different cobalt concentrations ([Co] = 1.0, 1.5, 2.0, 2. 5, and 3.0 mM) at 25.0 ± 0.1 °C.

The rate of hydrogen generation calculated from the slope of the linear portion of plots in Figure 38 increases with the increasing cobalt catalyst concentration, as expected. Figure 39 shows the plot of rate of hydrogen generation versus cobalt catalyst concentrations, both in logarithmic scale. Based on Figure 39, A straight line with a slope of almost 1 is obtained from Figure 39 indicates that the hydrolysis of $NaBH_4$ in basic medium proceeds via first order with respect to cobalt catalyst concentration.

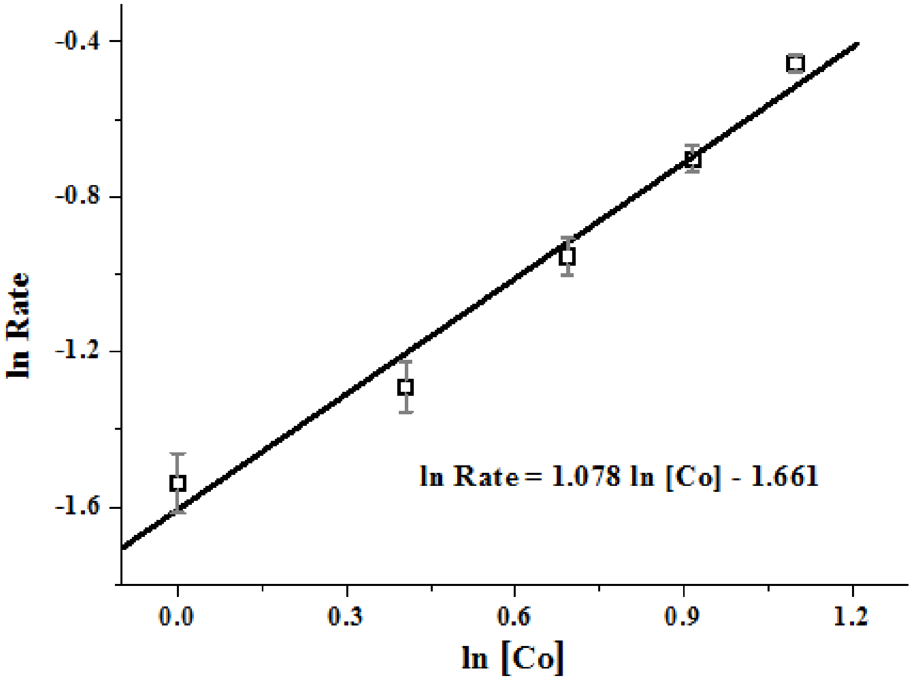

Figure 39. Plot of the hydrogen generation rate versus the catalyst concentration (both in logarithmic scale) for the zeolite confined cobalt(0) nanoclusters catalyzed hydrolysis of $NaBH_4$ ([$NaBH_4$] = 150 mM) in 10 wt % NaOH solution at 25.0 ± 0.1 °C.

The effect of $NaBH_4$ concentration on the rate of hydrogen generation was also investigated by carrying out a series of experiments starting with different initial concentrations of $NaBH_4$ while keeping the cobalt catalyst concentration constant at 2.0 mM in 10 wt % NaOH solution at 25.0 ± 0.1 °C. Figure 40 shows the plot of the generated hydrogen gas volume versus time for different initial concentrations of $NaBH_4$ (150, 300, 450, 600, and 750 mM).

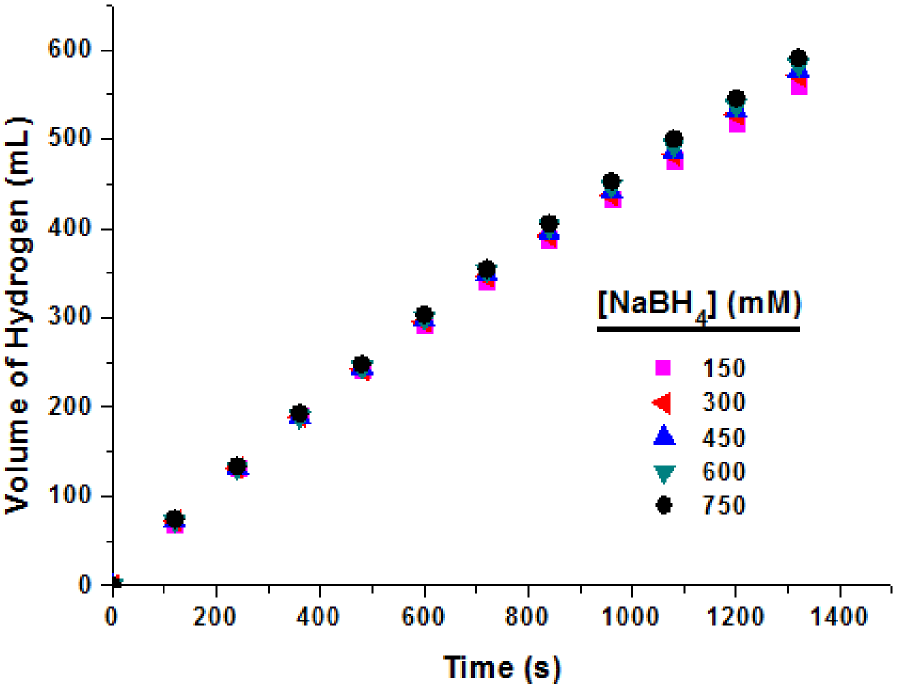

Figure 40. Plot of the volume of generated hydrogen gas (mL) versus time (s) for the zeolite confined cobalt(0) nanoclusters (with 0.85 wt % cobalt loading, [Co] = 2.0 mM) catalyzed hydrolysis of $NaBH_4$ solution (50 mL) in 10 wt % NaOH solution with different concentrations ([$NaBH_4$] = 150, 300, 450, 600, and 750 mM) at 25.0 ± 0.1 °C.

It is obvious from the plot of rate of hydrogen generation, calculated from the linear portion of the plots in Figure 40, versus $NaBH_4$ concentration, both in logarithmic scales (Figure 41) that the catalytic hydrolysis reaction proceeds via zero-order with respect to substrate concentration, and thus practically independent of the $NaBH_4$ concentration, at least in the studied range ([$NaBH_4$] = 150-750 mM) in the presence of 10 wt % NaOH.

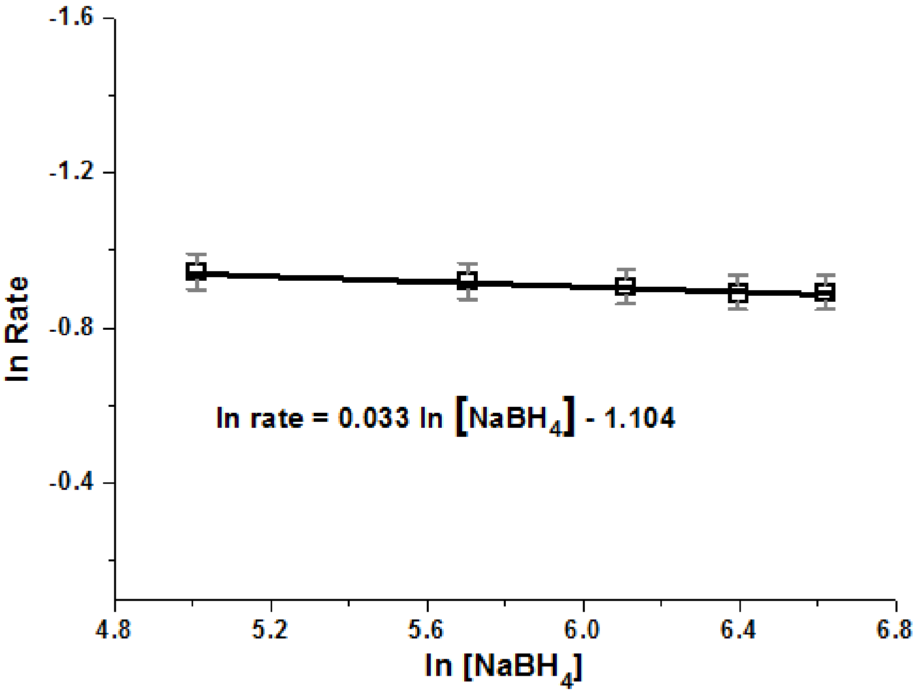

Figure 41. Plot of the rate of hydrogen generation versus the $NaBH_4$ concentration (both in logarithmic scale) in the hydrolysis of $NaBH_4$ catalyzed by zeolite confined cobalt(0) nanoclusters in 10 wt % NaOH solution at 25.0 ± 0.1 °C.

Consequently, the rate law for the catalytic hydrolysis of sodium borohydride in aqueous solution can be given as in Eq. 14,

$$\frac{-4d[NaBH_4]}{dt} = \frac{d[H_2]}{dt} = k[Co] \qquad (14)$$

The hydrolysis of sodium borohydride catalyzed by zeolite confined cobalt(0) nanoclusters was performed at various temperatures (25, 30, 35, 40, and 45 °C) starting with the initial substrate concentration of 150 mM $NaBH_4$ and an initial catalyst concentration of 2.0 mM Co in 10 wt % NaOH solution (Figure 42).

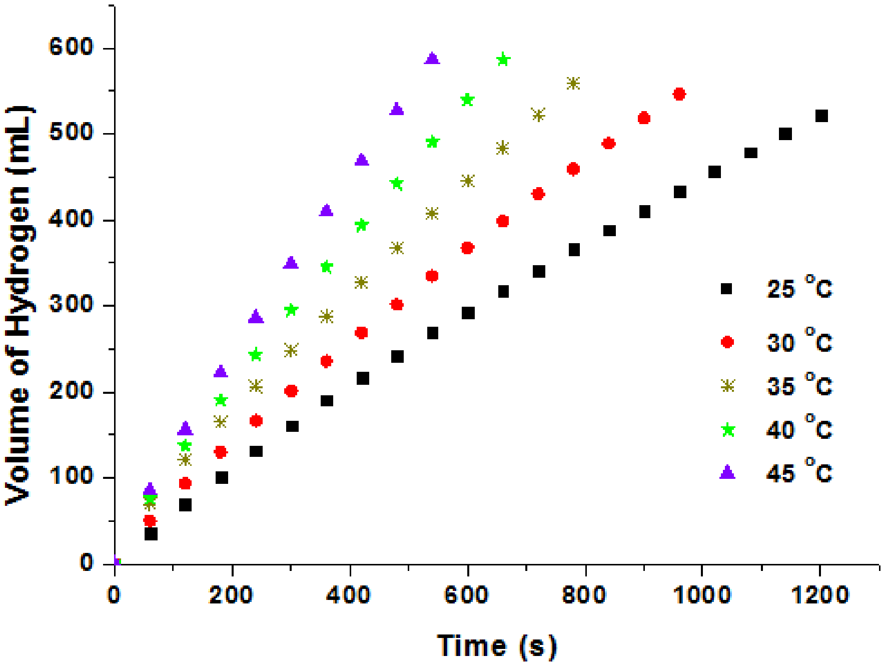

Figure 42. Plot of the volume of hydrogen (mL) versus time (s) for the hydrolysis of $NaBH_4$ (150 mM, 50 mL) catalyzed by zeolite confined cobalt(0) nanoclusters (with a cobalt content of 0.85 wt %, [Co] = 2.0 mM) in 10 wt % NaOH solution at different temperatures (25, 30, 35, 40, and 45 °C).

The values of rate constant k_{app} (Table A2 in the Appendix A) determined from the linear portions of the hydrogen volume versus time plots at five different temperatures are used to calculate the activation parameters. The activation energy was determined by using of Arrhenius Equation. A straight line with a slope of [-Ea/R] is obtained by the plot of ln k versus 1/T from Figure 43. The apparent activation energy, Ea^{app}, for the hydrolysis of $NaBH_4$ in basic medium is 34 ± 2 kJ/mol, which was calculated by using the slope of Arrhenius plot.

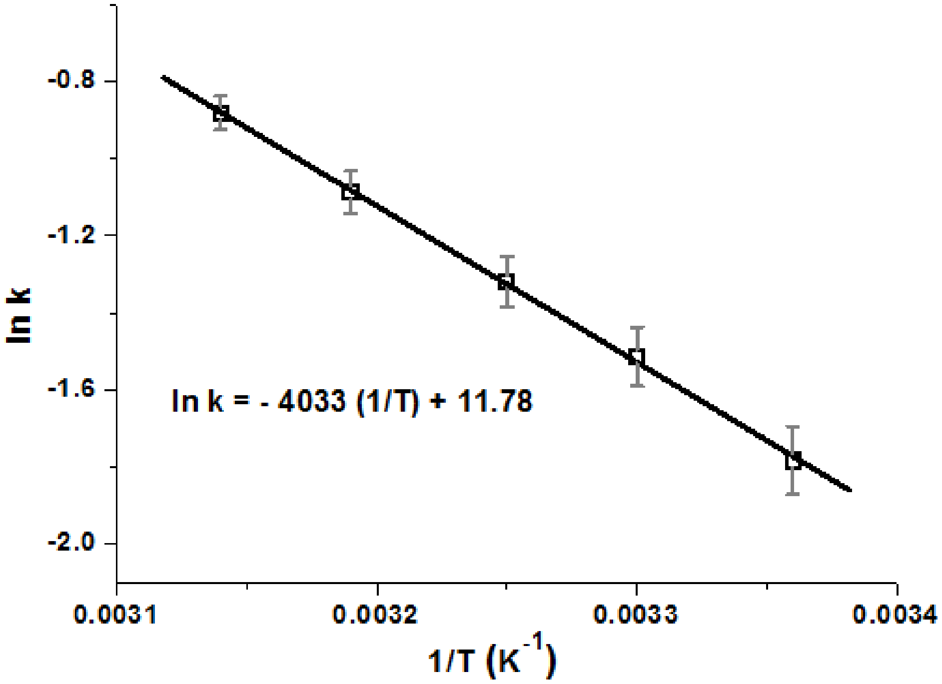

Figure 43. The Arrhenius plot for the zeolite confined cobalt(0) nanoclusters catalyzed hydrolysis of sodium borohydride in 10.0 wt % NaOH solution.

Activation energies for the hydrolysis of sodium borohydride in basic medium catalyzed by other catalysts and the catalyst used in this study are listed in Table 1 for comparison.

Table 1. The catalyst systems employed in the hydrolysis of sodium borohydride in the basic medium and obtained activation energies in different reaction conditions.

Catalyst	**Ea (kJ/mol)**	**$NaBH_4$**	**NaOH**	**Reference**
Ni-Co-B	62	0.16 g	15 %	[53]
Co-B/Ni foam	33	20 %	10 %	[55]
Ni_xB	38	1.5 %	10 %	[76]
Ru/IRA-400	47	20 %	10 %	[187]
Co/γ-Al_2O_3	33	5 %	5 %	[50]
Co/C	46	5 %	5 %	[50]
Carbon-supported Co-B	58	0.2 M	20 mmol	[107]
Pd-C powder	28	0.005 M	pH=13	[75]
Ru/$LiCoO_2$	68	10 %	5 %	[56]
Ru/IR-120	50	5 %	1 %	[78]
Ru/IRA-400	56	7.5 %	1 %	[25a]
Ni210 powder	63	0.2 g	10 %	[77]
Co powder	42	0.2 g	10 %	[77]
CoB	45	25 %	3 %	[188]
Co-Mn-B nanocomposites	55	5 %	5 %	[54]
PtPd-Carbon nanotubes	19	0.015 M	pH=13	[65]
Co-P	60	10 %	1 %	[59]
Co/AC	44	5 %	5 %	[58]
Co-W-B/Ni	29	20 %	5 %	[57]
PVP stabilized Co(0) NCs	37	0.15 M	5 %	[193]
Ru/Graphite	61	5 %	5 %	[70]
PtPd@CNT	19	0.15 M	1 %	[65]
Zeolite confined Co(0) NCs	34	0.15 M	10 %	[This study]

The enthalpy of activation, $\Delta H^{\#}$ and the entropy of activation, $\Delta S^{\#}$ were calculated by using of Eyring Equation. A straight line with a slope of [$-\Delta H^{\#}/R$] and an intercept of [$\ln k_b/h + \Delta S^{\#}/R$] are obtained by the plot of ln k/T versus 1/T from Figure 44.

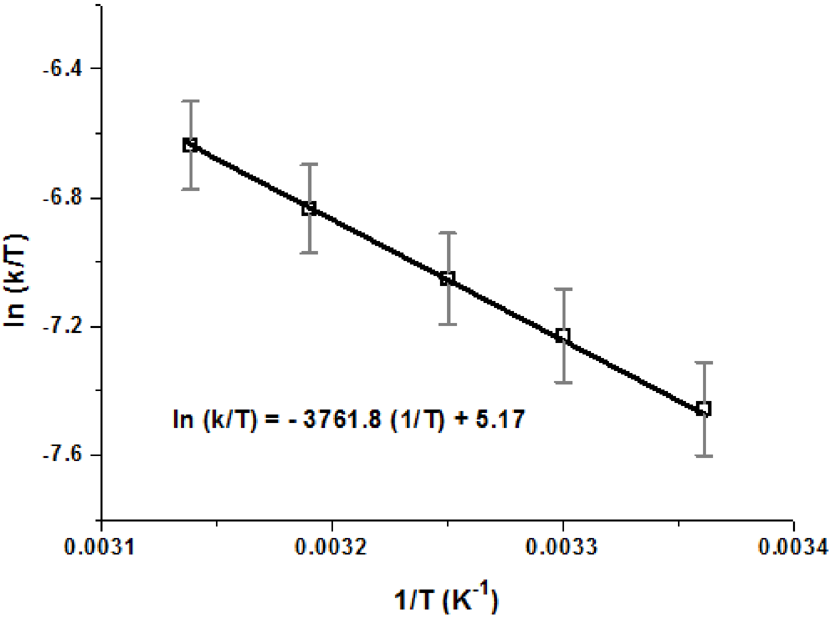

Figure 44. The Eyring plot for the zeolite confined cobalt(0) nanoclusters catalyzed hydrolysis of sodium borohydride in 10.0 wt % NaOH solution.

The enthalpy of activation, $\Delta H^{\#}$, for the hydrolysis of sodium borohydride in basic medium catalyzed by zeolite confined cobalt(0) nanoclusters is 31 ± 2 kJ/mol which was calculated by using the slope of Eyring plot while the entropy of activation, $\Delta S^{\#}$, obtained by using the intercept of Eyring plot was calculated as -154 ± 6 J/mol.K. It is noteworthy that the activation energy and enthalpy for the hydrolysis of sodium borohydride in basic solution are both lower than those found for the same reaction catalyzed by zeolite confined cobalt(0) nanoclusters in the absence of sodium hydroxide.

4.4.2. Isolability and Reusability of Zeolite Confined Cobalt(0) Nanoclusters in the Hydrolysis of Sodium Borohydride in Basic Medium

The isolability and reusability of the zeolite confined cobalt(0) nanoclusters in the hydrolysis of sodium borohydride solution were also tested. After the hydrolysis of sodium borohydride solution (150 mM, 50 mL) catalyzed by zeolite confined cobalt(0) nanoclusters ([Co] = 2.0 mM) in 10 wt % NaOH solution at 25 ± 0.1 °C, the catalyst was isolated as black powders. The isolated zeolite confined cobalt(0) nanoclusters are redispersible in basic solution of (10 wt % NaOH) sodium borohydride and still active catalyst. Figure 45 shows the plot of hydrogen volume generated versus time for zeolite confined cobalt(0) nanoclusters catalyzed hydrolysis of sodium borohydride in 10 wt % NaOH solution at 25.0 ± 0.1 °C at the first, third, and fifth catalytic runs, respectively. The inset in Figure 44 shows the corresponding percent retained catalytic activity and the conversion of sodium borohydride at those catalytic runs. It is noteworthy that zeolite confined cobalt(0) nanoclusters retain 59 % of their initial catalytic activity at the fifth run in the hydrolysis of sodium borohydride in basic medium. The activity loss may be attributed to the passivation of nanoclusters surface by increasing the amount of boron products, e.g. metaborate, which might decrease the accessibility of active sites. Besides, the slight decrease (from 0.85 to 0.79 wt %) in the cobalt content of the sample, determined by ICP analysis performed after fifth run of the catalytic hydrolysis of sodium borohydride in 10 wt % NaOH solution at 25.0 ± 0.1 °C, may account for the greater decrease in catalytic activity of the catalyst at the fifth run compared to previous ones. Despite this activity loss to some extent, it can be concluded that the zeolite confined cobalt(0) nanoclusters are isolable, redispersible, and yet catalytically active catalyst in the hydrolysis of sodium borohydride in basic medium, too. Additionally, it should be noted that there is no structural change in the framework of zeolite-Y after fifth catalytic run in the hydrolysis of sodium borohydride in basic medium as evidenced by XRD analysis (Figure B1 in Appendix B).

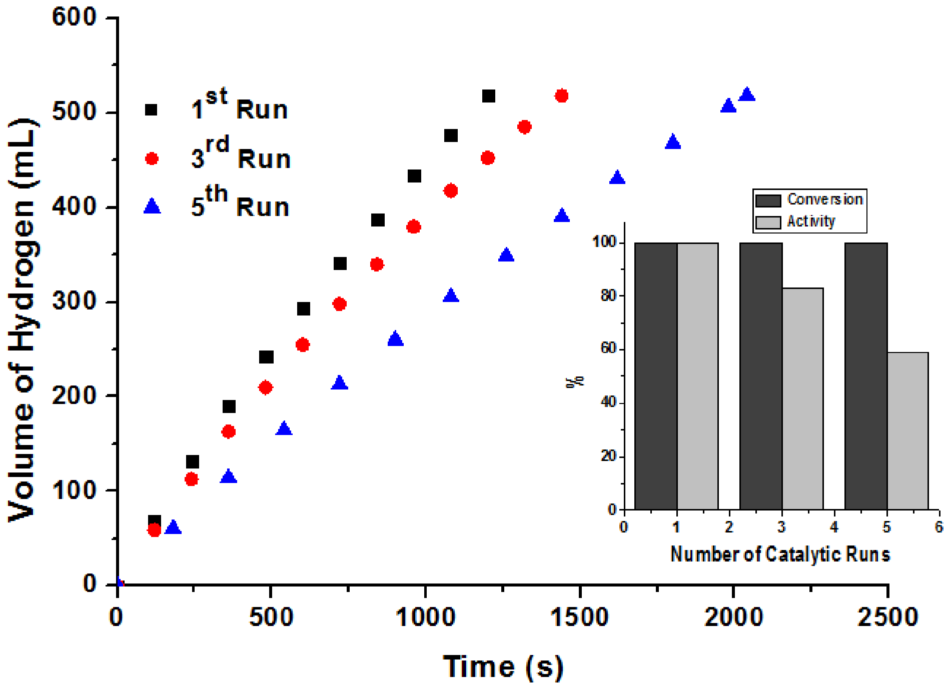

Figure 45. Plot of the volume of hydrogen (mL) versus time (s) for the hydrolysis of $NaBH_4$ (150 mM, 50 mL) catalyzed by zeolite confined cobalt(0) nanoclusters (with a cobalt content of 0.85 wt %, [Co] = 2.0 mM) in 10 wt % NaOH solution at first, third, and fifth catalytic runs. The inset shows the corresponding percent retained catalytic activity and the conversion of sodium borohydride at those catalytic runs.

4.4.3. Catalytic Lifetime of Zeolite Confined Cobalt(0) Nanoclusters in the Hydrolysis of Sodium Borohydride in Basic Medium

A lifetime experiment for the zeolite confined cobalt(0) nanoclusters catalyst in the hydrolysis of sodium borohydride was started with 2.0 mM zeolite confined cobalt(0) nanoclusters in 10 wt % NaOH solution at 25.0 ± 0.1 ºC. They provide a record total turnover value (36000) reported [189] for the hydrolysis of sodium borohydride in basic medium (Figure 46) and maximum TOF value of 880 mol H_2 (mol Co)$^{-1}$ h^{-1}. The rate of hydrogen generation also slowed down as the reaction proceeds may be because of increasing viscosity of the solution that makes it to be hardly stirred. Therefore, this TTO value should be considered as a lower limit and a much higher value might be obtained when the increase in viscosity is avoided.

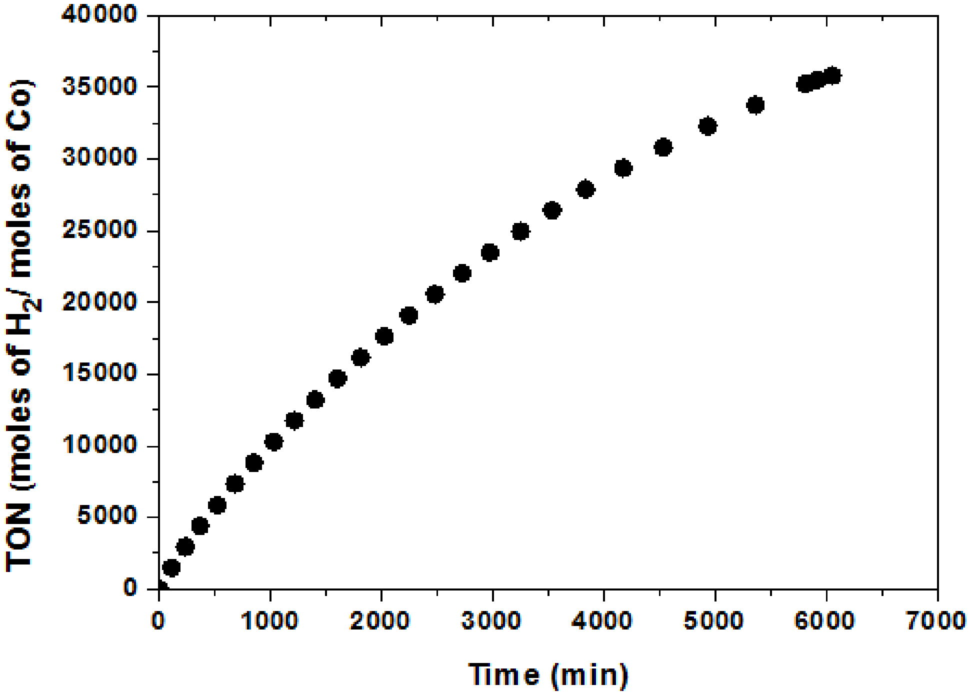

Figure 46. Graph of variation in TON with time for the zeolite confined cobalt(0) nanoclusters catalyzed hydrolysis of $NaBH_4$ in 10 wt % NaOH at 25 ± 0.1 °C.

4.5. The Catalytic Activity of Zeolite Confined Cobalt(0) Nanoclusters in the Hydrolysis of Ammonia Borane

4.5.1. The Effect of Cobalt Loading on the Catalytic Activity of Zeolite Confined Cobalt(0) Nanoclusters in the Hydrolysis of Ammonia Borane

Zeolite cobalt(0) nanoclusters were tested as catalyst in the hydrolysis of ammonia borane and found to be highly active catalyst in liberating hydrogen gas. The first issue to be addressed is the dependence of the catalytic activity of zeolite confined cobalt(0) nanoclusters in the hydrolysis of ammonia borane on the cobalt loading of zeolite-Y. As expected, cobalt content of the catalyst is dependent on the concentration of aqueous solution of cobalt(II) nitrate used for ion-exchange. Thus, the cobalt content in the catalyst can be regulated by changing the concentration of cobalt(II) ion in the slurry used for ion exchange.

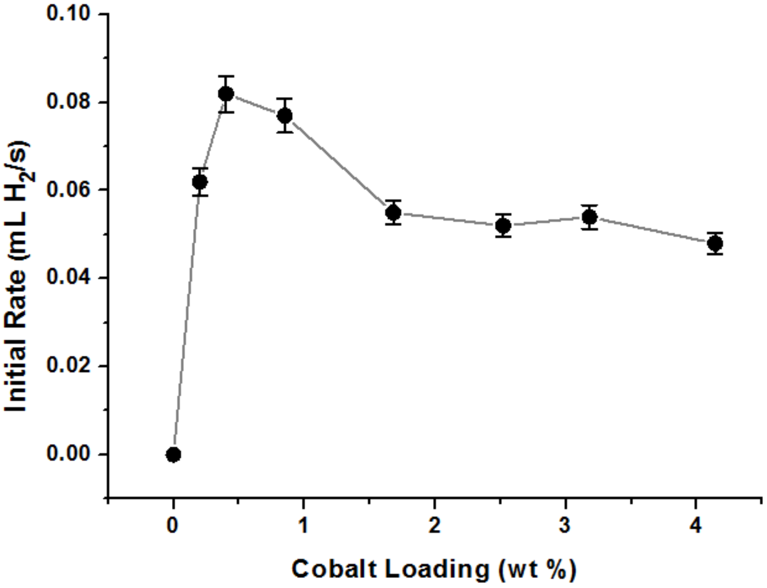

Figure 47. The initial rate of hydrogen generation (mL of H_2/s) versus cobalt loadings (in wt % Co) for the zeolite confined cobalt(0) nanoclusters (in all [Co] = 2.0 mM) catalyzed hydrolysis of H_3NBH_3 (100 mM, 20 mL) at 25 ± 0.1 °C.

In this way, the catalysts with different cobalt loading were prepared and tested in the hydrolysis of ammonia borane. Figure 47 shows the variation in the catalytic activity of zeolite confined cobalt(0) nanoclusters with cobalt loading of the zeolite in the hydrolysis of ammonia borane, which is similar to the activity variation observed for the hydrolysis of sodium borohydride [189].

The variation in catalytic activity reflects the accessibility of cobalt(0) nanoclusters in the zeolite cages by the substrate. The highest catalytic activity is obtained by using the zeolite confined cobalt(0) nanoclusters containing 0.40 wt % Co, most probably in the supercage (α-cage) of zeolite-Y, where the substrate more readily access cobalt(0) nanoclusters compared to the β-cage of zeolite-Y. As the cobalt loading increases, the nanoclusters might go to the less accessible sodalite cages as well, or nanoclusters in the supercages become larger and block the entrance to the supercages. In order to keep the cobalt concentration at a certain level in the catalytic reaction using the total catalyst amount as small as possible, the zeolite confined cobalt(0) nanoclusters catalyst with 0.85 wt % cobalt loading was chosen to be used in the further experiments.

4.5.2. Kinetic Studies and the Determination of Activation Parameters for the Hydrolysis of Ammonia Borane Catalyzed by Zeolite Confined Cobalt(0) Nanoclusters

The kinetics of the hydrolysis of ammonia borane catalyzed by the zeolite confined cobalt(0) nanoclusters was studied depending on the catalyst concentration, substrate concentration and temperature. The zeolite confined cobalt(0) nanoclusters were also found to be highly active catalyst in the hydrolysis of ammonia borane liberating hydrogen gas. Figure 48 shows the plots of the volume of hydrogen generated versus time during the catalytic hydrolysis of ammonia borane solution in the presence of zeolite confined cobalt(0) nanoclusters with a cobalt loading of 0.85 wt % in different cobalt concentrations at 25.0 ± 0.1 °C.

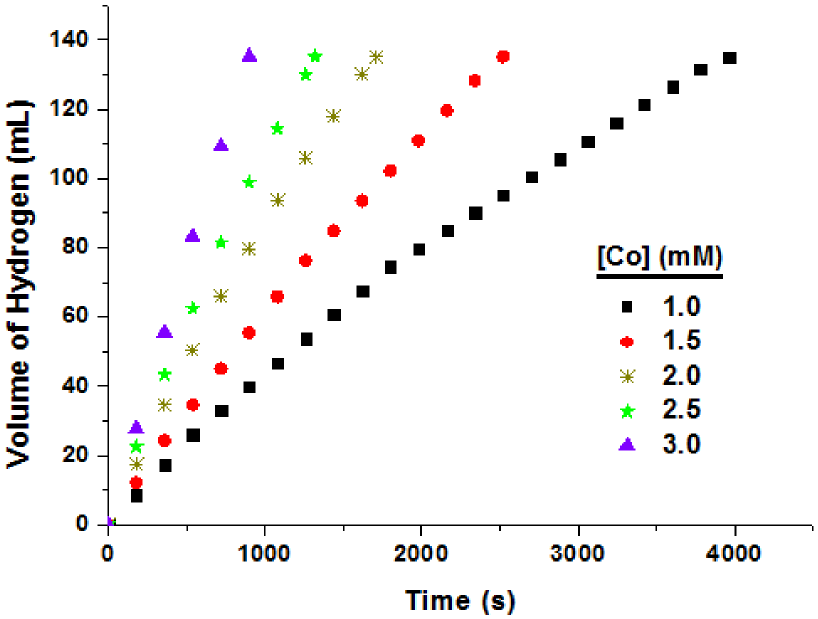

Figure 48. Plot of the volume of hydrogen (mL) versus time (s) for the hydrolysis of ammonia borane ([H_3NBH_3] = 100 mM) catalyzed by zeolite confined cobalt(0) nanoclusters (with a cobalt content of 0.85 wt %) at different cobalt concentrations ([Co] = 1.0, 1.5, 2.0, 2. 5, and 3.0 mM) at 25.0 ± 0.1 °C.

The rate of hydrogen generation calculated from the slope of the linear portion of the plots in Figure 48 increases with the increasing cobalt catalyst concentration, as expected. Figure 49 shows the plot of hydrogen generation rate versus cobalt catalyst concentrations, both in logarithmic scale. A straight line with a slope of almost 1 obtained from Figure 49 indicates that hydrolysis of H_3NBH_3 proceeds via first order with respect to cobalt catalyst concentration.

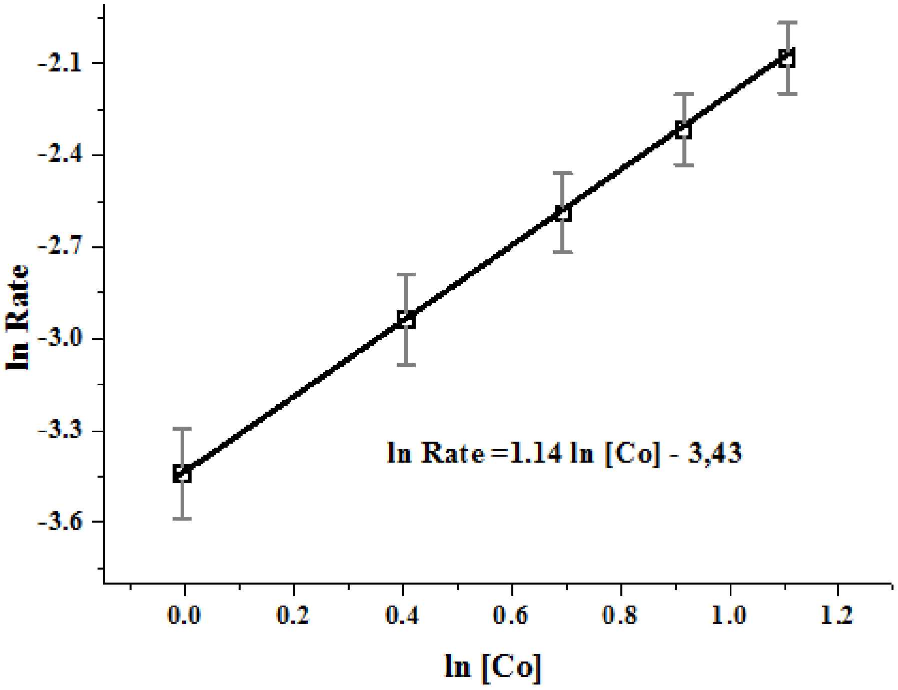

Figure 49. Plot of the hydrogen generation rate versus the catalyst concentration (both in logarithmic scale) for the zeolite confined cobalt(0) nanoclusters catalyzed hydrolysis of H_3NBH_3 ($[H_3NBH_3]$ = 100 mM) at 25.0 ± 0.1 °C.

The effect of H_3NBH_3 concentration on the rate of hydrogen generation was also investigated by carrying out a series of experiments starting with different initial concentrations of H_3NBH_3 while keeping the cobalt catalyst concentration constant at 2.0 mM at 25.0 ± 0.1 °C. Figure 50 shows the plot of the volume of hydrogen gas generated versus time for different initial concentrations of H_3NBH_3 (100, 150, 200, 250, and 300 mM).

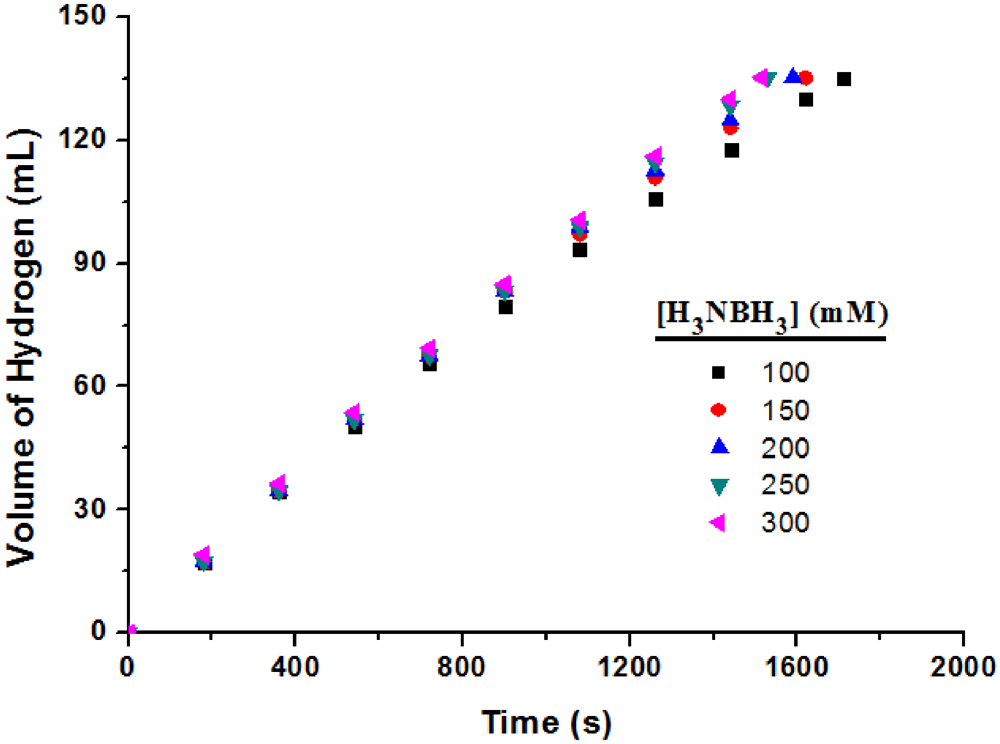

Figure 50. Plot of the volume of hydrogen (mL) versus time (s) for the zeolite confined cobalt(0) nanoclusters (with a cobalt content of 0.85 wt %, [Co] = 2.0 mM) catalyzed hydrolysis of H_3NBH_3 solution (20 mL) with different concentrations ([H_3NBH_3] = 100, 150, 200, 250, and 300 mM) at 25.0 ± 0.1 °C.

It is obvious from the plot of the rate of hydrogen generation, calculated from the linear portion of the plots in Figure 50, versus H_3NBH_3 concentration, both in logarithmic scales (Figure 51) that the catalytic hydrolysis reaction of H_3NBH_3 proceeds via zero-order with respect to H_3NBH_3 concentration, and thus practically independent of the H_3NBH_3 concentration, at least in the studied range.

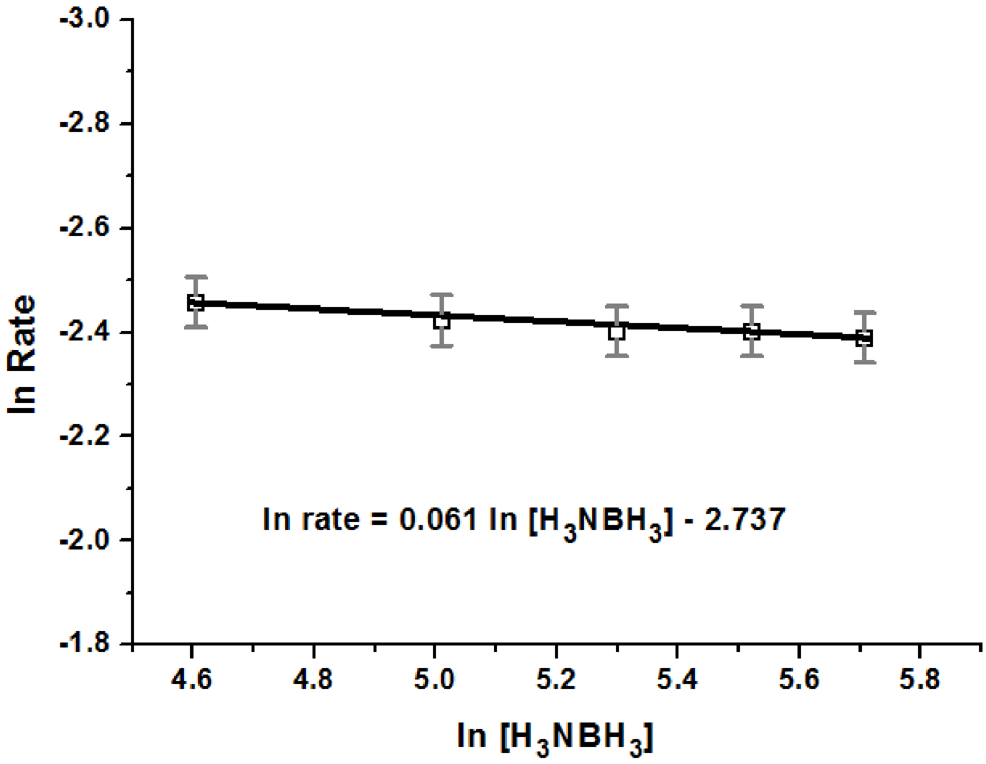

Figure 51. Plot of the hydrogen generation rate versus the substrate concentration (both in logarithmic scale) in the hydrolysis of H_3NBH_3 catalyzed by zeolite confined cobalt(0) nanoclusters at 25.0 ± 0.1 °C.

Consequently, the rate law for the catalytic hydrolysis of ammonia borane can be given as in Eq. 15,

$$\frac{-3d[\mathrm{NH_3BH_3}]}{dt} = \frac{d[\mathrm{H_2}]}{dt} = k[\mathrm{Co}] \tag{15}$$

The hydrolysis of ammonia borane catalyzed by zeolite confined cobalt(0) nanoclusters was performed at various temperatures (25, 30, 35, 40, and 45 °C) starting with the initial substrate concentration of 100 mM H_3NBH_3 and an initial catalyst concentration of 2.0 mM Co (Figure 52).

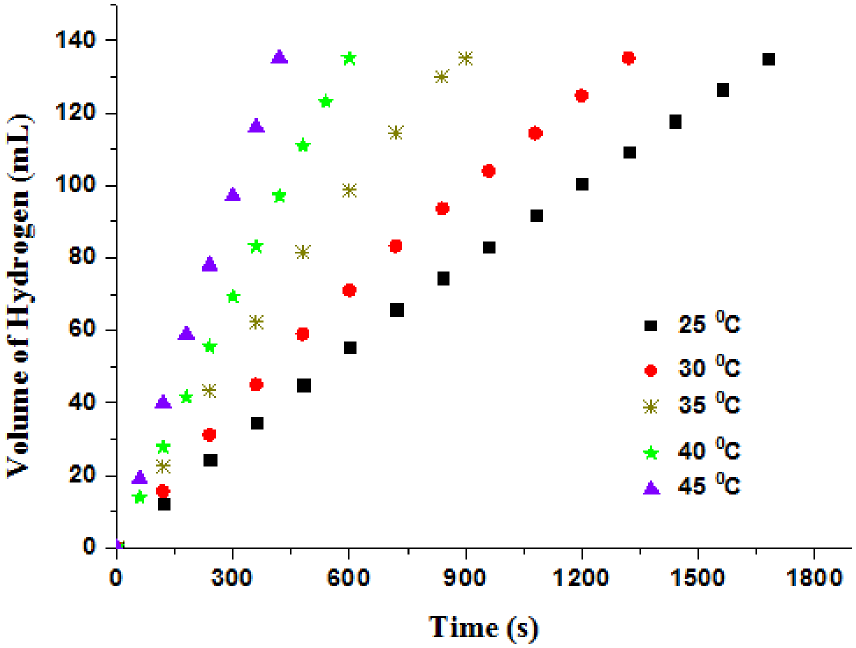

Figure 52. Plot of the volume of hydrogen (mL) versus time (s) for the hydrolysis of H_3NBH_3 (100 mM, 20 mL) catalyzed by zeolite confined cobalt(0) nanoclusters (with a cobalt content of 0.85 wt %, [Co] = 2.0 mM) at different temperatures (25, 30, 35, 40, and 45 °C).

The values of rate constant k_{app} (Table A3 in the Appendix A) determined from the linear portions of the hydrogen volume versus time plots at five different temperatures are used to calculate the activation parameters. The activation energy was determined by using of Arrhenius Equation. A straight line with a slope of [-Ea/R] is obtained by the plot of ln k versus 1/T from Figure 53. The apparent activation energy, Ea^{app}, for the hydrolysis of H_3NBH_3 is 56 ± 2 kJ/mol, which was calculated by using the slope of Arrhenius plot.

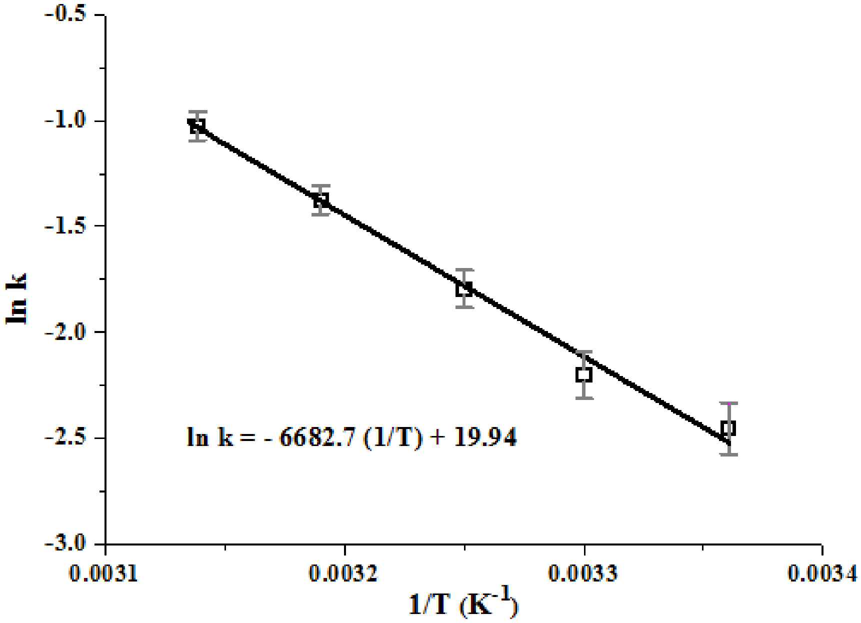

Figure 53. The Arrhenius plot for the zeolite confined cobalt(0) nanoclusters catalyzed hydrolysis of ammonia borane.

Activation energies for the hydrolysis of ammonia borane catalyzed by other catalysts and the catalyst used in this study are listed in Table 2 for comparison. Apart from the γ-Al_2O_3 supported Pt, Rh, Ru particles [190], carbon supported Ni-Ag particles [92], laurate-stabilized ruthenium(0) nanoclusters [194], PSSA-co-MA stabilized ruthenium(0) and palladium(0) nanoclusters [110], and $Pt_{0.65}Ni_{0.35}$ nanoparticles [97]; the zeolite confined cobalt(0) nanoclusters provide the lowest activation energy for the hydrolysis of ammonia borane.

Table 2. Activation energies for the hydrolysis of ammonia borane obtained by using various catalyst systems.

Catalyst	**Ea (kJ/mol)**	**Reference**
Pt/γ-Al_2O_3	21	[190]
Rh/γ-Al_2O_3	21	[190]
Ru/γ-Al_2O_3	23	[190]
K_2PtCl_6	87	[86]
$Ni_{0.97}$-$Pt_{0.03}$	57	[87]
Co/γ-Al_20_3	62	[85]
Ru/C	76	[88]
NiAg/C	52	[92]
Bulk Nickel	70	[191]
$Pt_{0.65}Ni_{0.35}$ NPs	39	[97]
ZFS Rh(0) NCs	67	[192]
PVP-stabilized Co(0) NCs	63	[193]
PSSA-co-MA stabilized Ru(0) NCs	54	[110]
PSSA-co-MA stabilized Pd(0) NCs	44	[110]
Laurate-stabilized Ru(0) NCs	47	[194]
Co-Ni-P/Pd-TiO_2	55	[104]
Pd-PVB-TiO_2	56	[105]
Co-Mo-B/Ni foam	44	[99]
Zeolite confined Co(0) NCs	56	[This study]

The enthalpy of activation, $\Delta H^{\#}$ and the entropy of activation, $\Delta S^{\#}$ were calculated by using of Eyring Equation. A straight line with a slope of [$-\Delta H^{\#}/R$] and an intercept of [$\ln k_b/h + \Delta S^{\#}/R$] are obtained by the plot of ln k/T versus 1/T from Figure 54.

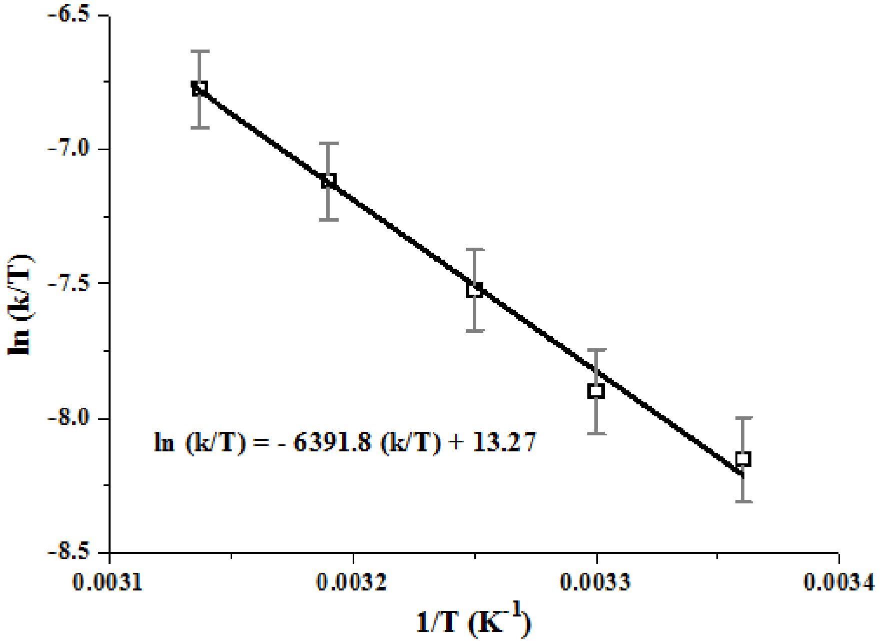

Figure 54. The Eyring plot for the zeolite confined cobalt(0) nanoclusters catalyzed hydrolysis of ammonia borane.

The enthalpy of activation, $\Delta H^{\#}$, for the hydrolysis of ammonia borane catalyzed by zeolite confined cobalt(0) nanoclusters is 53 ± 2 kJ/mol which was calculated by using the slope of Eyring plot while the enthropy of activation, $\Delta S^{\#}$, obtained by using the intercept of Eyring plot was calculated as - 87 ± 4 J/mol.K. A plausible mechanism for the metal-catalyzed hydrolysis of ammonia borane including overall reaction may be as follows (Figure 55);

$$M + H_3NBH_3 + 4\,H_2O \longrightarrow M + NH_4B(OH)_4 + 3\,H_2$$

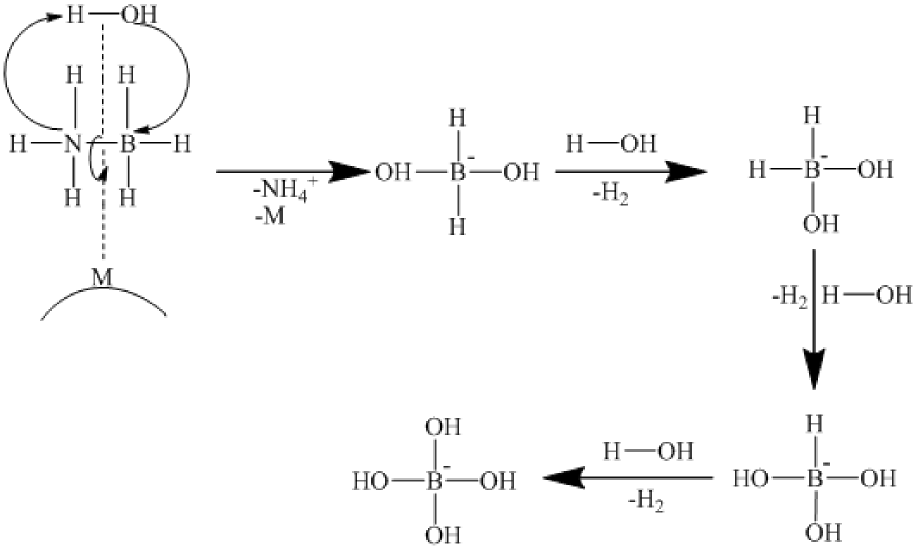

Figure 55. The overall reaction and the plausible mechanism for the metal-catalyzed hydrolysis of ammonia borane.

4.5.3. Isolability and Reusability of Zeolite Confined Cobalt(0) Nanoclusters in the Hydrolysis of Ammonia Borane

The zeolite confined cobalt(0) nanoclusters catalyst was also tested for the isolability and reusability in the hydrolysis of ammonia borane. After the complete hydrolysis of 100 mM ammonia borane solution catalyzed by 2.0 mM zeolite confined cobalt(0) nanoclusters at 25.0 ± 0.1 °C, the catalyst was isolated by suction filtration and dried under nitrogen atmosphere. The isolated zeolite confined cobalt(0) nanoclusters are redispersible in aqueous solution, and yet active catalyst in the hydrolysis of ammonia borane. Figure 56 shows the plot of hydrogen volume generated versus time for zeolite confined cobalt(0) nanoclusters catalyzed hydrolysis of ammonia borane at 25.0 ± 0.1 °C at the first, third, and fifth catalytic runs, respectively. The inset in Figure 56 shows the corresponding percent retained catalytic activity and the conversion of ammonia borane at those catalytic runs. The zeolite confined cobalt(0) nanoclusters still retain 69 % of their initial catalytic activity at the fifth run with a complete release of hydrogen. The decrease in catalytic activity in subsequent runs may be due to the passivation of nanoclusters surface by increasing amount of boron products, e.g. metaborate, which might decrease the accessibility of active sites [195], since the ICP analysis of the catalyst sample after catalytic reaction gave the same cobalt content for the zeolite confined cobalt(0) nanoclusters as before the reaction. Additionally, it should be noted that there is no structural change in the framework of zeolite-Y after fifth catalytic run in the hydrolysis of ammonia borane as evidenced by XRD analysis (Figure B2 in Appendix B).

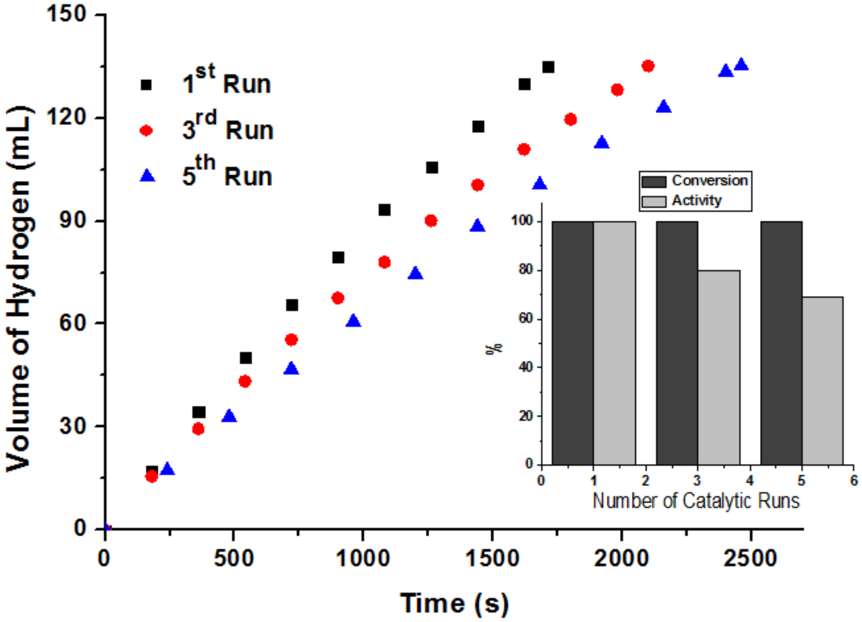

Figure 56. Plot of the volume of hydrogen (mL) versus time (s) for the hydrolysis of H_3NBH_3 (100 mM, 20 mL) catalyzed by zeolite confined cobalt(0) nanoclusters (with a cobalt content of 0.85 wt %, [Co] = 2.0 mM) at first, third, and fifth catalytic runs. The inset shows the corresponding percent retained catalytic activity and the conversion of ammonia borane at those catalytic runs.

4.5.4. Catalytic Lifetime of Zeolite Confined Cobalt(0) Nanoclusters in the Hydrolysis of Ammonia Borane

A lifetime experiment for the zeolite confined cobalt(0) nanoclusters catalyst in the hydrolysis of ammonia borane was started with 2.0 mM zeolite confined cobalt(0) nanoclusters at 25.0 ± 0.1 ºC. Figure 57 shows the variation in turnover number (TON) during the hydrolysis of ammonia borane catalyzed by zeolite confined cobalt(0) nanoclusters at 25.0 ± 0.1 °C.

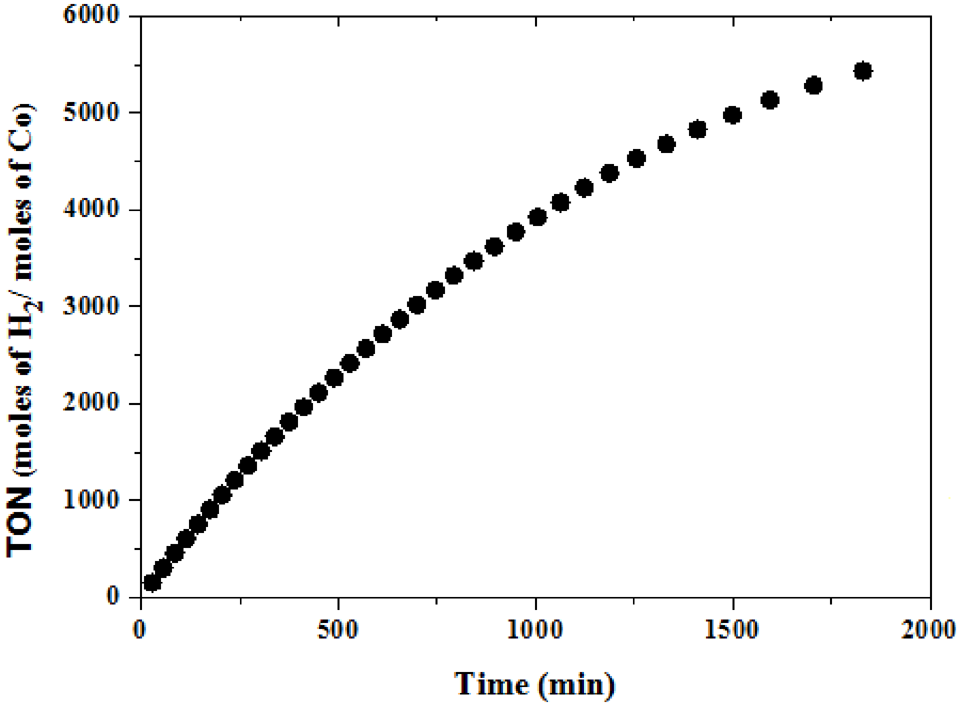

Figure 57. Graph for the variation in TON (turnover number) with time (min) for the zeolite confined cobalt(0) nanoclusters catalyzed hydrolysis of ammonia borane at 25 ± 0.1 °C.

They provide 5450 turnovers over 30 h in the hydrolysis of ammonia borane. This is a reasonable value obtained by using such a first raw transition metal, since the highest TTO number for the catalytic hydrolysis of ammonia borane at room temperature has been reported to be 51720 obtained by using the precious ruthenium metal [110]. The hydrogen generation slows down as the reaction proceeds, may be because of increasing viscosity of the solution or deactivation effect of increasing metaborate concentration. Therefore, this TTON value should be considered as a lower limit and much higher value might be obtained when the increase in viscosity is avoided.

CHAPTER 5

CONCLUSIONS

In summary, my study on the preparation and characterization of zeolite confined cobalt(0) nanoclusters as catalyst for hydrogen generation from the hydrolysis of sodium borohydride and ammonia borane has led to the following conclusions and insights;

Part I. Preparation and Characterization of Zeolite Confined Cobalt(0) Nanoclusters

- The zeolite confined cobalt(0) nanoclusters were easily prepared by following a two-step procedure: the ion exchange of Co^{2+} ions with the extra framework Na+ cations in zeolite-Y, followed by reduction of the Co^{2+} ions in the cavities of zeolite-Y by sodium borohydride in aqueous solution at room temperature.

- The zeolite confined cobalt(0) nanoclusters were characterized by using ICP-OES, XRD, IR, HRTEM, SEM, EDX, XPS, DR-UV-Vis, Raman spectroscopy and N_2 adsorption-desorption technique.

- The XRD and IR analyses confirm that the preparation method did not cause any alteration in the framework lattice and the crystallinity of zeolite-Y.

- HRTEM and DR-UV-Vis analyses confirm that zeolite confined cobalt(0) nanoclusters were formed within the cavities of zeolite-Y.

Part II. Hydrolysis of Sodium Borohydride

- The kinetic studies of the zeolite confined cobalt(0) nanoclusters catalyzed hydrolysis of sodium borohydride performed individually in aqueous and basic (10 wt % NaOH) solutions show that the catalytic hydrolysis reaction proceeds with first order dependency with respect to the catalyst concentration and zeroth order dependency with respect to the substrate concentration for both cases.

$$NaBH_4 + 2\,H_2O \xrightarrow[\text{at RT in } H_2O \text{ or 10 wt \% NaOH solution}]{\text{zeolite confined cobalt(0) nanoclusters}} NaBO_2 + 4\,H_2$$

$$-\frac{4\,d[NaBH_4]}{dt} = \frac{d[H_2]}{dt} = k\,[Co]$$

- The plausible mechanism of the hydrolysis of $NaBH_4$ in the presence of metal catalysts in aqueous solution may be as follows:

$$M + NaBH_4 + 4\,H_2O \longrightarrow M + NaB(OH)_4 + 4\,H_2$$

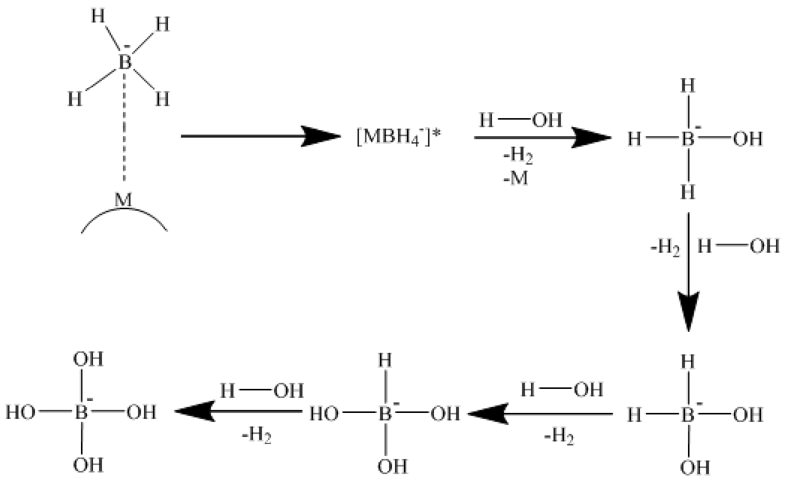

- The established mechanism [185] for the accelerating effect of NaOH concentration on the hydrogen generation rate from the hydrolysis of $NaBH_4$ can be best described as follows;

$$2\,M + BH_4^- \longleftrightarrow MBH_3^- + M\text{-}H$$

$$MBH_3^- \longleftrightarrow BH_3 + M + e^-$$

$$BH_3 + OH^- \longrightarrow BH_3(OH)^-$$

$$M + e^- + H_2O \longrightarrow M\text{-}H + OH^-$$

$$M\text{-}H + M\text{-}H \longrightarrow 2\,M + H_2$$

- The accelerating effect of NaOH concentration on the hydrogen generation rate from the hydrolysis of $NaBH_4$ ensures a good efficiency for hydrogen generation during the hydrolysis reaction, compensating for a possible negative effect caused by reduced activity of water and a lower solubility of the reaction product at higher hydroxide concentrations.

- Zeolite confined cobalt(0) nanoclusters formed in situ during the hydrolysis of sodium borohydride provided TTO numbers of 12000 and 35000 mol H_2 (mol Co)$^{-1}$ in aqueous and basic (10 wt % NaOH) solutions at room temperature, respectively. The value obtained from the hydrolysis of basic sodium borohydride is a record TTO number reported in the literature for this hydrolysis reaction and may stem from the enhancement effect of NaOH.

- The activation energies for the zeolite confined cobalt(0) nanoclusters catalyzed hydrolysis of sodium borohydride in aqueous and basic media were calculated to be $E_a = 55 \pm 2$ and $E_a = 34 \pm 2$ kJ/mol, respectively.

- The activation enthalpy ($\Delta H^{\#}$) and activation entropy ($\Delta S^{\#}$) of zeolite confined cobalt(0) nanoclusters catalyzed hydrolysis of sodium borohydride were calculated to be $\Delta H^{\#} = 52 \pm 2$ kJ/mol (in aqueous medium) and $\Delta H^{\#} = 31 \pm 2$ kJ/mol (in basic medium); $\Delta S^{\#} = -94 \pm 4$ J/K·mol (in aqueous medium) and $\Delta S^{\#} = -154 \pm 6$ J/K·mol (in basic medium). These values are indicative for an associative mechanism for the zeolite confined cobalt(0) nanoclusters catalyzed hydrolysis of sodium borohydride in both aqueous and basic media.

Part III. Hydrolysis of Ammonia Borane

- The kinetic studies of the zeolite confined cobalt(0) nanoclusters catalyzed hydrolysis of ammonia borane show that the catalytic hydrolysis reaction proceeds with first order dependency with respect to the catalyst concentration and zeroth order dependency with respect to the substrate concentration.

$$H_3NBH_3 + 2\,H_2O \xrightarrow[\text{at RT in } H_2O]{\text{zeolite confined cobalt(0) nanoclusters}} NH_4^+ + BO_2^- + 3\,H_2$$

$$-\frac{3\,d[H_3NBH_3]}{dt} = \frac{d[H_2]}{dt} = k[Co]$$

- The plausible mechanism of the hydrolysis of H_3NBH_3 in the presence of metal catalysts may be as follows;

$$M + H_3NBH_3 + 4\,H_2O \longrightarrow M + NH_4B(OH)_4 + 3\,H_2$$

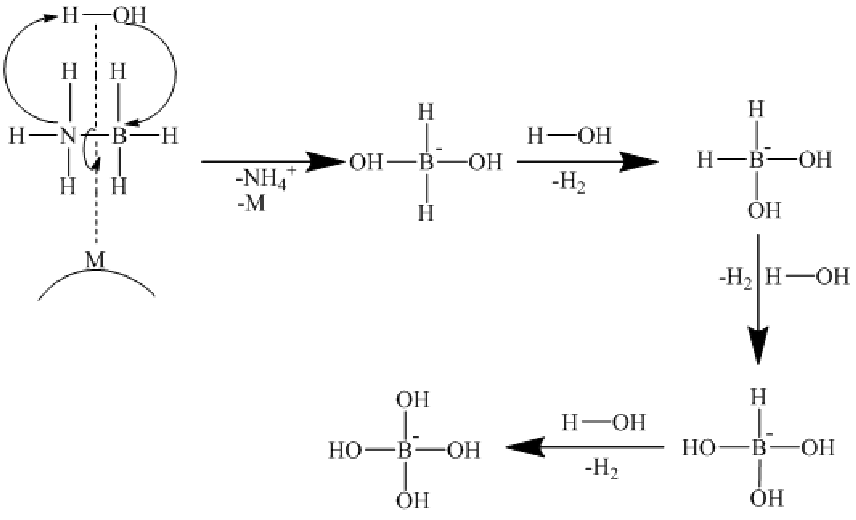

- Zeolite confined cobalt(0) nanoclusters provided TTO number of 5450 mol H_2 (mol Co)$^{-1}$ during the hydrolysis of ammonia borane in aqueous solution at 25 ± 0.1 ^{0}C.

- The activation energy for the zeolite confined cobalt(0) nanoclusters catalyzed hydrolysis of ammonia borane in aqueous solution was calculated to be $Ea = 56 \pm 2$ kJ/mol.

- The activation enthalpy ($\Delta H^{\#}$) and activation entropy ($\Delta S^{\#}$) of zeolite confined cobalt(0) nanoclusters catalyzed hydrolysis of ammonia borane was calculated to be $\Delta H^{\#} = 53 \pm 2$ kJ/mol and $\Delta S^{\#} = -87 \pm 4$ J/K·mol, respectively. These values also imply an associative mechanism for the zeolite confined cobalt(0) nanoclusters catalyzed hydrolysis of ammonia borane in aqueous solution.

- Although the rate of hydrogen generation from the catalytic hydrolysis of sodium borohydride was faster than that of ammonia borane under the same catalyst concentrations and reaction conditions, hydrogen generation from ammonia borane has a major advantage over sodium borohydride for practical on-board applications since the aqueous solutions of sodium borohydride have to be stabilized against self-hydrolysis by the addition of sodium hydroxide.

As a final remark; easy preparation, reusability, high catalytic activity, and low cost of zeolite confined cobalt(0) nanoclusters make them promising candidate to be employed as catalyst in developing highly efficient portable hydrogen generation systems using either sodium borohydride or ammonia borane as solid hydrogen storage material.

REFERENCES

[1] (a) Rand, D.A.J., Dell, R.M., *J. Power Sources* **2005**, 144, 568. (b) Zhang, J., Fisher, T.S., Gore, J.P., Hazra, D., Ramachandran, P.V., *Int. J. Hydrogen Energy* **2006**, 31, 2292. (c) Shang, Y., Chen, R.,. Thring, R., *World J. Engineering* **2005**, 2, 1.

[2] (a) U. S. Department of Energy, Office of Science, Basic Research Needs For the Hydrogen Economy, Report of the Basic Energy Sciences Workshop on Hydrogen Production, Storage and Use , www.sc.doe.gov/bes/hydrogen.pdf, May 13-15, **2003**. (b) Energy Information Administration, Annual Energy Outlook 2005 With Projections To 2025, www.eia.doe.gov/oiaf/aeo/pdf/0383(2005).pdf, February, **2005**. (c) Turner, J., Sverdrup, G., Mann, K., Maness, P.G., Kroposki, B., Ghirardi, M., Evans, R.J., Blake, D., *Int. J.Energy Res.* **2008**, 32, 379.

[3] (a) Ellison, H., Hydrogen, in Energy *for Sustainable World: From the Oil Age to a Sun-Powered Future*, Wiley-VCH, Weinheim, **2011**. (b) Grimes, C.A., Varghese, O.K., Ranjan, S., *Light, Water, Hydrogen*: *The Solar Generation of Hydrogen by Water Photoelectrolysis*, Springer, **2008**.

[4] Züttel, A., Borgschulte, A., Schlapbach, L., *Hydrogen as a Future Energy Carrier*, Wiley-VCH, Weinheim, **2008**.

[5] Rand, D.A.J., Dell, R.M., *Hydrogen Energy*: *Challenges and Prospects, RSC Publishing*, **2008**.

[6] Collot, A.G., *Prospects for Hydrogen from Coal*, Report CCC/78, IEA, Clean Coal Centre, London, December, **2003**.

[7] Gupta, R.B., *Hydrogen Fuel: Production, Transport, and Storage*, CRC Press, **2009**.

[8] (a) Hussain, M.M., Dincer, I., Li, X., *Appl. Thermal Eng.*, **2007**, 27, 2294. (b) Rifkin, J., *The Hydrogen Economy*, Penguin Putnam Inc., New York, **2002**.

[9] (a) Schlapbach, L., Züttel, A., *Nature* **2001**, 414, 353. (b) Orimo, S., Nakamori, Y., Eliseo, J.R., Züttel, A., Jensen, C.M., *Chem. Rev.*, **2007**, 107, 4111. (c) Berg, A.W.C.V., Arean, C.O., *Chem. Commun.*, **2008**, 668. (c) Berry, G.D., Aceves, S.M., *Energ. Fuels* **1998**, 12, 49.

[10] (a) Grochala, W., Edwards, P.P., *Chem. Rev.*, **2004**, 104, 1283. (b) Ross, D.K., *Vacuum* **2006**, 80, 1084.

[11] (a) Hu, J.J., Wu, G.T., Liu, Y.F., Xiong, Z.T., Chen, P., Murata, K., Sakata, K., Wolf, G., *J. Phys. Chem. B* **2006**, 110, 14688. (b) Chen, P., Xiong, Z.T., Luo, J.Z., Lin, J.Y., Tan, K.L., *Nature* **2002**, 420, 302.

[12] (a) Browning, D.J., Gerrard, M.L., Lakeman, J.B., Mellor, I.M., Mortimer, R.J., Turpin, M.C., *Nano Lett.*, **2002**, 2, 201. (b) Dillion, A.C., Jones, K.M., Bekkedahl, T.A., Kiang, C.H., Bethune, D.S., Heben, M., *Nature* **1997**, 386, 377.

[13] Schüth, F., Bogdanovic, B., Felderhoff, M., *Chem. Commun.*, **2004**, 2249.

[14] (a) Chen, J., Li, S.L., Tao, Z.L., Shen, Y.T., Cui, C.X., *J. Am. Chem. Soc.*, **2003**, 125, 5284. (b) Chen, J., Kuriyama, N., Yuan, H.T., Takeshita, H.T., Sakai, T., *J. Am. Chem. Soc.*, **2001**, 123, 11813.

[15] (a) Rosi, N.L., Eckert, J., Eddaoudi, M., Vodak, D.T., Kim, J., O'Keeffe, M., Yaghi, O.M., *Science* **2003**, 300, 1127. (b) Zhao, X.B., Xiao, B., Fletcher, A.J., Thomas, K.M., Bradshaw, D., Rosseinsky, M.J., *Science* **2004**, 306, 1012.

[16] Rood, J.A., Noll, B.C., Henderson, K.W., *Inorg. Chem.*, **2006**, 45, 5521.

[17] (a) Stephens, F.H., Pons, V., Baker, R.T., *Dalton Trans*., **2007**, 25, 2613. (b) Satyapal, S., Read, C., Ordaz, G., Thomas, G., U.S-D.O.E., Annual Hydrogen Program, www.hydrogen.energy.gov/pdfs/review06/satyapal.pdf, Washington, D.C., **2006**.

[18] Züttel, A., *Mater. Today* **2003**, 6, 24.

[19] Jones, R.H., Thomas, G.J., *Materials for the Hydrogen Economy*, CRC Press, **2008**.

[20] Demirci, U.B., Akdim, O., Andrieux, J., Hannauer, J., Chamoun, R., Miele, P., *Fuel Cells* **2010**, 10, 335.

[21] Wee, J.H., *J. Power Sources* **2006**, 155, 329.

[22] Nakamori, Y., Li, H.W., Matsuo, M., Miwa, K., Towata, S., Orimo, S., *J. Phys. Chem. Solids* **2008**, 69, 2292.

[23] Wee, J.H., Lee, K.Y., Kim, S.H., *Fuel Proc.Technol*., **2006**, 87, 811.

[24] (a) Liu, B.H., Li, Z.P., *J. Power Sources* **2009**, 187, 527. (b) Cakanyildirim, C., Gürü, M., *Int. J. Hydrogen Energy* **2008**, 33, 4634. (c) Züttel, A., Borgschulte, A., Orimo, S.I., *Scr. Mater*., **2007**, 56, 823. (d) Züttel, A., *Mitig. Adapt. Strat. Glob. Change* **2007**, 12, 343.

[25] (a) Amendola, S.C., Janjua, J.M., Spencer, N.C., Kelly, M.T., Petillo, P.J., Sharp-Goldman, S.L., Binder, M., *Int. J. Hydrogen Energy* **2000**, 25, 969. (b) Lee, J.Y., Lee, H.H., Lee, J.H., Kim D.M., Kim J.H., *J. Electrochem. Soc*., **2002**, 149, A 603. (c) Demirci, U.B., *L'Act. Chim*., **2008**, 316, 22.

[26] Padro, C.E.G., Lau, F., *Advances in Hydrogen Energy*, Kluwer Academic Publishers, **2002**.

[27] Aiello, R., Sharp, J.H., Matthews, M.A., *Int. J. Hydrogen Energy* **1999**, 24**,** 1123.

[28] (a) Levy, A., Brown, J.B., Lyons, C.J., *Ind. Eng. Chem.*, **1960**, 52, 211. (b) Kaufman, C.M., Sen, B., *J. Am. Chem. Soc. Dalton Trans.*, **1985**, 307. (c) Brown, H.C., Brown, C.A., *J. Am. Chem. Soc.*, **1962**, 84, 1493.

[29] James, B.D., Wallbridge, M.G.H., *Prog. Inorg. Chem.*, **1970,** 11, 99-231.

[30] Vielstich, W., Lamm, A., Gateiger, H.A., *Handbook of Fuel Cells: Fundamental, Technology, and Applications*, Wiley, West Sussex, **2003**.

[31] Norskov, J.K., Bligaard, T., Rossmeisl, J., *Nat. Chem.*, **2009**, 1, 37.

[32] U.S. Department of Energy, *Independent Review*, NREL/MP-150-42220, November **2007**.

[33] (a) Principi, G., Agresti, F., Maddalena, A., Russo, S.L., *Int. J. Hydrogen Energy* **2009**, 34, 2087. (b) Demirci, U.B., Miele, P., *Energy Environ. Sci.*, **2009**, 2, 627.

[34] (a) Peng, B., Chen, D., *Energy Environ. Sci.*, **2008**, 1, 479. (b) Umegaki, T., Yan, J.M., Zhang, X.B., Shioyama, H., Kuriyama, N., Xu, Q., *Int. J. Hydrogen Energy* **2008**, 34, 2303.

[35] Wang, P., Kang, X.D., *Dalton Trans.*, **2008**, 5400.

[36] (a) Parvanov, V.M., Schenter, G.K., Hess, N.J., Daemen, L.L., Hartl, M., Stowe, A.C., Camaioni, D.M., Autrey, T., *Dalton Trans.*, **2008**, 4514. (b) Custelcean, R., Dreger, Z.A., *J. Phys. Chem. B* **2003**, 107, 9231.

[37] (a) Shore, S.G., Parry, R.W., *J. Am. Chem. Soc.*, **1958**, 80, 8. (b) Mayer, E., *Inorg. Chem.*, **1972**, 11, 866. (c) Shore, S.G., Parry, R.W., *J. Am. Chem. Soc.*, **1955**, 77, 6084. (d) Hu, M.G., Van Paasschen, J.M., Geanangel, R.A., *J. Inorg. Nucl. Chem.*, **1977**, 39, 2147.

[38] (a) Baitalow, F., Baumann, J., Wolf, G., Jaenicke, K., Leitner, G., *Thermochim. Acta* **2002**, 391, 159. (b) Wolf, G., Baumann, J., Baitalow, F., Hoffman, F.P., *Thermochim. Acta* **2000,** 343, 19.

[39] Bluhm, M.E., Bradley, M.G., Butterick, R., Kusari, U., Sneddon, L.G., *J. Am. Chem. Soc.*, **2006**, 128, 7748.

[40] Umegaki, T., Yan, J.M., Zhang, X.B., Shioyama, H., Kuriyama, N., Xu, Q., *Int. J. Hydrogen Energy* **2009**, 34, 3816.

[41] Hausdorf, S., Baitalow, F., Wolff, G., Mertens, F.O.R.L., *Int. J. Hydrogen Energy* **2008**, 33, 608.

[42] (a) Kelly, H.C., Marriott, V.B., *Inorg. Chem.*, **1979**, 18, 2875. (b) Chandra, M., Xu, Q., *J. Power Sources* **2006**, 159, 855.

[43] Chandra, M., Xu, Q., *J. Power Sources* **2006**, 156, 190.

[44] Kojima, Y., Suzuki, K., Fukumoto, K., Sasaki, M., Yamamoto, T., Kawai, Y., Hayashi, H., *Int. J. Hydrogen Energy* **2002**, 27, 1029.

[45] Wu, C., Zhang, H., Yi, B., *Catal. Today* **2004**, 93-95, 477.

[46] Krishnan, P., Yang, T.H., Lee, W.Y., Kim, C.S., *J. Power Sources* **2005**, 143, 17.

[47] Xia, Z.T., Chan, S.H., *J. Power Sources* **2005**, 152, 46.

[48] Pinto, A.M.F.R., Falcao, D.S., Silva, R.A., Rangel, C.M., *Int. J. Hydrogen Energy* **2006**, 31, 1341.

[49] Cho, K.W., Kwon, H.S., *Catal. Today* **2007**, 120, 298.

[50] Ye, W., Zhang, H., Xu, D., Ma, L., Yi, B., *J. Power Sources* **2007**, 164, 544.

[51] Kim, S.J., Lee, J., Kong, K.Y., Jung, C.R., Min, I., Lee, S.Y., Kim, H.J., Nam, S.W., Lim, T.H., *J. Power Sources* **2007**, 170, 412.

[52] Xu, D., Zhang, H., Ye, W., *Catal. Commun.*, **2007**, 8, 1767.

[53] Ingersoll, J.C., Mani, N., Thenmozhiyal, J.C., Muthaiah, A., *J. Power Sources* **2007**, 173, 450.

[54] Mitov, M., Rashkov, R., Atanassov, N., Zielonka, A., *J. Mater. Sci.*, **2007**, 42, 3367.

[55] Dai, H.B., Liang, Y., Wang, P., Cheng, H.M., *J. Power Sources* **2008**, 177, 17.

[56] Liu, Z., Guo, B., Chan, S.H., Tang, E.H., Hong, L., *J. Power Sources* **2008**, 176, 306.

[57] Dai, H.B., Liang, Y., Wang, P., Yao, X.D., Rufford, T., Lu, M., Cheng, H.M., *Int. J. Hydrogen Energy* **2008**, 33, 4405.

[58] Xu, D., Dai, P., Liu, X., Cao, C., Guo, Q., *J. Power Sources* **2008**, 182, 616.

[59] Eom, K.S., Cho, K.W., Kwon, H.S., *J. Power Sources* **2008**, 180, 484.

[60] Hung, A.J., Tsai, S.F., Hsu, Y.Y., Ku, J.R., Chen, Y.H., Yu, C.C., *Int. J. Hydrogen Energy* **2008**, 33, 6205.

[61] Huang, Y., Wang, Y., Zhao, R., Shen, P.K., Wei, Z., *Int. J. Hydrogen Energy* **2008**, 33, 7110.

[62] Demirci, U.B., Garin, F., *J. Mol. Catal. A : Chem.*, **2008**, 279, 57.

[63] Liu, C.H., Chen, B.H., Hsueh, C.L., Ku, J.R., Jeng, M.S., Tsau, F., *Int. J. Hydrogen Energy* **2009**, 34, 2153.

[64] Akdim, O., Demirci, U.B., Brioude, A., Miele, P., *Int. J. Hydrogen Energy* **2009**, 34, 5417.

[65] Alonso, R.P., Sicurelli, A., Callone, E., Carturan, G., Raj, R., *J. Power Sources* **2007**, 165, 315.

[66] Demirci, U.B., Akdim, O., Miele, P., *J. Power Sources* **2009**, 192, 310.

[67] Akdim, O., Demirci, U.B., Miele, P., *Int. J. Hydrogen Energy* **2009**, 34, 7231.

[68] Fernandes, R., Patel, N., Miotello, A., *Appl. Catal. B: Environ.*, **2009**, 92, 68.

[69] Liang, Y., Wang, P., Dai, H.B., *J. Alloys Compd.*, **2010**, 491, 359.

[70] Liang, Y., Dai, H.B., Ma, L.P., Wang, P., Cheng, H.M., *Int. J. Hydrogen Energy* **2010**, 35, 3023.

[71] Tian, H., Guo, Q., Xu, D., *J. Power Sources* **2010**, 195, 2136.

[72] Patel, N., Fernandes, R., Bazzanella, N., Miotello, A., *Thin Solid Films* **2010**, 518, 4779.

[73] Fernandes, R., Patel, N., Miotello, A., Filippi, M., *J. Mol. Cat. A: Chem.*, **2009**, 298, 1.

[74] Ding, X.L., Yuan, X., Jia, C., Ma, Z.F., *Int. J. Hydrogen Energy* **2010**, 35, 11077.

[75] Patel, N., Patton, B., Zanchetta, C., Fernandes, R., Guella, G., Kale, A., Miotello, A., *Int. J. Hydrogen Energy* **2008**, 33, 287.

[76] Hua, D., Hanxi, Y., Xinping, A., Chuansin, C., *Int. J. Hydrogen Energy* **2003**, 28, 1095.

[77] Liu, B.H., Li, Z.P., Suda, S., *J. Alloy Compd.* **2006**, 415, 288.

[78] Hsueh, C.L., Chen, C.Y., Ku, J.R., Tsai, S.F., Hsu, Y.Y., Tsau, F., Jeng, M.S., *J. Power Sources* **2008**, 177, 485.

[79] Zhang, Q., Wu, Y., Sun, X., Ortega, J., *Ind. Eng. Chem. Res.*, **2007**, 46, 1120.

[80] Zhang, Z.S., Delgass, W.N., Fisher, T.S., Gore, J.P., *J. Power Sources* **2007**, 164, 772.

[81] Hu, L., Ceccato, R., Raj, R., *J. Power Sources* **2011**, 196, 69.

[82] Kim, H.J., Shin, K.J., Kim, H.J., Han, M.K., Kim, H., Shul, Y.G., Jung, K.T., *Int. J. Hydrogen Energy* **2010**, 35, 12239.

[83] Santos, D.M.F., Sequeira, C.A.C., Lobo, R.F.M., *Int. J. Hydrogen Energy* **2010**, 35, 9901.

[84] Ramachandran, P.V., Gagare, P.D., *Inorg. Chem.*, **2007**, 46, 7810.

[85] Xu, Q., Chandra, M., *J. Power Sources* **2006**, 163, 364.

[86] Mohajeri, N., T-Raissi, A., Adebiyi, O., *J. Power Sources* **2007**, 167, 482.

[87] Cheng, F., Ma, H., Li, Y., Chen, J., *Inorg. Chem.*, **2007**, 46, 788.

[88] Basu, S., Brockman, A., Gagore, P., Zheng, Y., Ramachandran, P.V., Delgass, W.N., *J. Power Sources* **2009**, 188, 238.

[89] Clark, T.J., Whittell, G.R., Manners, I., *Inorg. Chem.*, **2007**, 46, 7522.

[90] Kalidindi, S.B., Sanyal, U., Jagirdar, B.R., *Phys. Chem. Chem. Phys.*, **2008**, 10, 5870.

[91] Umegaki, T., Yan, J.M., Zhang, X.B., Shioyama, H., Kuriyama, N., Xu, Q., *J. Power Sources* **2009**, 191, 209.

[92] Yao, C.F., Zhuang, L., Cao, Y.L., Hi, X.P., Yang, H.X., *Int. J. Hydrogen Energy* **2008**, 33, 2462.

[93] Yan, J.M., Zhang, X.B., Han, S., Shioyama, H., Xu, Q., *Angew. Chem. Int. Ed.* **2008**, 47, 2287.

[94] Yan, J.M., Zhang, X.B., Han, S., Shioyama, H., Xu, Q., *J. Power Sources* **2009**, 194, 478.

[95] Yan, J.M., Zhang, X.B., Shioyama, H., Xu, Q., *J. Power Sources* **2010**, 195, 1091.

[96] Yan, J.M., Zhang, X.B., Han, S., Shioyama, H., Xu, Q., *Inorg. Chem.*, **2009**, 48, 7389.

[97] Yang, X., Cheng, F., Liang, J., Tao, Z., Chen, J., *Int. J. Hydrogen Energy* **2009**, 34, 8785.

[98] Rakap, M., Özkar, S., *Int. J. Hydrogen Energy* **2010**, 35, 1305.

[99] Dai, H.B., Gao, L.L., Liang, Y., Kang, X.D., Wang, P., *J. Power Sources* **2010**, 195, 307.

[100] Tong, D.G., Zeng, X.L., Chu, W., Wang, D., Wu, P., *J. Mater. Sci.*, **2010**, 45, 2862.

[101] Patel, N., Fernandes, R., Guella, G., Miotello, A., *Appl. Catal. B* **2010**, 95, 137.

[102] Jiang, H.L., Umegaki, T., Akita, T., Zhang, X.B., Haruta, M., Xu, Q., *Chem. Eur. J.* **2010**, 16, 3132.

[103] Yamada, Y., Yano, K., Xu, Q., Fukuzumi, S., *J. Phys. Chem. C* **2010**, 114, 16456.

[104] Rakap, M., Kalu, E.E., Özkar, S., *Int. J. Hydrogen Energy* **2011**, 36, 254.

[105] Rakap, M., Kalu, E.E., Özkar, S., *Int. J. Hydrogen Energy* **2011**, 36, 1448.

[106] Umegaki, T., Yan, J.M., Zhang, X.B., Shioyama, H., Kuriyama, N., Xu, Q., *J. Power Sources* **2010**, 195, 8209.

[107] Zhao, J., Ma, H., Chen, J., *Int. J. Hydrogen Energy* **2007**, 32, 4711.

[108] Zahmakıran, M., Özkar, S., *J. Mol. Cat. A: Chem.*, **2006**, 258, 95.

[109] (a) Metin, Ö., Özkar, S., *Int. J. Hydrogen Energy* **2007**, 32, 1707. (b) Metin, Ö., Özkar, S., *J. Mol. Cat. A: Chem.*, **2008**, 295, 39.

[110] Metin, Ö., Şahin, Ş., Özkar, S., *Int. J. Hydrogen Energy* **2009**, 34, 6304.

[111] Aiken III, J.D., Lin, Y., Finke, R.G., *J. Mol. Catal. A: Chem.,* **1996,** 114, 29.

[112] (a) Pool, R., *Science*, **1990**, 248, 1186. (b) Jongh, L.J., *Physics and Chemistry of Metal Cluster Compounds*, Kluwer Publishers, Dordrect, **1994.**

[113] Feldheim, D.R., Foss, C.A., *Metal Nanoparticles: Synthesis, Characterization, and Applications*, Marcel Dekker, NewYork, **2002**.

[114] (a) Zhou, B., Hermans, S., Somorjai, G.A., *Nanotechnology in Catalysis*, Kluwer Academic Publishers, New York, **2004**. (b) Bönnemann, H., Nagabhushana, K.S., Chemical Synthesis of Nanoparticles, in *Encyclopedia of Nanoscience and Nanotechnology*, American Scientific Publishers, Stevenson Ranch, **2004**.

[115] Cui, C., Lieber, C.M., *Science* **2001**, 291, 851.

[116] Eychmuller, A., *J. Phys. Chem. B*, **2001**, 104, 6514.

[117] (a) Puntes, V.F., Krishnan, K.M., Alivisatos, A.P., *Science* **2001**, 291, 2115. (b) Sun, S., *Science* **2000**, 287, 1989.

[118] (a) Rao, C.N.R., Kulkarni, G.U., Thomas, P.J., *Chem. Soc. Rev*., **2000**, 29, 27. (b) Chen, S., *Adv. Mater*., **2000**, 12, 186.

[119] (a) Niemeyer, C.M., *Angew. Chem. Int. Ed. Engl*., **2001**, 40, 4128. (b) Kumar, C.S.S.R., Hormes, J., Leuschner, C., *Nanofabrication Towards Biomedical Applications*, Wiley, Weinheim, **2005**.

[120] (a) Schmid, G., Bäumle, M., Geerkens, M., Heim, I., Osemann, C., Sawitowski, T., *Chem. Soc. Rev.*, **1999**, 128, 79. (b) Schmid, G., *Chem. Rev.*, **1992**, 92, 1709.

[121] Corain, B., Schmid, G., Toshima N., *Metal Nanoclusters in Catalysis and Materials Science*, Elsevier, Amsterdam, Netherlands, **2008.**

[122] Gaffet, E., Tachikart, M., El Kedim, O., Rahouadj, R., *Mater. Charact.*, **1996**, 36, 185.

[123] Richards, R.M., *Surface and Nanomolecular Catalysis*, Taylor & Francis, Boca Raton, **2006**.

[124] (a) Fu, X., Wang, Y., Wu, N., Gui, L., *Langmuir* **2002**, 18, 4619. (b) Henglein, A., *J. Phys. Chem. B*, **2000**, 104, 2201.

[125] Esumi, K., Tano, T., Meguro, K., *Langmuir* **1989**, 5, 268.

[126] Henglein, A., Lille, J., *J. Phys. Chem.*, **1981**, 85, 1246.

[127] Ershov, B.G., Janata, E., Michaelis, M., Henglein, A., *J. Phys. Chem.*, **1991**, 95, 8996.

[128] Dhas, A., Gedanken, A., *J. Mater. Chem.*, **1998**, 8, 445.

[129] Faraday, M., *Philos. Trans. R. Soc. London* **1857**, 147, 145.

[130] Schmid, G., *Clusters and Colloids: From Theory to Applications*, VCH Publishers, New York, **1994**.

[131] (a) Tano, T., Esumi, K., Meguro, K., *J. Colloid Interface Sci.*, **1989**, 133, 530. (b) Esumi, K., Suzuki, M., Tano, T., Torigoe, K., Meguro, K., *Colloids Surf.*, **1991**, 55, 9. (c) Esumi, K., Tano, T., Meguro, K., *Langmuir* **1989**, 5, 268. (d) Esumi, K., Sadakane, O., Torigoe, K., Meguro, K., *Colloids Surf.*, **1992**, 62, 255.

[132] Aiken III, J.D., Finke, R.G., *J. Mol. Catal. A: Chem.,* **1999**, 145, 1.

[133] (a) Duteil, A., Queau, R., Chaudret, B., Mazel, R., Roucau, C., Bradley, J.S., *Chem. Mater*., **1993**, 5, 341. (b) Bradley, J.S., Millar, J.M., Hill, E.W., Behal, S., Chaudret, B., Duteil, A., *Faradays Discuss*., **1991**, 92, 255.

[134] Turkevich, J., Stevenson, P.C., Hillier, J., *Discuss. Faraday Soc*., **1951**, 11, 55.

[135] Hirai, H., Nakao, Y., Toshima, N., Adachi, K., *Chem. Lett*., **1976**, 5, 905.

[136] Giersig, M., Mulvaney, P., *Langmuir* **1993**, 9, 3408.

[137] Astruc, D., Lu, F., Aranzaes, J.R., *Angew. Chem. Int. Ed*., **2005**, 44, 7852.

[138] Bönnemann, H., Brijoux, W., *Nanostruct. Mater*., **1995**, 5, 135.

[139] Reetz, M.T., Lohmer, G., *Chem. Commun*., **1996**, 16, 1921.

[140] Toshima, N., Harada, M., Yonezawa, T., Kushihashi, K., Asakura, K., *J. Phys. Chem*., **1991**, 95, 7448.

[141] Rothenberg, G., *Catalysis: Concepts and Green Applications*, Wiley-VCH, Weinheim, **2008**.

[142] Thomas, J.M., Thomas, W.J., *Principles and Practice of Heterogeneous Catalysis*, VCH, New York, **1997**.

[143] Gates, B.C., *Catalytic Chemistry*, Academic Press: New York, **1992**.

[144] Anthonsen, T., *Reactions Catalyzed by Enzymes In Applied Biocatalysis*, Harwood Academic Publishers, UK, **1999**.

[145] Mortimer, R.G., *Physical Chemistry*, Academic Press, San Diego, **2000**.

[146] Özkar, S., *Appl. Surf. Sci.,* **2009,** 256, 1272.

[147] Klabunde, K.J., Stark, J., Koper, C., Park, D., *J. Phys. Chem.*, **1996**, 100, 12142.

[148] Lin, Y., Finke, R.G., *J. Am. Chem. Soc.*, **1994**, 116, 8335.

[149] Bönnemann, H., Braun, G.A., *Angew. Chem., Int. Ed. Engl.*, **1996**, 35, 1992.

[150] Wilcoxon, J.P., Martinho, T., Klavetter, E., Sylwester, A.P., *Nanophase Mater.*, **1994**, 771.

[151] Lewis, L.N., Lewis, N., *J. Am. Chem. Soc.*, **1986**, 108, 7228.

[152] Vargaftik, M.N., Zargorodnikov, V.P., Stolarov, I.P., Moiseev, I.I., Kochubey, D.I., Likholobov, V.A., Chuvilin, A.L., Zamaraev, K.I., *J. Mol. Catal.*, **1989**, 53, 315.

[153] Schmidt, T.J., Noeske, M., Gasteiger, H.A., Behm, R.J., Britz, P., Brijoux, W., Bönnemann, H., *Langmuir* **1997**, 13, 2591.

[154] Reetz, M.T., Breinbauer, R., Wedemann, P., Binger, P., *Tetrahedron* **1998**, 54, 1233.

[155] Reetz, M.T., Quaiser, S.A., Merk, C., *Chem. Ber.*, **1996**, 129, 741.

[156] Reetz, M.T., Breinbauer, R., Wanninger, K., *Tetr. Lett.*, **1996**, 37, 4499.

[157] Reetz, M.T., Lohmer, G., *J. Chem. Soc. Chem. Comm.*, **1996**, 1921.

[158] Grassian, V. H., *J. Phys. Chem. C*, **2008**, 112*,* 18303.

[159] (a) Özkar, S., Finke, R.G., *J. Am. Chem. Soc.*, **2002**, 124, 5796. (b) Özkar, S., Finke, R.G., *Langmuir* **2002**, 18, 7653. (c) Özkar, S., Finke, R.G., *Langmuir* **2003**, 19, 6247.

[160] Tosheva, L., Valtchev, V. P., *Chem. Mater.*, **2005**, 17, 2494.

[161] (a) Sun, Y., Sun, T., Seff, K., *Chem. Rev*. **1994**, 94, 857. (b) Ryoo, R., June-Cho, S., Pak, C., Guk-Kim, J., Ki-Ihm, S., Yong-Lee, J., *J. Am. Chem. Soc*. **1992**, 114, 76. (c) Guczi, L., Kiricsi, I., *Appl. Catal. A: Chem*., **1999**, 186, 375. (d) Guczi, L., Beck, A., Horvath, D., *Top. Catal*. **2002**, 19, 157.

[162] (a) Tzou, M.S., Teo, B.K., Sachtler, W.M.H., *J. Catal*., **1988**, 113, 220. (b) de Graaf, J., van Dillen, A.J., de Jong, K.P., Koningsberger, D.C., *J. Catal*., **2001**, 203, 307. (c) Kawi, S., Chang, J.R., Gates, B.C., *J. Am. Chem. Soc*., **1993**, 115, 4830.

[163] (a) Homeyer, S.T., Sachtler, W.M.H., *J. Catal*., **1989**, 117, 91. (b) Zhang, Z., Zhang, Y.D., Hines, W.A., Budnick, J.I., Sachtler, W.M.H., *J. Am. Chem. Soc*., 1992, **114**, 4834. (c) Wang, Y., Wu, H., Zhang, Q., Tang, Q., Micropor. Mesopor. Mat., **2005**, 86, 38.

[164] Guczi, L., *Catal. Lett*., **1991**, 7, 205.

[165] Tang, Q., Zhang, Q., Wang, P., Wang, Y., Wan, H., *Chem. Mater*., **2004**, 16, 1967.

[166] (a) Glavee, G.N., Klabunde, K.J., Sorensen, C.M., Hadjipanayis, G.C., *Langmuir* **1992**, 8, 771. (b) Glavee, G.N., Klabunde, K.J., Sorensen, C.M., Hadjipanayis, G.C., *Langmuir* **1993**, 9, 162. (c) Glavee, G.N., Klabunde, K.J., Sorensen, C.M., Hadjipanayis, G.C., *Inorg. Chem*., **1993**, 32, 474.

[167] Yan, J.M., Zhang, X.B., Han, S., Shioyama, H., Xu, Q., *Inorg. Chem*., **2009**, 48, 7389.

[168] Walspurger, S., Sommer, J., *Reactions in Zeolites, Molecular Encapsulation; Organic Reactions in Constrained Systems*, Wiley, UK, **2010**.

[169] Auerbach, S.M., Carrado, K.A., Dutta, P.K., *Handbook of Zeolite Science and Technology*, Marcel Dekker, New York, **2003**.

[170] Wright, P.A., *Microporous Framework Solids*, RSC Publishing, Cambridge, **2008**.

[171] Kulprathipanja, S., *Zeolites in Industrial Separation and Catalysis*, Wiley-VCH, Weinheim, **2010**.

[172] Madon, R.J., Boudart, M., *Ind. Eng. Chem. Fundam.*, **1982**, 21, 438.

[173] Baerlocher, C., Meier, W.M., Olson, D.H., *Atlas of Zeolite Framework Types*, 5th revised edition, Elsevier, Amsterdam, **2001**.

[174] Mandale, A.B., Badrinarayanan, S., Date, S.K., Sinha, A.P.B., *J. Electron Spectrosc. Relat. Phenom*. **1984**, 33, 61.

[175] (a) Guczi, L., Bazin, D., *Appl. Catal. A: Chem.*, **1999**, 188, 163. (b) Fukuoko, A., Higashimoto, N., Sakamoto, Y., Inagaki, S., Fukushima, Y., Ichikawa, M., *Top. Catal.*, **2002**, 18, 73.

[176] (a) Jiang, Y.X., Weng, W.Z., Si, D., Sun, S.G., *J. Phys. Chem. B* **2005**, 109, 7637.

[177] Okitsu, K., Yue, A., Tanabe, S., Matsumoto, H., *Bull. Chem. Soc. Jpn.*, **2002**, 75, 449.

[178] Klebanoff, L.E., Van Campen, D.G., Pouliot, R.J., *Phys. Rev. B* **1994**, 49, 2047.

[179] Isambert, A., Angot, E., Hebert, P., Haines, J., Levelut, C., Le Parc, R., Ohishi, Y., Kohara, S., Keen, D.A., *J. Mater. Chem.*, **2008**, 18, 5746.

[180] (a) Gallant, D., Pezolet, M., Simard, S., *J. Phys. Chem. B* **2006**, 110, 6871. (b) Knops-Gerrits, P.P., Cuypers, M., *Stud. Surf. Sci. Catal.*, **2002**, 142, 263.

[181] (a) Verberckmoes, A.A., Weckhuysen, B.M., Schoonheydt, R.A., *Micropor. Mesopor. Mat.*, **1998**, 22, 165. (b) Nakashima, D., Ichihashi, Y., Nishiyama, S., Tsuruya, S., *J. Mol. Cat. A: Chem.*, **2006**, 259, 108. (c) Seiki, T., Nakato, A., Nishiyama, S., Tsuruya, S., *Phys. Chem. Chem. Phys.*, **2003**, 5, 3818. (d) Patil, M.V., Yadav, M.K., Jasra, R.V., *J. Mol. Cat. A: Chem.*, **2007**, 277, 72.

[182] Storck, S., Bretinger, H., Maier, W.F., *Appl Catal A: Chem.*, **1998**, 174, 137.

[183] Davis, R.E., Swain, C.G., *J. Am. Chem. Soc.*, **1960**, 82, 5950.

[184] Jeong, S.U., Kim, R.K., Cho, E.A., Kimb, H.J., Nam, S.W., Oh, I.H., Hong, S.A., Kim, S.H., *J. Power Sources* **2005**, 144, 129.

[185] Holbrook, K.A., Twist, P.J., *J. Chem. Soc. A*, **1971**, 890.

[186] Walter, J.C., Zurawski, A., Montgomery, D., Thornburg, M., Revankar, S., *J. Power Sources* **2008**, 179, 335.

[187] Amendola, S.C., Sharp-Goldman, S.L., Janjua, M.S., Kelly, M.T., Petillo, P.J., Binder, M., *J. Power Sources* **2000**, 85, 186.

[188] Lee, J., Kong, K.Y., Jung, C.R., Cho, E., Yoon, S.P., Han, J., Lee, T.G., Nam, S.W., *Catal. Today* **2007**, 120, 305.

[189] Rakap, M., Özkar, S., *Appl. Catal. B: Environ.*, **2009**, 91, 21.

[190] Chandra, M., Xu, Q., *J. Power Sources* **2007**, 168, 135.

[191] Kalidindi, S.B., Indirani, M., Jagirdar, B.R., *Inorg. Chem.*, **2008**, 47, 7424.

[192] Zahmakıran, M., Özkar, S., *Appl. Catal. B: Environ.*, **2009**, 89, 104.

[193] Metin, Ö., Özkar, S., *Energy Fuels* **2009**, 23, 3517.

[194] Durap, F., Zahmakıran, M., Özkar, S., *Int. J. Hydrogen Energy* **2009**, 34, 7223.

[195] (a) Clark, T.J., Whittell, G.R., Manners, I., *Inorg. Chem.*, **2007**, 46, 7522. (b) Jaska, C.A., Clark, T.J., Clendenning, S.B., Groeza, D., Turak, A., Lu, Z.H., Manners, I., *J. Am. Chem. Soc.*, **2005**, 127, 5116-24

APPENDIX A

TABLES

Table A1. The values of rate constant (k_{app}) calculated from the volume of hydrogen versus time data for the catalytic hydrolysis of sodium borohydride solution ([$NaBH_4$] = 150 mM, 50 mL) in the presence of 2.0 mM zeolite confined cobalt(0) nanoclusters at different temperatures.

Temperature (K)	**Rate Constant, k_{app} mol H_2.(mol Co)$^{-1}$.s^{-1}**
298	0.056
303	0.085
308	0.128
313	0.162
318	0.230

Table A2. The values of rate constant (k_{app}) calculated from the volume of hydrogen versus time data for the catalytic hydrolysis of sodium borohydride solution ([$NaBH_4$] = 150 mM, 50 mL) in the presence of 2.0 mM zeolite confined cobalt(0) nanoclusters and 10.0 wt % NaOH at different temperatures.

Temperature (K)	**Rate Constant, k_{app} mol H_2.(mol Co)$^{-1}$.s^{-1}**
298	0.168
303	0.220
308	0.267
313	0.337
318	0.414

Table A3. The values of rate constant (k_{app}) calculated from the volume of hydrogen versus time data for the catalytic hydrolysis of ammonia borane solution ($[H_3NBH_3]$ = 100 mM, 20 mL) in the presence of 2.0 mM zeolite confined cobalt(0) nanoclusters at different temperatures.

Temperature (K)	**Rate Constant, k_{app} mol H_2.(mol Co)$^{-1}$.s^{-1}**
298	0.0868
303	0.1106
308	0.1662
313	0.2534
318	0.3613

APPENDIX B

FIGURES

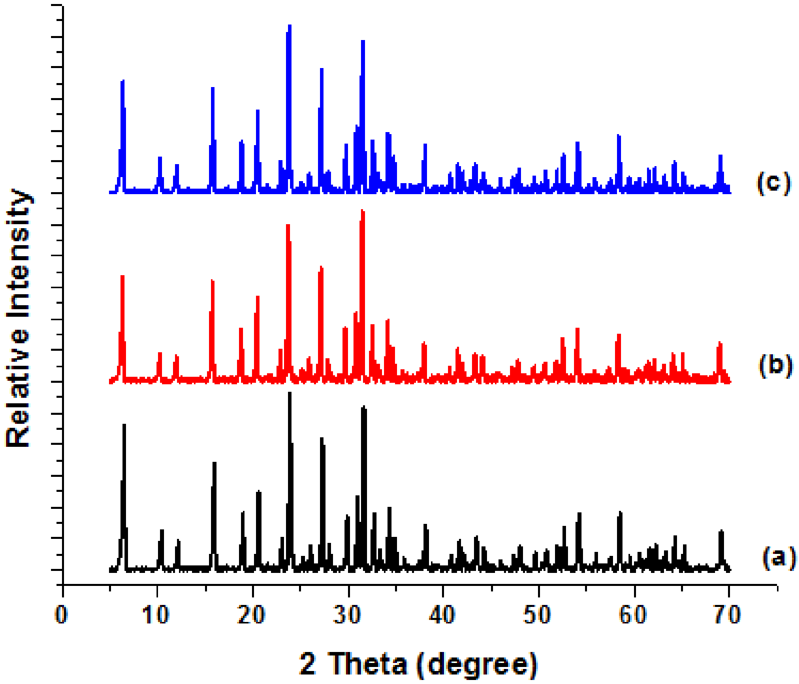

Figure B1. The powder XRD patterns of (a) zeolite-Y, (b) zeolite confined cobalt(0) nanoclusters prepared by borohydride reduction of cobalt(II)-exchanged zeolite-Y sample with a cobalt content of 0.85 wt % in basic solution, and (c) zeolite confined cobalt(0) nanoclusters after fifth use in the hydrolysis of sodium borohydride in basic solution.

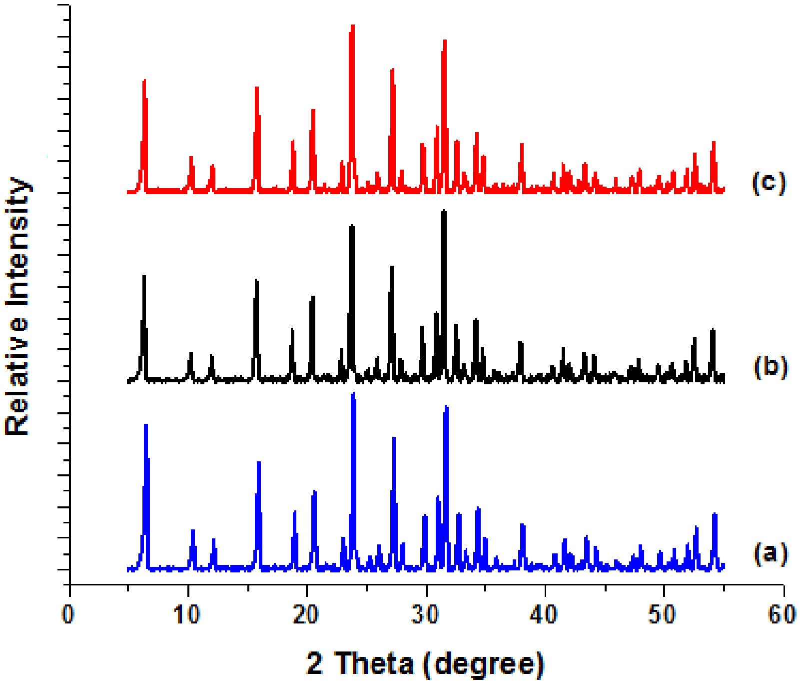

Figure B2. The powder XRD patterns of (a) zeolite-Y, (b) zeolite confined cobalt(0) nanoclusters with a cobalt content of 0.85 wt %, and (c) zeolite confined cobalt(0) nanoclusters after fifth use in the hydrolysis of ammonia borane.

CURRICULUM VITAE

Name	**:** Murat RAKAP
Date of Birth	**:** July 14, 1977
Place of Birth	**:** Çarşamba / Samsun
Status	**:** Married

Education

1995-1999 **BS in Chemistry**, Department of Chemistry, Karadeniz Technical University, Trabzon, Turkey, GPA: 3.27 / 4.00

2000-2002 **MS in Chemistry**, Inorganic Chemistry Division, Department of Chemistry, Karadeniz Technical University, Trabzon, Turkey, GPA: 3.93 / 4.00

Thesis Title: Synthesis and characterization of symmetrical phthalocyanines containing 20-membered crown ether units

Supervisor: Assoc. Prof. Dr. Halit Kantekin

2004-2011 **PhD in Chemistry**, Inorganic Chemistry Division, Department of Chemistry, Middle East Technical University, Ankara, Turkey, GPA: 3.57 / 4.00

Thesis Title: Preparation and characterization of zeolite confined cobalt(0) nanoclusters as catalyst for hydrogen generation from the hydrolysis of sodium borohydride and ammonia borane

Supervisor: Prof. Dr. Saim Özkar

Positions

2000-02	Teaching Assistant In General Chemistry Laboratory, Karadeniz Technical University, Trabzon, Turkey
2000-02	Teaching Assistant In Inorganic Chemistry Laboratory, Karadeniz Technical University, Trabzon, Turkey
2001-02	Teaching Assistant In Industrial Chemistry Laboratory, Karadeniz Technical University, Trabzon, Turkey
2003-04	Teaching Assistant In General Chemistry Laboratory, Middle East Technical University, Ankara, Turkey
2005-09	Teaching Assistant In Analytical Chemistry Laboratory, Middle East Technical University, Ankara, Turkey
2006-11	Teaching Assistant In Inorganic Chemistry Laboratory, Middle East Technical University, Ankara, Turkey
2010	Visiting Researcher at the Department Chemical and Biomedical Engineering, Florida State University, Tallahassee, FL, USA

Awards and Scholarships

1999	The Second Best Undergraduate Student of Department of Chemistry, Karadeniz Technical University
1995-99	Scholarship for Undergraduate Students by The Prime Ministry Social Assistance and Solidarity Fund
2000-02	National Scholarship for MSc Students by The Scientific and Technological Research Council of Turkey (TUBITAK-2210)
2006-09	National Scholarship for PhD Students by The Scientific and Technological Research Council of Turkey (TUBITAK-2211)

Publications

1- Halit Kantekin, **Murat Rakap**, Yaşar Gök, Halil Zeki Şahinbaş**;** Synthesis and characterization of new metal-free and phthalocyanine nickel(II) complex containing macrocyclic moieties; *Dyes and Pigments*, 74, 2007, 21-25.

2- Halit Kantekin, **Murat Rakap**, Miraç Nedim Mısır, Halil Zeki Gök, İrfan Acar; The synthesis and characterization of new metal-free and metallo phthalocyanines substituted with four dithiatetraoxa macrocyclic moieties; *Journal of Coordination Chemistry*, 60, 2007, 1965-1972.

3- Murat Rakap, Saim Özkar; Intrazeolite cobalt(0) nanoclusters as low-cost and reusable catalyst for hydrogen generation from the hydrolysis of sodium borohydride; *Applied Catalysis B: Environmental*, 91, 2009, 21-29.

4- Murat Rakap, Saim Özkar; Zeolite confined palladium(0) nanoclusters as effective and reusable catalyst for hydrogen generation from the hydrolysis of ammonia-borane; *International Journal of Hydrogen Energy*, 35 (3), 2010, 1305-1312.

5- Murat Rakap, Saim Özkar; Hydrogen generation from the hydrolysis of ammonia-borane using intrazeolite cobalt(0) nanoclusters catalyst; *International Journal of Hydrogen Energy*, 35, 2010, 3341-3346.

6- Feyyaz Durap, **Murat Rakap**, Murat Aydemir, Saim Özkar; Room temperature aerobic Suzuli cross-coupling reactions in DMF/water mixture using zeolite confined palladium(0) nanoclusters as efficient and recyclable catalyst; *Applied Catalysis A: General*, 382, 2010, 339-344.

7- Murat Rakap, Egwu Eric Kalu, Saim Özkar; Hydrogen generation from the hydrolysis of ammonia borane using cobalt-nickel-phosphorus (Co-Ni-P) catalyst supported on Pd-activated TiO_2 by electroless deposition; *International Journal of Hydrogen Energy*; 36, 2011, 254-261.

8- Murat Rakap, Egwu Eric Kalu, Saim Özkar; Polymer-immobilized palladium supported on TiO_2 (Pd-PVB-TiO_2) as highly active and reusable catalyst for hydrogen generation from the hydrolysis of unstirred ammonia-borane solution; *International Journal of Hydrogen Energy*; 36, 2011, 1448-1455.

9- Murat Rakap, Saim Özkar; Hydroxyapatite-supported palladium(0) nanoclusters as effective and reusable catalyst for hydrogen generation from the hydrolysis of ammonia-borane; *International Journal of Hydrogen Energy*; 36, 2011, 7019-7027.

10- Murat Rakap, Egwu Eric Kalu, Saim Özkar; Cobalt-nickel-phosphorus supported on Pd-activated TiO_2 (Co-Ni-P/Pd-TiO_2) as cost-effective and reusable catalyst for hydrogen generation from hydrolysis of alkaline sodium borohydride solution; *Journal of Alloys and Compounds*; 509, 2011, 7016-7021.

11- Murat Rakap, Egwu Eric Kalu, Saim Özkar; Effect of stirring on the kinetics of hydrogen generation from the hydrolysis of ammonia-borane using Pd-PVB-TiO_2 and Co-Ni-P/Pd-TiO_2 as highly active and reusable catalyst; *International Journal of Hydrogen Energy*; submitted.

12- **Murat Rakap**, Saim Özkar; Hydroxyapatite-supported cobalt(0) nanoclusters as efficient and cost-effective catalyst for hydrogen generation from the hydrolysis of both sodium borohydride and ammonia-borane; *Catalysis Today*; doi:10.1016/j.cattod.2011.04.022.

International Symposiums

1. Murat Rakap, Saim Özkar, Hydroxyapatite-Supported Palladium(0) Nanoclusters as Active and Reusable Catalyst for Hydrogen Generation from the Hydrolysis of Ammonia-Borane. *Energy Challenges for Advanced Materials and Processes: Harvesting, Storage, and Efficient Utilization (EnCAMP-2011)*, May 25-29, 2011, Cappadocia / Turkey (Oral Presentation).

National Symposiums

1. Murat Rakap, Saim Özkar. İntrazeolit Kobalt(0) Nanokümeleri: Hazırlanması, Tanımlanması ve Sodyum Borhidrürün Hidrolizindeki Katalitik Etkinliğinin İncelenmesi, II. Ulusal Anorganik Kimya Kongresi, 16-19 Mayıs 2009, Fırat Üniversitesi (Elazığ) (Poster Presentation).

2. Murat Aydemir, **Murat Rakap**, Feyyaz Durap, Akın Baysal, Saim Özkar, İntrazeolit Palladyum(0) Nanokümelerinin Suzuki Tepkimelerindeki Katalitik Etkinliği, 24. Ulusal Kimya Kongresi, 29 Haziran-2 Temmuz 2010, Zonguldak Karaelmas Üniversitesi (Zonguldak) (Poster Presentation).

3. Murat Rakap, Saim Özkar, Hidroksiapatit Üzerine Tutturulmuş Palladyum(0) Nanokümelerinin Hazırlanması, Tanımlanması ve Amonyak Boranın Hidrolizindeki Katalitik Etkinliğinin İncelenmesi, III. Ulusal Anorganik Kimya Kongresi, 19-22 Mayıs 2011, Çanakkale Onsekiz Mart Üniversitesi (Çanakkale) (Poster Presentation).